



저작자표시-비영리-변경금지 2.0 대한민국

이용자는 아래의 조건을 따르는 경우에 한하여 자유롭게

- 이 저작물을 복제, 배포, 전송, 전시, 공연 및 방송할 수 있습니다.

다음과 같은 조건을 따라야 합니다:



저작자표시. 귀하는 원저작자를 표시하여야 합니다.



비영리. 귀하는 이 저작물을 영리 목적으로 이용할 수 없습니다.



변경금지. 귀하는 이 저작물을 개작, 변형 또는 가공할 수 없습니다.

- 귀하는, 이 저작물의 재이용이나 배포의 경우, 이 저작물에 적용된 이용허락조건을 명확하게 나타내어야 합니다.
- 저작권자로부터 별도의 허가를 받으면 이러한 조건들은 적용되지 않습니다.

저작권법에 따른 이용자의 권리는 위의 내용에 의하여 영향을 받지 않습니다.

이것은 [이용허락규약\(Legal Code\)](#)을 이해하기 쉽게 요약한 것입니다.

[Disclaimer](#)

Doctor of Philosophy

**Biosynthesis, chemical synthesis and application of  
nitrogen-containing aryl compounds.**

The Graduate School  
of the University of Ulsan  
Department of Chemical Engineering  
and Bioengineering  
**Yuanyuan Wang**

**Biosynthesis, chemical synthesis and application of  
nitrogen-containing aryl compounds.**

**Supervisor: Prof. Soon-Ho Hong, Prof. Zhihua Sun**

A Dissertation

Submitted to  
the Graduate School of the University of Ulsan  
In partial Fulfillment of the Requirements  
for the Degree of

Doctor of Philosophy

by

Yuanyuan Wang

Department of Chemical Engineering and Bioengineering

University of Ulsan, Korea

February 2021

## Acknowledgements

I am very grateful to my tutor, *Prof. Soon-Ho Hong* for giving me selfless guidance and help with his profound knowledge and valuable experience, allowing me to learn and grow in a comfortable and friendly laboratory. And keep timely emails with me during my stay in China to make the paper and thesis work go smoothly. I would never forget about this.

I am thankful to the *University of Ulsan*, for supporting my projects and providing a good research environment during this study.

I will undoubtedly give my thanks to *Vidhya, Murali, Sivachandiran, Ngan and Jaehoon*, they help me like brothers and sisters in every possible way, no matter in experiments, paper works or daily life. I feel really honored to have such good lab mates. I wish them a bright future and a happy family.





Thank my parents and younger brother for keeping me calm and spending the past few years without any burden.

Thank Office Manager *Lim kyoung Jo* and all office staffs in our department, and *Dr. Zhen Guo* in international office, without whom I will feel troubled in the process. Thank all friends who stay with me and stand by me.

In the past five years, I learned much knowledge, knew many people, made many friends, went through many things, and inevitably I grew older. The only things that might be lost are weight and collagen in my body. This period is coming to the end in the unforgettable year 2020. The life at Ulsan University and city Ulsan left me many good memories. Hope the city will always be peaceful and people here will always stay away from diseases.

**Biosynthesis, chemical synthesis and application of  
nitrogen-containing aryl compounds.**

This certifies that the dissertation of Yuanyuan Wang is  
approved.

위원장	교수	유익근 
Committee Chair	Prof.	Yoo, Ik-Keun
위원	교수	류근갑 
Committee Member	Prof.	Ryu, Kuen-Garp
위원	교수	홍순호 
Committee Member	Prof.	Hong, Soon-Ho
위원	교수	엄경태 
Committee Member	Prof.	Eom, Gyeong-Tae
위원	교수	孙智华 
Committee Member	Prof.	Zhihua Sun

Department of Chemical Engineering and bioengineering

University of Ulsan, Korea

February 2021

## Table of Contents

<b>NOMENCLATURE</b>	<b>9</b>
<b>LIST OF TABLES</b>	<b>10</b>
<b>LIST OF FIGURES</b>	<b>11</b>
<b>Abstract</b>	<b>1</b>
<b>Chapter 1</b>	<b>3</b>
<b>Introduction</b>	<b>3</b>
<b>Chapter 2</b>	<b>5</b>
<b>Development of fenitrothion adsorbing recombinant <i>Escherichia coli</i> by cell surface display of pesticide-binding peptide</b>	<b>5</b>
<b>2.1 Abstract</b>	<b>5</b>
<b>2.2 Introduction</b>	<b>5</b>
<b>2.3 Material and methods</b>	<b>7</b>
<b>2.3.1 Bacterial strains and growth conditions</b>	<b>7</b>
<b>2.3.2 Plasmid construction</b>	<b>8</b>
<b>2.3.3 Expression study by SDS-PAGE</b>	<b>10</b>
<b>2.3.4 Fenitrothion biosorption by the recombinant strain</b>	<b>10</b>
<b>2.3.5 Molecular modeling and docking studies</b>	<b>11</b>
<b>2.3.6 Scanning emission microscopy (SEM) analysis</b>	<b>11</b>
<b>2.4 Results and discussion</b>	<b>11</b>
<b>2.4.1 Construction of fenitrothion-adsorbing recombinant strain</b>	<b>11</b>
<b>2.4.2 Optimization of adsorption conditions</b>	<b>12</b>

2.4.3 Construction of pesticide-binding peptide dimer	14
2.4.4 Modeling and docking studies	15
2.4.5 Cell morphology by FE-SEM	16
2.5 Conclusions	17
2.6 References	19
Chapter 3	21
Enhanced production of $\gamma$ -aminobutyric acid (GABA) from <i>E. coli</i> under acidic condition.	21
3.1 Abstract	21
3.2 Introduction	21
3.2.1 Gamma-aminobutanoic acid	21
3.2.2 Previous studies for enhanced production of $\gamma$ - aminobutyric acid	22
3.2.3 <i>Escherichia coli</i> -derived protein gene ycgZ-ymgABC	23
3.2.4 Gene DR1558 extracted from <i>Deinococcus radiodurans</i>	24
3.3 Materials and methods	24
3.3.1 Bacterial strains and growth conditions	24
3.3.2 Plasmid construction	26
3.3.3 Expression study by SDS-PAGE	29
3.3.4 GABA analysis	29
3.4 Results and discussion	30
3.4.1 Construction of acid-tolerance recombinant strain	30
3.4.2 Optimization of GABA production	31
3.5 Conclusions	32
3.6 References	34

<b>Chapter 4</b>	<b>36</b>
<b>Design, synthesis and antiproliferative activity of chiral 1, 4-disubstituted-3,4-dihydroquinazolin-2(<i>1H</i>)-one derivatives against common human cancer cell lines</b>	<b>36</b>
<b>4.1 Abstract</b>	<b>36</b>
<b>4.2 Introduction</b>	<b>36</b>
<b>4.3 Materials and methods</b>	<b>37</b>
<b>4.3.1 Synthesis and substance testing methods</b>	<b>37</b>
<b>4.3.2 Cell culture assays and MTT assay</b>	<b>38</b>
<b>4.3.3 In vitro antitumor activity and cytotoxicity assays [6]</b>	<b>38</b>
<b>4.3.4 Molecular docking</b>	<b>38</b>
<b>4.4 Results and discussion</b>	<b>39</b>
<b>4.4.1 Synthesis of products</b>	<b>39</b>
<b>4.4.2 Antitumor activities towards three kinds of tumor cells</b>	<b>41</b>
<b>4.4.3 Molecular docking studies</b>	<b>43</b>
<b>4.5 Conclusions</b>	<b>44</b>
<b>4.6 References</b>	<b>46</b>
<b>Chapter 5</b>	<b>48</b>
<b>Synthesis of phenylpropionate compounds and their potential antiproliferative activities.</b>	<b>48</b>
<b>5.1 Abstract</b>	<b>48</b>
<b>5.2 Introduction</b>	<b>48</b>
<b>5.3 Materials and methods</b>	<b>50</b>
<b>5.3.1 Synthesis and substance testing methods</b>	<b>50</b>
<b>5.3.2 Molecular docking studies</b>	<b>51</b>



<b>5.4 Results and discussion</b>	<b>51</b>
<b>5.4.1 Molecular docking studies</b>	<b>51</b>
<b>5.4.2 Synthesis of target products</b>	<b>55</b>
<b>5.5 Conclusions</b>	<b>58</b>
<b>5.6 References</b>	<b>59</b>
<b>6 Conclusions</b>	<b>61</b>
<b>Supplementary Information (SI)</b>	<b>62</b>
<b>1. Synthesis of quinazolinone derivatives (Chapter 4)</b>	<b>62</b>
<b>2. <sup>1</sup>H NMR and <sup>13</sup>C NMR spectra of quinazolinone derivatives</b>	<b>65</b>
<b>3. Synthesis of phenylpropionate compounds (Chapter 5)</b>	<b>72</b>
<b>4. <sup>1</sup>H NMR and <sup>13</sup>C NMR spectra of phenylpropionate compounds</b>	<b>76</b>

## NOMENCLATURE

Abbreviations used throughout the thesis are according to the recommendations of the IUPAC-IUBMB commission of biochemical nomenclature and of the ACS Style Guide.

The following abbreviations were used:

Kb	Kilo base (1000 base pairs)
bp	base pair
kD	Kilo Dalton
IPTG	Isopropyl $\beta$ -D-1-Thiogalactopyranoside
PCR	polymerase chain reaction
LB	Luria-Bertani broth
SDS-PAGE	sodium dodecyl sulfate polyacrylamide gel electrophoresis
DCM	dichloromethane
NBS	N-Bromosuccinimide
NMR	Nuclear Magnetic Resonance
LC-MS	liquid chromatograph-mass spectrometer

## **LIST OF TABLES**

<b>Table 2.1 List of bacterial strains and plasmids used in this study</b>	<b>8</b>
<b>Table 2.2 Primers used in this study</b>	<b>9</b>
<b>Table 3.1 List of bacterial strains and plasmids used in this study</b>	<b>25</b>
<b>Table 3.2 Primers used in this study</b>	<b>26</b>
<b>Table 4.1 Half maximal inhibitory concentrations (<math>IC_{50}</math>, <math>\mu M</math>) in vitro tumor cell lines and L02 of 8 compounds.</b>	<b>42</b>
<b>Table 5.1 The docking scores of 9 preferred compounds, one reported tumor inhibitor and other 5 compounds for comparison.</b>	<b>52</b>
<b>Table 5.2 Synthesis of final products</b>	<b>56</b>

## LIST OF FIGURES

<b>Fig. 1.1 Cell surface display technology</b>	<b>3</b>
<b>Fig. 1.2 Interactions between anti-cancer drugs and tumor cells.</b>	<b>4</b>
<b>Fig. 2.1 Molecular structure of Fenitrothion.</b>	<b>6</b>
<b>Fig. 2.2 (A) Schematic diagram of pesticide-binding peptide display. (B) Map of pETPBx2 plasmid containing the OmpC–pesticide-binding peptide fusion protein.</b>	<b>9</b>
<b>Fig. 2.3 SDS-PAGE expression analysis of OmpC–pesticide-binding peptide monomer (left) and dimer (right) fusion proteins at various concentrations of IPTG.</b>	<b>12</b>
<b>Fig. 2.4 The fenitrothion adsorption at various temperatures (A), pH levels (B), fenitrothion (C) concentrations using recombinant <i>E. coli</i> (pETPB).</b>	<b>13</b>
<b>Fig. 2.5 (A) The fenitrothion adsorption using recombinant <i>E. coli</i> displaying monomer (■) and dimer (●) of the pesticide-binding peptide at various fenitrothion concentrations. (B) Fenitrothion adsorption in the artificial polluted soil. <i>E. coli</i> BL21 (DE3), <i>E. coli</i> (pETPB), and <i>E. coli</i> (pETPBx2) were tested.</b>	<b>15</b>
<b>Fig. 2.6 Modeling and docking of OmpC pesticide-binding peptide with (A) monomer of pesticide-binding peptide and (B) dimer of pesticide-binding peptide with fenitrothion.</b>	<b>16</b>
<b>Fig. 2.7 Cell morphology of <i>E. coli</i> BL21 (DE3), <i>E. coli</i> (pETPB), and <i>E. coli</i> (pETPBx2) with fenitrothion by FE-SEM.</b>	<b>17</b>
<b>Fig. 3.1 GABA pathway in TCA cycle</b>	<b>22</b>

- Fig. 3.2 Acid tolerance of *ycgZ-ymgABC* and other genes in W3110 strain under acid stress of pH 2.5. Combined strains were inoculated into LB media (Amp), induced at OD=0.5 with 200ng/ml AHT. After 2h induction, cells were harvested, washed, and diluted to an equal OD=1.0. Tested under acid stress for 2h and processed serial dilution and spotting.** 23
- Fig. 3.3 Gene clean of DR1558 (middle) and *ycgZ-ymgABC* (left and right).** 31
- Fig. 3.4 Production of total GABA concentration after 30h of cultivation, under various conditions such as: (A)(B) IPTG and (C)(D) pH with DR1558 or *ycgZ-ymgABC* scaffold architecture.** 32
- Fig. 4.1 Quinazolinone derivatives with biological activity in previous studies.** 37
- Fig. 4.2 Synthetic routes of chiral 1, 4-disubstituted-3, 4-dihydroquinazolin-2(1H)-one.** 40
- Fig. 4.3 Structures of 7 synthetic compounds, as well as one known quinazolines derivative 12h with antitumor activity in Table 4.1.** 40
- Fig. 4.4 10 compounds were synthesized in previous study. It showed that compounds with R of alkyl substituent (compound p10) possessed best tumor cell validity.** 41
- Fig. 4.5 (A) Schematic depiction of the compound 12d within the binding pocket. Pink arrows denote hydrogen-bonding to backbone (solid lines) or side chains (dotted), while straight line (green) represents  $\pi$ -stacking interactions, and straight line (red)**

represents salt bridge; (B) Compound 12d in oncogenic tyrosine phosphatase SHP2 in the crystal structure 43

**Fig. 5.1** Molecular structures of L-Phenylalanine (left) and isothiourreas (right). 49

**Fig. 5.2** Structures of Lesinurad (a), JTP-59557 (b), CXCR4 (c) and resolution of isothiourrea structure synthesis (d). 50

**Fig. 5.3** Schematic depiction of compound 4 with retinoic acid receptor related orphan C (RORC) (PDB ID: 4WPF) within the binding pocket. Straight line (green) represents  $\pi$ -stacking interactions. 54

**Fig. 5.4** A Synthetic route of Lesinurad explored by us in previous study. B Compared with existing synthetic methods, our method has advantages in synthetic pathway and yield. C Synthesis of CXCR4 through our synthesis method. D Synthesis method of potential cancer cell inhibitor with phenylalanine group and isothiourrea group. 56

## Abstract

Fenitrothion is a nitrophenolic pesticide with nitrogen-containing aryl structures that has been widely used in agriculture. However, the major hydrolysis metabolite of fenitrothion is toxic to many living organisms, raising environmental safety concerns. It is necessary and promising to remove fenitrothion from pesticide-polluted soil and water by biology methods. On the other hand, nitrogen-containing aryl structure is an important pharmacophore of anticancer drugs. In recent years, cancer has become the biggest threat to human health and the research of cancer drugs is particularly important. The pesticide-binding peptide SPPWPPRP monomer and dimer were introduced respectively and displayed in *E. coli*, the binding efficiency under different temperatures, pH levels, and fenitrothion concentrations were evaluated. The recombinant strain with peptide dimer provided the highest amount of fenitrothion adsorption (136.0  $\mu\text{mol fenitrothion/g DCW}$ ), while the strain with the monomer adsorbed somewhat less (117.2  $\mu\text{mol fenitrothion/g DCW}$ ). The results indicated that the peptide-displaying recombinant strain can efficiently adsorb fenitrothion present in actual soil, and can be used to decontaminate fenitrothion-contaminated soil. All the tested *E. coli* strains remain intact under contaminated conditions.

Acid tolerance peptides DR1558 and *ycgZ-ymgABC* were introduced and displayed in *E. coli*, the GABA production under different pH levels was evaluated. Final GABA concentration was increased by 11.3% via the inactivation of competing pathways at initial MSG concentration of 10g/L. Both of DR1558 combined strain and *ycgZ-ymgABC* combined strain produced higher GBAB yields under relatively lower pH conditions, showing that the introduction of acid-tolerance peptides can help increase GABA production. However, conditions including temperature and initial MSG concentration need to be further optimized to achieve better GABA output.

1, 4-disubstituted-3,4-dihydroquinazolin-2(1*H*)-one derivatives and phenylpropionate compounds were synthesized, and their potential in cancer inhibition was evaluated by computer aided drug design (Discovery Studio) and tested in K562, A549, U251 and

L02 cell lines by MTT assay. Among these synthesized quinazolinone derivatives, (S)-6-chloro-1-(cyclopropylmethyl)-4-(2-fluorophenyl)-3,4-dihydroquinazolin-2(*1H*)-one (12d) possessed more optimal antiproliferative activity with IC<sub>50</sub> values lower than 30  $\mu$ M. As for tested cell lines, better inhibition effect was implied on lung cancer cell A549.

Phenylpropionate compounds which considered to have good anti-tumor activity in the preliminary drug-assisted design were synthesized through convenient routes. Active molecules of isothiourea with phenylalanine group were successfully synthesized. A multicomponent protocol that involves electrophilic center and isocyanide is proved to be suitable for the formation of these and other important isothiourea compounds, including an anti-gout drug and CXCR4 antibody. The advantages of mild reaction conditions, reduced purification steps, and ease of starting material accessibility is a useful addition to existing methodologies.



## Chapter 1

### Introduction

Surface display technique, which displays the fusion protein of a short protein or peptide (target protein) and microbial outer membrane protein (OMP, carrier protein) through genetic engineering technology, has already been established for several decades. A number of surface display systems and gene fusion strategies since then have been constructed in succession. Based on variable structure and function of microbial cell surface, cell surface display technology is applied in biosorbent, biosensor, antibody production and biocatalyst *et al.* in recently years Fig. (1.1).

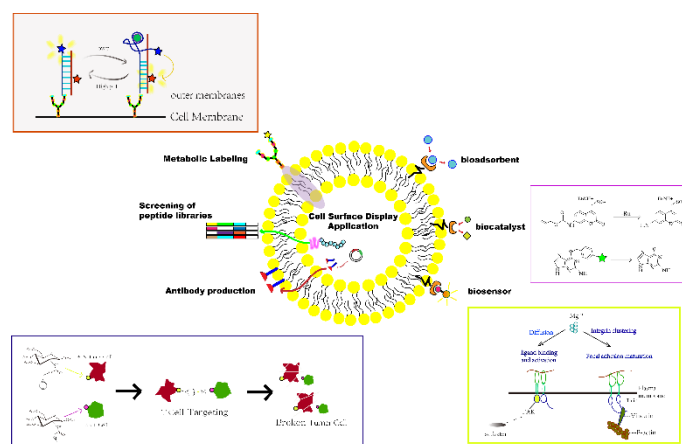


**Fig. 1.1** Cell surface display technology

The incidence of malignant tumors is rising worldwide and cancer has become the first fatal disease. Objective factors such as poor living environment and lifestyle, aging, and increasing survival pressure can lead to cancer. In cancer treatment, drug therapy is very important, and the use of effective anti-cancer drugs can help patients live longer. At present, the common anti-cancer drugs include chemotherapy drugs, traditional Chinese medicine, Biopharmaceuticals and targeted drugs, *etc.* The mechanism of anticancer activities is showed in Fig. 1.2. According to different mechanism, cancer medicines can be divided into five categories: Synthesis inhibition of nucleoside acid,

such as fluorouracil and methotrexate; Protein synthesis inhibition, such as vincristine and asparaginase; Direct damage towards DNA, such as nitrogen mustard and busulfan; DNA template interference, such as doxorubicin and mithomycin; Hormones affection, such as sex hormones and adrenal cortex hormones. However, effective and specific drugs are scarce and need to be developed, both of the chemical synthesis methods and biosynthesis methods are good choices.

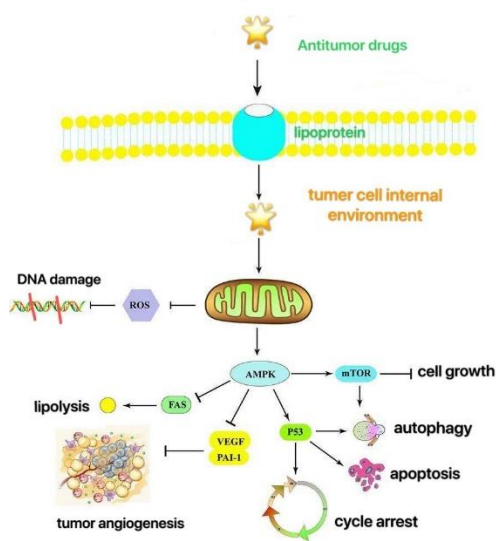


**Fig. 1.2** Interactions between anti-cancer drugs and tumor cells.

## Chapter 2

### Development of fenitrothion adsorbing recombinant *Escherichia coli* by cell surface display of pesticide-binding peptide

#### 2.1 Abstract

Constructed *Escherichia coli* could efficiently adsorb fenitrothion by displaying a pesticide-binding peptide on it using the anchoring motif OmpC. A codon-optimized, pesticide-binding peptide was attached to the C-terminus of OmpC at loop 7 (993 bp). The efficiency of fenitrothion binding by the monomer peptide was evaluated under different temperatures, pH levels, and fenitrothion concentrations. To enhance fenitrothion adsorption, a dimer of pesticide-binding peptide was also constructed and displayed. Compared with the peptide monomer, the dimer-displaying strain showed superior fenitrothion-binding ability. The performance of the strains was evaluated in artificial polluted soil, and their morphology was analyzed by FE-SEM. The results showed that these two kinds of constructed strains can adsorb fenitrothion in contaminated environments with no cellular activity reduction.

#### 2.2 Introduction

Organophosphorus pesticides have been used extensively all over the world, especially in agriculture for more than 60 years. Currently, about 100 organophosphorus pesticides, such as chlorpyrifos, fenitrothion, and parathion are in use, since they are considered to have specific toxicity towards insects. However, after the substantial and long-term agricultural use of these pesticides, it was found that they actually also exhibit toxicity to non-target animals and humans. Recently, it has been reported that applying chlorpyrifos, fenitrothion, and parathion leads to soil, groundwater, and surface water contamination, making organophosphorus pesticides a major public health concern. Fenitrothion, or *O*, *O*-dimethyl *O*-(3-methyl-4-nitrophenyl) phosphorothioate (Fig. 2.1), is a nitrophenolic pesticide that has been widely used in agriculture. The inhibition of

acetylcholine esterase activity and inhibition of acetylcholine breakdown in synapses result in the accumulation of acetylcholine in synapses, which causes convulsions, paralysis, and death of insects [1]. However, under aerobic conditions, the major hydrolysis metabolite of fenitrothion, 3-methyl-4-nitrophenol, is toxic to many living organisms, raising environmental safety concerns.

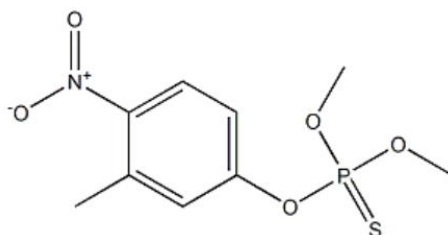


**Fig. 2.1** Molecular structure of Fenitrothion.

Intensive studies have been carried out on removing fenitrothion from pesticide-polluted soil and water. To achieve this goal, various strategies, such as the use of nano- $\alpha$ -Al<sub>2</sub>O<sub>3</sub> sorbent, organo-mineral complexes, and bacterial culture, have been evaluated. Wei et al. (2012) presented the first study on polishing-activated nano- $\alpha$ -Al<sub>2</sub>O<sub>3</sub> sorbent for sensing nitroaromatic organophosphate pesticides by square-wave anodic stripping voltammetry (SWASV) [2]; they found that polished  $\alpha$ -Al<sub>2</sub>O<sub>3</sub> nanoparticles have strong affinity towards the phosphoric group in fenitrothion. Arani et al. (2006) reported Fe-TAML/H<sub>2</sub>O<sub>2</sub> (TAML: tetraamido macrocyclic ligand) activators degraded organophosphorus pesticides [3]. Also, fenitrothion can be adsorbed efficiently by organo-mineral complexes, including organo-montmorillonite, organoclinoptilolite, and organo-sepiolite, via hydrophobic interactions [4].

Various studies were also carried out for biological removal of fenitrothion. *Sphingomonas* sp. TFEE and *Burkholderia* sp. MN1 were isolated from a fenitrothion-treated soil, and indicating that fenitrothion can be degraded by syntrophic culture of both strains. *Sphingomonas* sp. TFEE degrades fenitrothion to 3-methyl-4-nitrophenol (3M4N), which is further degraded by *Burkholderia* sp. MN1 [5]. Five organophosphorus pesticides (chlorpyrifos, diazinon, fenitrothion, malathion, and

methyl parathion) were inoculated with lactic acid bacteria; the results revealed the degradation rate increased by 0.8%–225% [6]. The fenitrothion-utilizing strain *Burkholderia* sp. NF100 was isolated from fenitrothion-contaminated soil, and it was found that this strain uses fenitrothion as a sole carbon source [7].

Bacterial cell surface display is a novel biotechnological strategy by which a desired protein can be expressed on the surface of bacteria with the help of a matched anchoring motif. For efficient, stable display of a desired protein or peptide, selection of an appropriate anchoring motif is essential. Several anchoring motifs, including TraT, LamB, FhuA, OmpA, and OmpC, have been widely used in various Gram-negative bacteria for various applications [8]. Among them, *Escherichia coli* OmpC has been characterized as one of the most efficient anchoring motif proteins. It was reported that osmoporin *E. coli* OmpC has a stable  $\alpha$ -barrel structure [9] and a high expression titer of  $2 \times 10^5$  molecules per cell. Therefore, OmpC is considered an appropriate anchoring motif for peptide surface expression.

In this study, fenitrothion-adsorbing recombinant *E. coli* was constructed through the display of pesticide-binding peptide, using OmpC as an anchoring motif. To elevate the fenitrothion-binding capacity, a dimer of pesticide-binding peptide was also displayed and evaluated. The fenitrothion-binding conditions were optimized by testing the recombinant *E. coli* under different conditions of pH, temperature, IPTG concentration, and fenitrothion concentration.

## **2.3 Material and methods**

### **2.3.1 Bacterial strains and growth conditions**

The *E. coli* strains and plasmids used in this study are listed in Table 2.1. All the strains were cultivated in Luria–Bertani medium (LB medium) (10 g/L bacto tryptone, 5 g/L bacto yeast extract, and 5 g/L NaCl), supplemented with ampicillin (100 mg/L) at 37 °C,

with vigorous shaking at 200 rpm. No carbon source was added to culture media.

**Table 2.1** List of bacterial strains and plasmids used in this study

Strain/plasmid	Relevant genotype/property	Source
<i>Escherichia coli</i>		
strain		
BL21(DE3)	$F^- ompT gal dcm lon hsdS_B(r\bar{B} m\bar{B})$ $\check{e}(DE3 [lacI lacUV5-T7 gene 1$ $ind1sam7 nin5])$	Novagen
Plasmid		
pET-21a	Ap <sup>R</sup>	NEB <sup>a</sup>
pETPBP	pET-21a containing <i>ompC-PBP</i> gene	This work
pETPBPx2	pET-21a containing <i>ompC-PBP</i> (x2) gene	This work

<sup>a</sup> New England Biolabs, Beverly, MA, USA

### 2.3.2 Plasmid construction

The codon-optimized pesticide-binding peptide (SPPWPPRP) was fused to the C-terminus of the OmpC gene at loop 7 (993 bp) (Fig. 2.2a) [10]. Polymerase chain reaction (PCR) was performed with MJ Mini Personal Thermal Cycler (Bio-Rad Laboratories, Hercules, CA, USA) using the Expand High Fidelity PCR system (Roche Molecular Biochemicals, Mannheim, Germany). The PCR product was cloned into the pET21a plasmid, using NdeI and XhoI restriction enzymes, to construct plasmid pETPBP. The PCR primers used in this study are listed in Table 2.2. OmpC–pesticide peptide expression was induced by the T7 promoter after adding isopropyl b-D-1-thiogalactopyranoside (IPTG). These plasmids were transformed into 1 *E. coli* BL21 (DE3) strain for further studies. For the construction of the dimeric pesticide peptide, a

new reverse primer containing two pesticide peptides and linkers (GCGGAAGCGGCGGCGAAAGCG) in the middle of peptides was used. The PCR product was cloned into the pET21a plasmid, using NdeI and XhoI restriction enzymes, to construct the dimeric plasmid pETPBPx2 (Fig. 2.2b). Then, the constructed plasmid was transformed into the BL21 (DE3) strain for further studies.

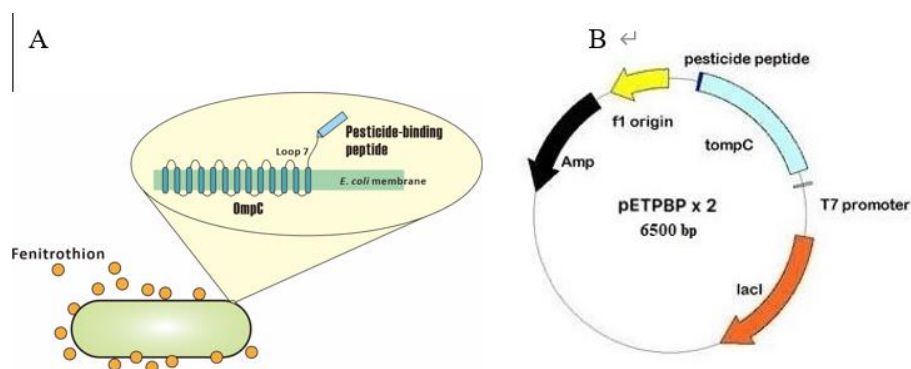


**Fig. 2.2** (A) Schematic diagram of pesticide-binding peptide display. (B) Map of pETPBPx2 plasmid containing the OmpC–pesticide-binding peptide fusion protein.

**Table 2.2** Primers used in this study

Name	Sequence (5'-3')
Optimized pesticide-binding peptide	AGC CCG CCG TGG CCG CCG CGC CCG
Monomer Ompc_Frw	CATATGAAAGTTAAAGTACTGTC
Monomer Ompc_Rev	CTCGAGTTACGGGCGCGGCGGCCACGG CGGGCTCATGTTTTTGT
Dimer Ompc_Frw	CATATGATGAAAGTTAAAGTACTG
Dimer Ompc_Rev	CTCGAGTTATTACGGGCGCGGCGGCCAC GGCGGGCTCGCTTTCGCCGCCGCTTCCG CCGGGCGCGGCGGCCACGGCGGGCT
Linker	GCGGAAGCGGCGGCGAAAGCG

### **2.3.3 Expression study by SDS-PAGE**

The recombinant *E. coli* strains were cultured in 10 mL tubes with an antibiotic at 37 °C overnight and diluted 100-fold in a flask containing 250 mL of LB medium. When optical density at 600 nm (OD600) reached 0.6, IPTG was added to the culture broth. After 6 h of culture at 30 °C, the protein was isolated using B-7M urea buffer. The treated cells were analyzed by 12% (w/v) sodium dodecyl sulfate-polyacrylamide gel electrophoresis (SDS-PAGE). The fractionated protein samples were stained with Coomassie Brilliant Blue R-250 (Bio-Rad Laboratories, Hercules, CA, USA).

### **2.3.4 Fenitrothion biosorption by the recombinant strain**

The recombinant *E. coli* strains were incubated in LB medium with 100 mg/L ampicillin at 37 °C for 12 h and diluted 100-fold in LB medium. Then, they were further incubated until OD600 reached 0.5–0.8. The cells were induced with 1 mM IPTG and cultured for 5 h at 20 °C. The strains were washed twice with autoclaved distilled water. Then 10 mL autoclaved distilled water and fenitrothion-containing acetonitrile solution (with different fenitrothion concentration of 10, 20, 30, 40, 50, or 60 ppm) were added to LB medium, cells were incubated for 30 min to adsorb fenitrothion. Other conditions, such as pH (5, 6, 7, 8, 9) and temperature (20, 25, 30°C), were also varied and tested. Next, the cells were washed again with autoclaved distilled water and centrifuged at 8000 rpm for 15 min (The distilled water after this step were examined through HPLC and no fenitrothion was detected). After that, 2mL of acetonitrile was added to the cells to elute the pesticide from the cells. These suspensions were mixed well and centrifuged to collect the solutions. The Fenitrothion containing samples were transferred in HPLC sample bottles for quantitative testing after filtration. The amount of adsorbed fenitrothion was analyzed using high-performance liquid chromatography (HPLC). Each result was corrected by a calibration curve. Different amounts of fenitrothion were dissolved in acetone to prepare a series of calibration solutions of 0.5, 1, 5, 10, 20, 50,



and 100 ppm.

### **2.3.5 Molecular modeling and docking studies**

Fusion proteins' binding efficiency towards fenitrothion was further validated by molecular modeling studies and docking analysis. The molecular modeling was performed by Easy Modeller 4.0 using 2JIN as a template. The homology model's refined structure was obtained by 3Drefine Protein Structure Refinement Server. The molecular docking was performed with auto dock.

### **2.3.6 Scanning emission microscopy (SEM) analysis**

After fenitrothion adsorption, the recombinant strains were visualized by field emission scanning emission microscopy (FE-SEM) (JEOL JSM-6500F). The cells were washed and fixed by incubation at 23 °C in 2.5% glutaraldehyde for 14 h. The fixed cells were washed with PBS, and then the cells were mounted on ultra-flat silicon wafers and dried for visualization by FE-SEM.

## **2.4 Results and discussion**

### **2.4.1 Construction of fenitrothion-adsorbing recombinant strain**

Although some studies of fenitrothion adsorption by native and recombinant bacteria have been performed, cell surface display has not been employed for its adsorption. By expressing pesticide-binding peptide on the outer bacteria membrane, a dramatic increase of the fenitrothion-adsorbing capacity of bacteria could potentially be achieved. To realize this, a peptide (SPPWPPRP) was integrated into the C-terminus of the *E. coli* outer membrane protein OmpC. A previous study indicated the pesticide-binding peptide used in this study showed high sensitivity to fenitrothion [10]. The peptide

needs to be displayed outside of the membrane for efficient fenitrothion adsorption. In a previous study, it was suggested that loop 7 of *E. coli* OmpC could act as a stable motif for peptide anchoring based on homology studies [11]. Therefore, the codon-optimized, pesticide-binding peptide was fused to the C-terminus of the OmpC gene at loop 7 between the amino acids XS and QL.

The OmpC–pesticide-binding peptide fusion protein was cloned into the pET21 plasmid and expressed by the addition of the inducing agent IPTG. The findings showed that the fusion protein was successfully expressed, as revealed by SDS-PAGE (Fig.2.3).

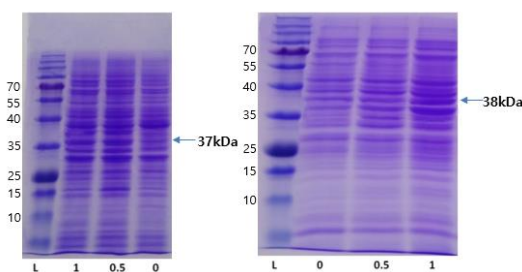


**Fig. 2.3** SDS-PAGE expression analysis of OmpC–pesticide-binding peptide monomer (left) and dimer (right) fusion proteins at various concentrations of IPTG.

#### 2.4.2 Optimization of adsorption conditions

To find the optimal conditions for fenitrothion adsorption, the constructed recombinant strain was cultured under various temperatures, pH levels, and fenitrothion concentrations (Fig. 2.4). The amount of fenitrothion adsorbed at the surface was measured using wild-type *E. coli* as a control.

To determine the optimal temperature, the absorption reactions were performed at 20, 25, and 30°C (Fig. 2.4a). The results show decreased fenitrothion adsorption at higher temperatures, possibly because of more complicated membrane protein-related processes, such as secretion and folding, which take a longer processing time. At 20°C, about 60  $\mu\text{mol}$  fenitrothion/g DCW was adsorbed on the recombinant strain surface.

Although higher fenitrothion adsorption was obtained at the lowest temperature, an even lower temperature was not tested considering the associated recombinant *E. coli* low growth rate.

To evaluate the effect of pH on fenitrothion adsorption, the recombinant strain was cultured at various pH levels of 6, 7, 8, and 9 (Fig. 2.4b). Maximum fenitrothion adsorption was obtained at pH 7, at which as much as 78.8  $\mu\text{mol}$  fenitrothion/g DCW was adsorbed on the recombinant strain surface. The amount of fenitrothion adsorption decreased as pH increased, and only 52.8  $\mu\text{mol}$  fenitrothion/g DCW was adsorbed at pH 9. This indicates that the displayed peptide's structure was affected by pH, and the most stable structure formed at pH 7.

Although organophosphorus pesticides exerted specific toxicity on insects, fenitrothion's effects on the recombinant strain's cell growth and metabolism should be examined. The recombinant strain was cultured with various fenitrothion concentrations (0.1–20 ppm) (Fig. 2.4c). The amount of adsorbed fenitrothion increased as the fenitrothion concentration increased from 0.1 to 20 ppm. Therefore, the constructed strain's intracellular activity appeared unaffected by the addition of fenitrothion, and the strain can be used for fenitrothion adsorption, even at higher fenitrothion concentrations.

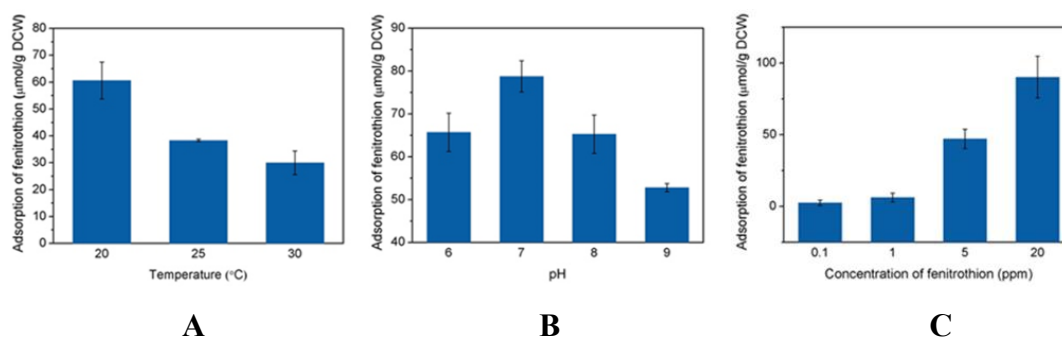


**Fig. 2.4** The fenitrothion adsorption at various temperatures (A), pH levels (B), fenitrothion (C) concentrations using recombinant *E. coli* (pETPBP).

### 2.4.3 Construction of pesticide-binding peptide dimer

As described above, a recombinant strain displaying the pesticide-binding peptide was constructed, which successfully adsorbed fenitrothion. To improve the strain's capacity to adsorb fenitrothion, a dimer of the pesticide-binding peptide was constructed and displayed. By attaching a dimer of the peptide on the anchoring motif, more binding sites can be displayed on the surface of the recombinant strain, and more fenitrothion can be adsorbed by the same amount of the strain. To achieve this, a dimer of the pesticide-binding peptide was cloned at the N-terminus of OmpC, and the fusion protein expression was monitored by SDS-PAGE (Fig. 2.3).

The recombinant strains displaying peptide monomer and dimer were incubated with various initial fenitrothion concentrations (20, 30, 40, 50, and 60 ppm). In both strains, more fenitrothion was adsorbed as the fenitrothion concentration increased. At every fenitrothion concentration, the strain with peptide dimer showed superior fenitrothion adsorption than the strain with peptide monomer. When 60 ppm fenitrothion was used, 165.6  $\mu\text{mol}$  fenitrothion/g DCW was adsorbed by the strain displaying the dimer, while the equivalent value was 106.5  $\mu\text{mol}$  fenitrothion/g DCW for that displaying the monomer. These findings imply that, by displaying the peptide dimer, the capacity to adsorb fenitrothion was increased by 55.5%.

In actual contaminated soil, many other components are present besides fenitrothion, which might hinder fenitrothion's interaction with the displayed peptide. As such, to mimic fenitrothion adsorption in actual contaminated soil, artificial polluted soil was prepared by adding 20 ppm of fenitrothion into a sample of 5 g of actual soil, which was resolved in 100 mL of distilled water. The recombinant strain with peptide dimer provided the highest amount of fenitrothion adsorption (136.0  $\mu\text{mol}$  fenitrothion/g DCW), while the strain with the monomer adsorbed somewhat less (117.2  $\mu\text{mol}$  fenitrothion/g DCW; Fig. 2.3a). The *E. coli* BL21 (DE3) strain was used as a control strain, and it adsorbed 79.9  $\mu\text{mol}$  fenitrothion/g DCW (Fig. 2.5b). This indicated that the peptide-displaying recombinant strain can efficiently adsorb fenitrothion present in actual soil, and can be used to decontaminate fenitrothion-contaminated soil.

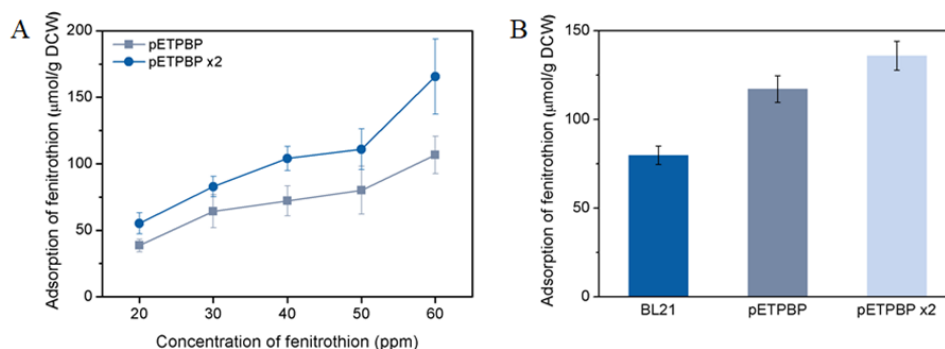


**Fig. 2.5** (A) The fenitrothion adsorption using recombinant *E. coli* displaying monomer (■) and dimer (●) of the pesticide-binding peptide at various fenitrothion concentrations. (B) Fenitrothion adsorption in the artificial polluted soil. *E. coli* BL21 (DE3), *E. coli* (pETPBP), and *E. coli* (pETPBPx2) were tested.

#### 2.4.4 Modeling and docking studies

For a detailed understanding of the interaction between fenitrothion and pesticide-binding peptide, molecular modeling of OmpC–peptide fusion proteins was carried out (Fig. 2.6). The OmpC–peptide monomer analysis results showed that the Pro 333 residue of the fusion protein interacts with fenitrothion (Fig. 2.6a). In the case of peptide dimer, fenitrothion interacts with Pro 349, Trp 350, and Pro 334 residues of the OmpC–peptide dimer fusion protein (Fig. 2.6b). This suggested that the dimer of pesticide-binding peptide can undertake stronger binding interaction with fenitrothion. This is consistent with the results of a wet experiment showing that the dimer-displaying strain adsorbed more fenitrothion on its surface. This study confirms improved fenitrothion-adsorbing capacity of peptide dimer from a bioinformatic perspective.

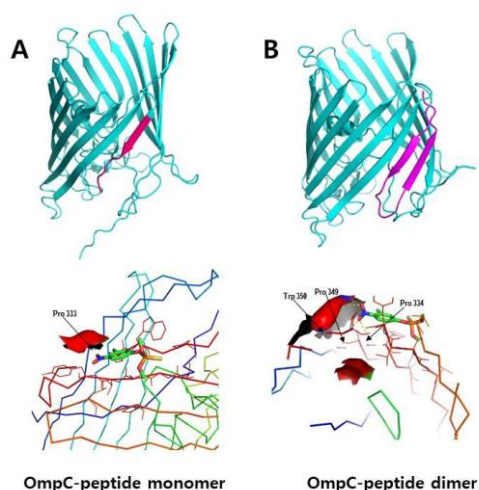


**Fig. 2.6** Modeling and docking of OmpC pesticide-binding peptide with (A) monomer of pesticide-binding peptide and (B) dimer of pesticide-binding peptide with fenitrothion.

#### 2.4.5 Cell morphology by FE-SEM

Based on the results of the studies described above, the constructed peptide-displaying strain can grow normally in the presence of fenitrothion, and it can adsorb fenitrothion efficiently in artificial polluted soil. For the industrial application of this strain, maintaining its health in a contaminated environment is essential. Therefore, the recombinant *E. coli* morphology was analyzed by FE-SEM after performing fenitrothion adsorption with a solution containing 20 ppm fenitrothion (Fig. 2.7). The SEM images show that all the tested *E. coli* strains remain intact under contaminated conditions. Because the fenitrothion adsorbed strain maintained their intact structure, fenitrothion can be removed by simple filtration from contaminated environment. This suggested that the constructed recombinant *E. coli* can be applied to actual polluted environments with no further modification.

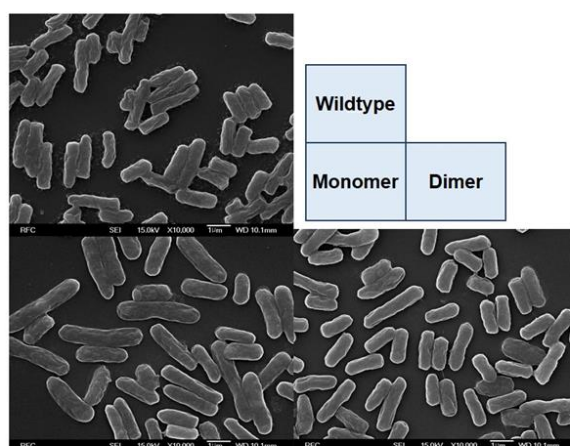


**Fig. 2.7** Cell morphology of *E. coli* BL21 (DE3), *E. coli* (pETPBP), and *E. coli* (pETPBPx2) with fenitrothion by FE-SEM.

## 2.5 Conclusions

In this study, pesticide-binding peptide displaying recombinant *E. coli* was constructed by using OmpC as an anchoring motif for efficient fenitrothion adsorption. The peptide dimer was constructed to elevate the recombinant strain's fenitrothion-binding capacity. Based on the results obtained with artificial polluted soil, we believe that the newly constructed peptide-displaying recombinant strain can be considered a strong candidate for an environmentally friendly system to remove fenitrothion or organophosphorus pesticides. Moreover, the strategy employed in this study can be applied to develop other systems for removing organophosphorus pesticides and contaminants. However, the effect of newly constructed recombinant bacteria needs to be investigated before real field application. What's more, the development of environmentally safe process such as immobilization might be required for real application.

Though the successful removal of fenitrothion by the newly constructed recombinant strain, the degradation of adsorbed fenitrothion still remains as a further challenge. Co-culture of fenitrothion adsorbing strain with fenitrothion degradation such as *Sphingomonas* sp. TFEE can be considered as a further modification of current system [5]. By coculturing the strains, the fenitrothion will not just removed from the

environment, but fenitrothion cleaning bacterial system can be constructed.



## 2.6 References

- [1] Cáceres L., Rovira J., García A., Torres R., 2011. Determination of the resistance to organophosphate, carbamate, and pyrethroid insecticides in Panamanian *Anopheles albimanus* (Diptera: Culicidae) mosquitoes. *Biomedica*, 31, 419–427.
- [2] Wei Y., Xu R.X., Gao C, Liu J.H., Huang X.J., 2012. Polishing-activated nano  $\alpha$ - $\text{Al}_2\text{O}_3$ : Adsorption and electrochemical behavior toward organophosphate pesticides, *Electrochem. Commun.* 18, 78–80.
- [3] Arani C., Sushil K. K., Deboshri B., Anindya G., Terrence J. C., 2006. Total degradation of fenitrothion and other organophosphorus pesticides by catalytic oxidation employing Fe-TAML peroxide activators, *J. Am. Chem. Soc.* 128, 12058–12059.
- [4] Dragana K., Jovan L., Milan D., Radivoj P., Đorđe J., Tanja S., 2011. Fenitrothion adsorption–desorption on organo–minerals, *Appl. Clay Sci.* 52, 109–114.
- [5] Chie K., Shinji N., Yasuhiro T., Kanako T., Masahito H., Kenji K., 2009. Complementary cooperation between two syntrophic bacteria in pesticide degradation. *J. Theor. Biol.* 256, 644–654.
- [6] Zhang Y.H., Xua D., Liu J.Q., Zhao X.H., 2014. Enhanced degradation of five organophosphorus pesticides in skimmed milk by lactic acid bacteria and its potential relationship with phosphatase production. *Food Chem.* 164. 173–178.
- [7] Masahito H., Motoko H., Shinichi T., 2000. Involvement of Two Plasmids in Fenitrothion Degradation by *Burkholderia* sp. Strain NF100, *Appl. Environ. Microbiol.* 4, 1737–1740.
- [8] Saleem M., Brim H., Hussain S., Arshad M., Leigh M.B., Zia U.H., 2008. Perspectives on microbial cell surface display in bioremediation, *Biotechnol. Adv.* 26, 151–161.
- [9] Sambandam R., Yoo I.K., Lee S.Y., Hong S.H., 2011. Construction of copper removing bacteria through the integration of two-component system and cell surface display. *Appl. Biochem. Biotechnol.* 165, 1674–1681.
- [10] Hua X.D., Liu X.F., Shi H.Y., Wang Y.R., Kim H.J., Gee S.J., Wang M.H., Liu F.Q.,

Hammock B.D., 2014. Development of a heterologous enzyme-linked immunosorbent assay for organophosphorus pesticides with phage-borne peptide, RSC Adv., 4, 42445–42453.

[11] Xu Z.H., LEE S.Y., 1999. Display of polyhistidine peptides on the *Escherichia coli* cell surface by using outer membrane protein C as an anchoring motif. Appl. Environ. Microbiol. 11, 5142–5147.

## **Chapter 3**

### **Enhanced production of $\gamma$ -aminobutyric acid (GABA) from *E. coli* under acidic condition.**

#### **3.1 Abstract**

In this study, *Escherichia coli* were engineered to produce gamma-aminobutyric acid from MSG by the introduction of acid tolerance synthetic scaffolds of peptide ycgZ-ymgABC from W3110 strain and DR1558 peptide from bacterium *Deinococcus radiodurans*. The GABA production was functioned by succinate dehydrogenase in the Krebs cycle. By introduction of peptide DR1558, production of 1.2 g/L GABA was achieved at 30oC and pH 2. By introduction of peptide ycgZ-ymgABC, production of 0.62 g/L GABA was achieved at 30oC and pH 2.

#### **3.2 Introduction**

##### **3.2.1 Gamma-aminobutanoic acid**

Gamma-aminobutanoic acid (GABA) is a non-protein amino acid, known as one of the core neurotransmitters in mammalian brains [1]. Considering the various beneficial effects of GABA, including decrease of blood pressure, inhibition of anxiety, enhancement of liver, kidney and cardiovascular, enhancement of immune response and repression of cancer cell proliferation, GABA has gained extensive use in pharmaceuticals and functional foods [2]. The general GABA pathway leads from the Krebs cycle to GABA via glutamate. Under the action of glutamate dehydrogenase, glutamic acid produces GABA, which is converted into succinic semialdehyde by GABA transaminase, and further to succinic acid (Fig. 3.1).

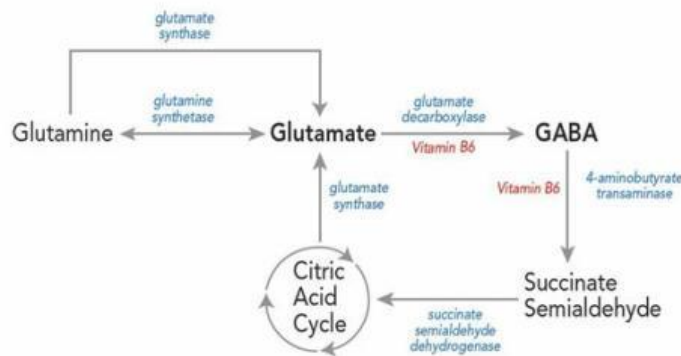


**Fig. 3.1** GABA pathway in TCA cycle

### 3.2.2 Previous studies for enhanced production of $\gamma$ -aminobutyric acid

Many attempts to synthesize GABA effectively have been made to date because of its beneficial functions and the increasing commercial demand.

As the traditional GABA production process involves the decarboxylation of glutamate, various recombinant strains overexpressing decarboxylase have been constructed to enhance GABA production, using monosodium L-glutamate (MSG) as carbon source. For example, 1.35-fold higher GABA concentration was obtained by overexpressing the glutamate decarboxylase from *Lactobacillus plantarum* [3]. 0.1 g/L of GABA was obtained from 30 g/L of MSG by overexpressing rice glutamate decarboxylase from *Bifidobacterium longum* [4]. 5.46 g/L of GABA was obtained from 10 g/L of MSG by overexpressing the glutamate decarboxylase and GABA transporter from *Escherichia coli* [5]. However, the results showed that the yield of GABA decreased in a low pH environment, which contradicted with the fact that the low pH environment is beneficial to the growth of *E. coli*.

Direct production of GABA from sugar in recombinant *E. coli* was explored and found to be a challenging task. Due to importance of glutamate in the *E. coli* metabolic network, it is not optimized to produce glutamate or GABA. Previous studies found that no GABA was produced in wild type *E. coli* when applying glucose as carbon source. To construct direct GABA producer, Pham et al. [6] developed a system of three

enzymes consisting GABA pathway including isocitrate dehydrogenase, glutamate synthase and glutamate decarboxylase were connected via synthetic protein scaffold. As a result, 0.92 g/L of GABA was produced from 10g/L of glucose.

Considering the fact in previous reports that GABA production is higher under acidic conditions which is not favorable for bacterial growth, we proposed a new idea of introducing the protein resistant to pH conditions into *E. coli* system to maintain the production of GABA, with MSG as a carbon source. *Escherichia coli*-derived protein gene *ycgZ-ymgABC* and gene DR1558 extracted from the bacteria *Deinococcus radiodurans* were selected for constructing the recombined *E. coli* strains respectively.

### 3.2.3 *Escherichia coli*-derived protein gene *ycgZ-ymgABC*

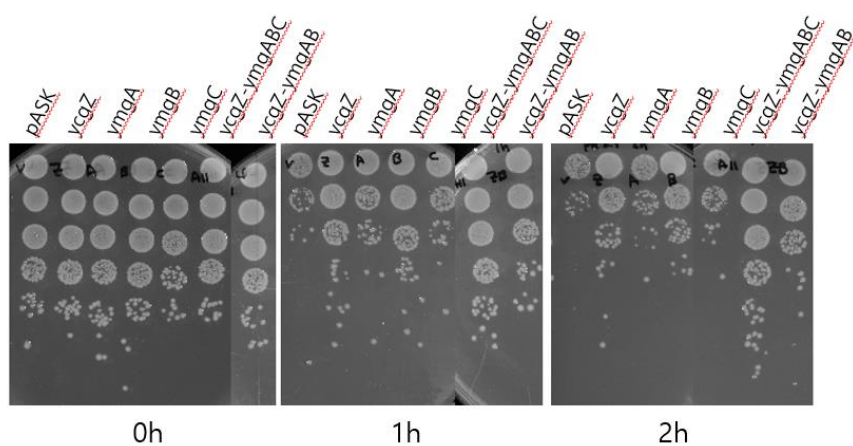


**Fig. 3.2** Acid tolerance of *ycgZ-ymgABC* and other genes in W3110 strain under acid stress of pH 2.5. Combined strains were inoculated into LB media (Amp), induced at OD=0.5 with 200ng/ml AHT. After 2h induction, cells were harvested, washed, and diluted to an equal OD=1.0. Tested under acid stress for 2h and processed serial dilution and spotting.

The present invention relates to *Escherichia coli*-derived transformants with tolerance to several environmental stresses (oxidation, acidity and heat) of micro-organisms, and uses thereof. More specifically, it relates to the production of microorganism strain with tolerance to oxidation, stress, acidity stress and heat stress of each transformants by transforming the recombinant plasmid vector including *Escherichia coli*-derived

protein genes such as *ycgZ-ymgABC* into *Escherichia coli*. The environmentally resistant microorganism strain produced by the present invention can be usefully used for food and industrial applications. Acid tolerance of *ycgZ-ymgABC* in W3110 strain under acid stress of pH 2.5 was showed in Fig. 3.2 [7]. Combined strains were inoculated into LB media (Amp), induced at OD=0.5 with 200ng/ml AHT. After 2h induction, cells were harvested, washed, and diluted to an equal OD=1.0. Tested under acid stress for 2h and processed serial dilution and spotting. The number of bacteria strains of genes *ycgZ-ymgABC* on the culture medium is obviously more than that of others, showing its superiority of enduring acidic environment.

#### **3.2.4 Gene DR1558 extracted from *Deinococcus radiodurans***

DR1558, a response regulator in the two-component signal transduction system, is extracted from the bacteria extremophilic bacterium *Deinococcus radiodurans*. By directly binding to the promoter regions of genes or binding to the effector molecules in response to environmental stress, DR1558 was reported to enhance cell robustness to help cells survive under harsh conditions including heat, salt, and acid conditions [8]. Appukuttan *et al.* studied production of succinate, 2,3-butanediol (2,3-BDO) and poly(3-hydroxybutyrate) [P(3HB)] by DR1558-engineered *E. coli* strains [9,10]. Taking the advantage of acid resistance, DR1558 may help *E. coli* in surviving under acidic condition.

In this study, *Escherichia coli* were engineered to produce gamma-aminobutyric acid from MSG by the introduction of acid tolerance synthetic scaffolds. The GABA production was functioned by succinate dehydrogenase in the Krebs cycle.

### **3.3 Materials and methods**

#### **3.3.1 Bacterial strains and growth conditions**

The *E. coli* strains and plasmids used in this study are listed in Table 3.1. *E. coli* XL1-Blue (XB) was used as the host strain. Chemically competent cells were prepared using

a standard procedure and were stored at -80°C until needed. All the strains were cultivated in Luria–Bertani medium (LB medium) (10 g/L bacto tryptone, 5 g/L bacto yeast extract, and 5 g/L NaCl), supplemented with ampicillin (50 mg/L) and 30 µg/mL of chloramphenicol sodium salt at 37 °C at 200 rpm overnight. Next, 100 mL of LB media supplemented 10 g/L MSG was inoculated with the overnight culture and cultured further at 30°C and 250 rpm. When the optical density at 600 nm (OD600) increased to 1.5-1.7. Samples were withdrawn and stored at -20°C for subsequent analysis.

**Table 3.1** List of bacterial strains and plasmids used in this study

Strain/plasmid	Relevant genotype/property	Source
<i>Escherichia coli</i>		
strain		
XL1-Blue	SupE44 hsdR17 recA1 endA1 gyrA96 thi relA1 lacF' (proAB+lacI <sup>q</sup> lacZΔM15 Tn10 (tet <sup>R</sup> ))	Laboratory stock
Plasmid		
pBAD 30	Ap <sup>R</sup>	NEB <sup>a</sup>
pET-21a	Ap <sup>R</sup>	NEB <sup>a</sup>
pH3BN	pMAL-p4X containing <i>N. crassa</i> <i>gadB-SH3D</i> and <i>E. coli</i> <i>gadC-SH3L</i> , C-terminal model	This work Laboratory
ycgZ-ymgABC	pET-21a containing <i>ycgZ-ymgABC</i> gene	stock
DR1558	pET-21a containing <i>DR1558</i> gene	Laboratory stock

<sup>a</sup> New England Biolabs, Beverly, MA, USA

### 3.3.2 Plasmid construction

*E. coli* gadC gene was amplified using the Expand high-fidelity polymerase chain reaction (PCR) system (Roche Molecular Biochemicals, Germany) from the genomic DNA of *E. coli*. The SH3 ligand gene was PCR amplified from the pJD758 plasmid (Laboratory stock). The SH3 ligand was attached to the C-terminus of the *E. coli* gadC gene to make gadCC-SH3L. The *E. coli* gadCC-SH3L gene was cloned into pHBD using BamHI and XbaI restriction sites to construct pH3BN expression plasmids [11]. This combined cell was used as the competent cell for next combined strain. Then DR1558 plasmid and ycgZ-ymgABC plasmid were cloned into pH3BN *E. coli* respectfully to construct pH3BN-DR1558 *E. coli* strain and pH3BN-ycgZ-ymgABC *E. coli* strain.

The size of gene DR1558 is 678bp, and the size of gene ycgZ-ymgZBC is 1208bp. The PCR product of DR1558 was cloned into the pBAD 30 plasmid, using SacI and XbaI restriction enzymes. The PCR primers used in this study are listed in Table 3.2. DR1558 peptide expression was induced after adding isopropyl b-D-1-thiogalactopyranoside (IPTG). These plasmids were transformed into pH3BN-XL1-Blue to be pH3BN-DR1558 *E. coli* strain for further studies.

The PCR product of ycgZ-ymgABC was cloned into the pET21a plasmid, using BamHI and SacI restriction enzymes. The PCR primers used in this study are listed in Table 3.2. ycgZ-ymgABC peptide expression was induced after adding isopropyl b-D-1-thiogalactopyranoside (IPTG). These plasmids were transformed into pH3BN-XL1-Blue to be pH3BN-ycgZ-ymgABC *E. coli* strain for further studies.

**Table 3.2** Primers used in this study

Name	Sequence (5'-3')
DR1558 peptide	5'- ATGACTCTGCCTCAAGGAGAATCTATGACCACCC



---

CCACTGTCCGTGTGCTGCTCGTTGACGACCACGC  
CGTCGTGCGCCAGGGTCTGCGCCTCTTTCTGGGG  
CTGGACGAAGGCATCGAAGTGGTGGGCGAGGCC  
GCCAACGGCGAAGAAGCCCTGCAAGAGGCCGAG  
CGCCTGCGCCCCGAAGTCGTCGTGATGGACCTGA  
TGATGCCGGTGATGGATGGCATTACCGCCACCCGT  
GAGCTGCGCCGCCCTGCCGACACCGAAGTC  
ATCGCGCTGACCTCCACCCTGGAAGAAAACAAG  
GTGAACGGCGCGATTGAGGCCGGGGCCATCTCGT  
ACATGCTCAAGGACGCCTCCAGCGACACCCTGGC  
CGACGCCATCCACGCGGGCGGCGCGGGCGAAGT  
GCGGCTGCATCCCGAAGCGGGCGGCGGGCTGGT  
GCGCGATTTCCGGTCGCCGGAGATGCGCGAGAGC  
CTGACCCCCAAGGAAACCGCCGTGCTGCAACTG  
CTGGCGCGCGGGCAGAGCAACAAGGACATCGCC  
GCCGAACAGGGCGTGAGCGAGGCGACGGTCAAG  
ACCCACGTGTCGCGGCTGCTGAGCAAGCTGGGG  
CTGGACAGCCGGACGCAGGCGGCGCTCTACGCC  
CTCAAATACGGGATTGCCAGTCTGGAGGGCGTGG  
AGTTGTGA-3'

ycgZ-ymgABC  
peptide

5'-  
ATGCATCAA AATTCAGTGACTTTAGATTCTGCGGG  
AGCAATCACTCGTTACTTTGCAA AAGCTAACTTG  
CATACTCAGCAGGAAACTCTCGGGGAAATTGTGA  
CTGAGATTTTGA AAGATGGACGTAATCTGAGTCG  
AAAGTCGCTTTGTGCCAAACTTCTTTGCCGACTG  
GAACACGCGACTGGGGAAGAGGAACAGAAACAT  
TATAATGCACTAATTGGGTTGCTTTTTGAATAATGC  
AACAGCCTGATTATTTAACAGGTTAGCTATGAAGT

CGTTATGAAGACATCTGATAATGAACGTATAAAAT  
ATGAAATTACTGGCCAGGCGGTGCTCCAGATACT  
GCGCATGAAGATAAATTTTTCATTGCAGACTCTTA  
TTAAGCAATTACTCGTAATGAAATCGGCTGAGGA  
AGATGCTTTCCGACGCGATTTAATTGACAGCATAA  
TTCGTGATTTTAGCAATAGTGATTCAGGAGGGCCA  
AACCGAAGAACAGCGACAGCTGACAATAAAAGT  
ATGTTCAATGGTAAGAAAATAAACAGAATACATTA  
AAATTCATAAGTAAGATGAGAGGTTACCATGCTT  
GAAGATACTACAATTCATAATGCAATAACTGATAA  
AGCGTTAGCAAGTTACTTTCGCAGTTCGGGTAATT  
TGTTAGAAGAAGAATCAGCAGTGTTAGGGCAGGC  
TGTCACCAATTTAATGCTTTCAGGCGATAATGTTA  
ATAATAAAAATATTATCTTAAGTCTGATACACTCCT  
TGGAAACAACAAGTGATATTCTCAAAGCTGATGT  
GATTAGAAAAACACTGGAAATCGTGTTGCGATAC  
ACAGCTGATGATATGTAACTTCTAATTATTAAGTAT  
AAGTTTATAGAAAACCTCATCTTATTTTTGTCT  
GTCGCTTTAGACTATACACAGCATAATTTTATTGG  
GTTAATATTTCTACGAGGCTGACATGAATAATTCA  
ATCCCAGAGAGATTTATTTTCAATGTGCTTTGTTT  
AAAAATCTCGAGAGGGAGGTGTTGATGACGCATG  
GGTATGTTGATAGTCATATTATTGATCAGGCTTTAC  
GCTTGCGTTTAAAAGATGAAACCAGTGTGATTCT  
TTCTGATCTCTATCTGCAAATATTGCAGTACATTGA  
AATGCATAAGACTACACTAACGGATATCATTATTA  
ATGACAGGGAATCCGTGCTCTCTTAG-3'

DR1558\_Frw

5' -CGGAGCTCATGACTCTGCCTCAAGGA-3'

DR1558\_Rev

5' -CGTCTAGATCACAACCTCCACGCCCTCCAG-3'

ycgZ-ymgABC	5'-
_Frw	ATATAT <b>GGATCC</b> ATGCATCAA <b>AATTC</b> AGTGACTTT AGATTCT-3'
ycgZ-ymgABC	5'-
_Rev	ATATAT <b>GAGCTC</b> CTAAGAGAGCACGGATTCCCTG TCATTAAT AAT-3'

---

\*Restriction enzyme sites are shown in bold.

### 3.3.3 Expression study by SDS-PAGE

The recombinant *E. coli* strains were cultured in 10 mL tubes with an antibiotic at 37 °C overnight and diluted 100-fold in a flask containing 250 mL of LB medium. When optical density at 600 nm (OD<sub>600</sub>) reached 0.6, IPTG was added to the culture broth. After 6 h of culture at 30 °C, the protein was isolated using B-7M urea buffer. The treated cells were analyzed by 12% (w/v) sodium dodecyl sulfate-polyacrylamide gel electrophoresis (SDS-PAGE). The fractionated protein samples were stained with Coomassie Brilliant Blue R-250 (Bio-Rad Laboratories, Hercules, CA, USA).

### 3.3.4 GABA analysis

GABA bioconversion was quantitatively analyzed by HPLC using an OptimaPak C18 column (4.6 × 150 mm, RS tech Corporation, Daejeon, Korea). Samples were centrifuged at 12,000 rpm for 5 min, and then 100 µL of the supernatant was added to an Eppendorf tube. Next, 200 µL of 1M sodium bicarbonate buffer pH 9.8, 100 µL of 80 g/L dansylchloride in acetonitrile and 600 µL of double-distilled water were added to make a 1 mL reaction mixture. The mixture was then incubated at 80°C for 40 min, after which 100 µL of 20 µL/mL acetic acid was added to stop the reaction. The mixture was centrifuged at 12,000 rpm for 5 min. The supernatant was then filtered through a 0.2 µm Millipore filter and analyzed by HPLC on an Agilent system using UV detection.

Separation of the derivatized samples was attained using a binary nonlinear gradient with eluent A [tetrahydrofuran/methanol/50 mM sodium acetate pH 6.2 (5:75:420, by vol.)] and eluent B (methanol).

The column temperature was set to 30°C. Elution conditions were as follows: equilibration (6 min, 20% B), gradient (20 min, 20 ~ 80% B) and cleaning (3 min, 100% B). The flow rate of the mobile phase was 1 mL/min, and detection of the samples was carried out at 286 nm. The standard curve for GABA was determined using the same procedure for eight standard solutions at 0.1, 0.2, 0.3, 1, 2, 3, 5, and 10 g/L GABA (Sigma, Missouri, USA).

### 3.4 Results and discussion

#### 3.4.1 Construction of acid-tolerance recombinant strain

*E. coli* gadC gene was amplified using the Expand high-fidelity polymerase chain reaction (PCR) system (Roche Molecular Biochemicals, Germany) from the genomic DNA of *E. coli*. The SH3 ligand gene was PCR amplified from the pJD758 plasmid (Laboratory stock). The SH3 ligand was attached to the C-terminus of the *E. coli* gadC gene to make gadCC-SH3L. The *E. coli* gadCC-SH3L gene was cloned into pHBD using BamHI and XbaI restriction sites to construct pH3BN expression plasmids. This combined cell was used as the competent cell for next combined strain. Then DR1558 plasmid and ycgZ-ymgABC plasmid were cloned into pH3BN respectfully to construct pH3BN-DR1558 *E. coli* strain and pH3BN-DR1558 *E. coli* strain.

Gene clean results of DR1558 (middle) and ycgZ-ymgABC (left and right) using different annealing temperatures are showed in Fig. 3.3. The DR1558–pesticide-binding peptide fusion protein was cloned into the pBAD 30 plasmid and expressed by the addition of the inducing agent IPTG. The ycgZ-ymgABC–pesticide-binding peptide fusion protein was cloned into the pET21a plasmid and expressed by the addition of the inducing agent IPTG. The findings showed that the fusion protein was successfully expressed, as revealed by SDS-PAGE (Fig.2.3).



**Fig. 3.3** Gene clean of DR1558 (middle) and *ycgZ-ymgABC* (left and right).

### 3.4.2 Optimization of GABA production

GABA production under various pH were tested. The recombinant XB strains were incubated at 0.1, 0.5, and 1 mM of IPTG at pH 2.5 to test the effect of IPTG concentration. The recombinant XB strains were cultured at pH 2.5, 3.5, 4.5, 5.5 and 6.5 with 0.5 mM of IPTG at 30°C to examine the effect of pH. The OD600 of the cultures were measured at the time of sample withdrawal. At least three measurements were obtained for each sample.

Production of total GABA concentration after 30h of cultivation, under various conditions of IPTG and pH with DR1558 or *ycgZ-ymgABC* scaffold architecture are showed in Fig. 3.4. The data showed production of 0.62 g/L GABA was achieved at 30°C and pH 2 by introduction of peptide DR1558, and production of 1.22 g/L GABA was achieved at 30°C and pH 2 by introduction of peptide *ycgZ-ymgABC*. Final GABA concentration was increased by 11.3% via the inactivation of competing pathways at initial MSG concentration of 10g/L.

Both of DR1558 combined strain and *ycgZ-ymgABC* combined strain produced higher GABA yields under relatively lower pH conditions, showing that the introduction of acid-tolerance peptides can help increase GABA production. This provided a preliminary experimental basis for subsequent industrialized large-scale production.

However, GABA production began to decrease after 6 hours, which may be related to the increase of pH in the culture medium over time, which also shows that two scaffolds are sensitive to pH increase.

From the perspective of the highest yield and trend line, ycgZ-ymgABC (1.22 g/L) combined strain is better than DR1558 (0.62 g/L) combined strain between these two scaffolds. Compared with other research which improved GABA production by optimizing metabolic pathways [12], the GABA yield of both combined strains reached a similar or higher level which higher than 0.6 g/L.

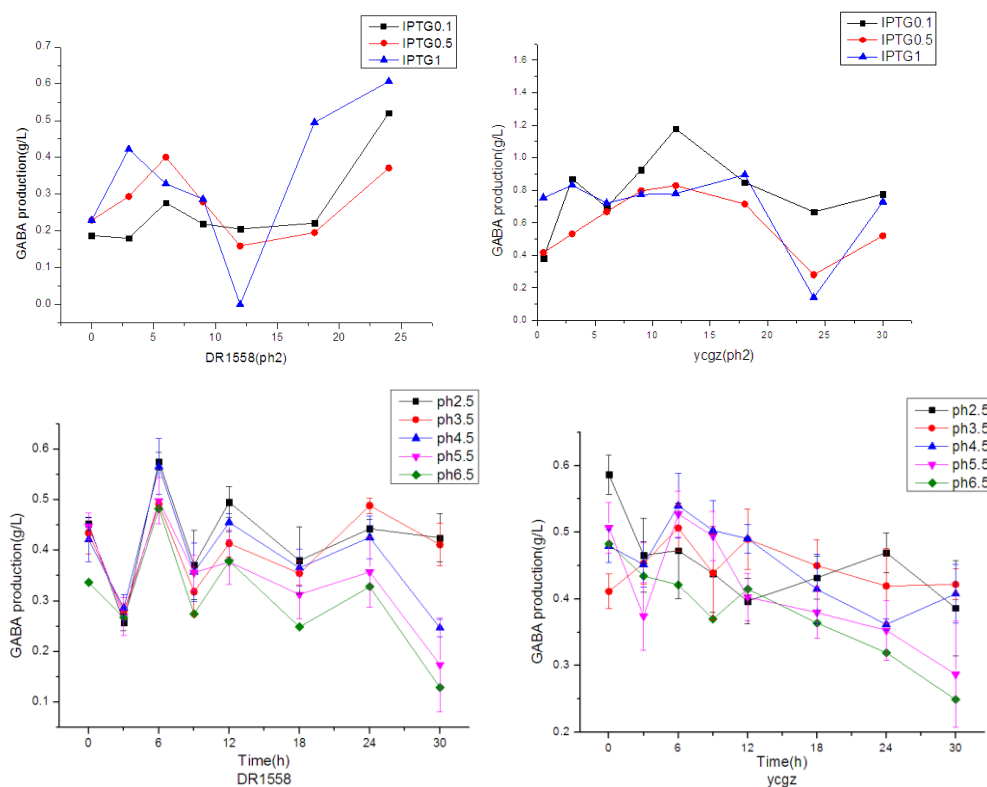


**Fig. 3.4** Production of total GABA concentration after 30h of cultivation, under various conditions such as: (A)(B) IPTG and (C)(D) pH with DR1558 or ycgZ-ymgABC scaffold architecture.

### 3.5 Conclusions

In this study, *Escherichia coli* were engineered to produce gamma-aminobutyric acid from MSG by the introduction of acid tolerance synthetic scaffolds of peptide DR1558

and peptide ycgZ-ymgABC. The data showed production of 0.62 g/L GABA was achieved by introduction of peptide DR1558, and production of 1.22 g/L GABA was achieved by introduction of peptide ycgZ-ymgABC. Final GABA concentration was increased by 11.3% via the inactivation of competing pathways at initial MSG concentration of 10g/L. Both of DR1558 combined strain and ycgZ-ymgABC combined strain produced higher GBAB yields under relatively lower pH conditions, showing that the introduction of acid-tolerance peptides can help increase GABA production. However, conditions including temperature and initial MSG concentration need to be further optimized to achieve better GABA output.

### 3.6 References

- [1] Vo TD, Kim TW, Hong SH. (2012). Effects of glutamate decarboxylase and gamma aminobutyric acid (GABA) transporter on the bioconversion of GABA in engineered *Escherichia coli*. *Bioprocess Biosyst. Eng.* 35: 645-650.
- [2] Hao R, Schmit, JC. (1993) Cloning of gene for glutamate decarboxylase and its expression during condition in *Neurospora crassa*. *Biochem. J.* 293: 735-738.
- [3] Vo TD, Ko JS, Lee SH, Park SJ, Hong SH (2013) Overexpression of *Neurospora crassa* OR74A Glutamate Decarboxylase in *Escherichia coli* for Efficient GABA production. *Biotechnol. Bioprocess Eng.* 18: 1062-1066.
- [4] Dueber JE, Wu GC, Malmirchegini GR, Moon TS, Petzold CJ, Ullal AV, Prather KLJ, Keasling JD (2009) Synthetic protein scaffolds provide modular control over metabolic flux. *Nat. Biotechnol.* 27: 753–759.
- [5] Baek JM, Mazumdar S, Lee SW, Jung MY, Lim JH, Seo SW, Jung GY, Oh MK (2013) Butyrate production in engineered *Escherichia coli* with synthetic scaffolds. *Biotechnol. Bioeng.* 110: 2790-2794.
- [6] Van Dung Pham, Seung Hwan Lee, Si Jae Park, Soon Ho Hong (2015) Production of gamma-aminobutyric acid from glucose by introduction of synthetic scaffolds between isocitrate dehydrogenase, glutamate synthase and glutamate decarboxylase in recombinant *Escherichia coli*. *Journal of Biotechnology* 207: 52–57.
- [7] Lim, Sang Yong; Kim, Dong Ho; Seo, Ho Seong (2018) Development of recombinant micro-organisms with resistance to environmental stress. Korean Patent KR 1818181.
- [8] Appukuttan D, Singh H, Park S-H, Jung J-H, Jeong S, Seo HS, Choi YJ, Lim S (2016) Engineering synthetic multistress tolerance in *Escherichia coli* by using a deinococcal response regulator, DR1558. *Appl Environ Microbiol.* 82:1154–1166.
- [9] Guo S, Yi X, Zhang W, Wu M, Xin F, Dong W, Zhang M, Ma J, Wu H, Jiang M (2017) Inducing hyperosmotic stress resistance in succinate-producing *Escherichia coli* by using the response regulator DR1558 from *Deinococcus radiodurans*. *Process Biochem.* 61: 30–7.



- [10] Park S-h, Kim GB, Kim HU, Park SJ, Choi J-I (2019) Enhanced production of poly-3-hydroxybutyrate (PHB) by expression of response regulator DR1558 in recombinant *Escherichia coli*. *Int J Biol Macromol.* 131: 29–35.
- [11] Sivachandiran Somasundaram, Murali Kannan Maruthamuthu, Irisappan Ganesh, Gyeong Tae Eom, and Soon Ho Hong (2017) Enhancement of Gamma-Aminobutyric Acid Production by Co-Localization of *Neurospora crassa* OR74A Glutamate Decarboxylase with *Escherichia coli* GABA Transporter Via Synthetic Scaffold Complex. *J. Microbiol. Biotechnol.* 27: 1664–1669.
- [12] Van Dung Pham, Sivachandiran Somasundaram, Seung Hwan Lee, Si Jae Park, and Soon Ho Hong (2016). Gamma-aminobutyric Acid Production through GABA Shunt by Synthetic Scaffolds Introduction in Recombinant *Escherichia coli*. *Biotechnology and Bioprocess Engineering.* 21: 261-267.

## Chapter 4

### Design, synthesis and antiproliferative activity of chiral 1, 4-disubstituted-3,4-dihydroquinazolin-2(*IH*)-one derivatives against common human cancer cell lines

#### 4.1 Abstract

Quinazolinone structures have been studied due to their biological activities against cancer. Herein a series of novel chiral 1, 4-disubstituted-3,4-dihydroquinazolin-2(*IH*)-one derivatives were synthesized with (*S*)-(-)-*tert*-butylsulfonamide as chiral inducer. In vitro antitumor activity was evaluated on 3 tumor cell lines using the 3-(4, 5-dimethylthiazol-2-yl)-2, 5-diphenyl tetrazolium bromide (MTT) assay, including lung cancer cell A549, leukemia cell K562 and glioma cell U251. Cell toxicity was tested with human hepatocyte cell line L02. Among these synthesized quinazolinone derivatives, (S)-6-chloro-1-(cyclopropylmethyl)-4-(2-fluorophenyl)-3,4-dihydroquinazolin 2(*IH*)-one (**12d**) possessed more optimal antiproliferative activity than others with IC<sub>50</sub> values lower than 30 μM. As for tested cell lines, better inhibition effect was implied on lung cancer cell A549.

#### 4.2 Introduction

Quinazolinones and their derivatives are widely used in the field of medicine due to their structural variability and broad-spectrum biological activities. The derivatives with different substituent at 3-position and 4-position respectively (Fig. 4.1, compound **1**) were reported to be good Na<sup>+</sup>/Ca<sup>2+</sup> ion exchange inhibitors, which is related to the management of ischemic heart disease [1-3]. The derivatives with structure of 3, 4 substituted-2(*IH*)-quinazoline (Fig. 4.1, compound **2**) were showed anticoccidial activity [4] and inhibition function for HIV infection [5]. As far as we know, no 1, 4-disubstituted-dihydroquinazolin derivatives were explored for antitumor activity. In this paper, 1, 4-disubstituted-3, 4- dihydroquinazolin-2(*IH*)-one directives with skeleton of compound **3** (Fig. 4.1) were synthesized through simple and efficient methods. The difference in anticancer ability due to different chiral structure was

also discussed. What's more, we explored antiproliferative potential of these new compounds in three kinds of common human tumor cell lines, including lung cancer cell A549, leukemia cell K562, and glioma cell U251.

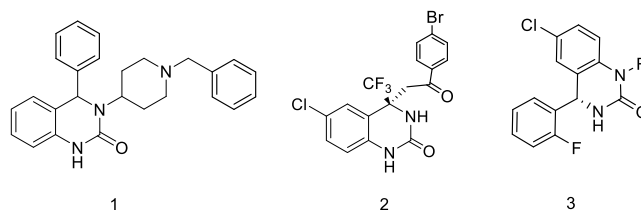


**Fig. 4.1** Quinazolinone derivatives with biological activity in previous studies.

## 4.3 Materials and methods

### 4.3.1 Synthesis and substance testing methods

All commercially available reagents were used without purification unless otherwise noted. Column chromatography was performed using silica gel (200 - 300 mesh). Reactions were magnetically stirred and monitored by NMR spectroscopy or analytical thin-layer chromatography (TLC). TLC plates were visualized by exposure to ultraviolet light (UV, 254 nm) and/or exposure to iodine.  $^1\text{H}$  NMR and  $^{13}\text{C}$  NMR spectra were recorded in  $\text{CDCl}_3$  operating at 400 MHz and 100 MHz, respectively. Proton chemical shifts are reported relative to the residual proton signals of the deuterated solvent  $\text{CDCl}_3$  (7.28 ppm) or TMS. Carbon chemical shifts were internally referenced to the deuterated solvent signals in  $\text{CDCl}_3$  (77.10 ppm). Chemical shifts are reported in  $\delta$  (parts per million) values. Coupling constants  $J$  are reported in Hz. Proton coupling patterns were described as singlet (s), doublet (d), triplet (t), quartet (q), and multiple (m). High-resolution mass spectra were recorded on a Liquid Chromatograph Mass Spectrometer (LCMS - IT - TOF).

### **4.3.2 Cell culture assays and MTT assay**

The K562, A549, U251 and L02 cell lines were grown in RPMI 1640 media (Gibco). Cells at the density of  $5 \times 10^3$  cells/well were seeded into 96-well plates at 37 °C with 5% CO<sub>2</sub> in humidified air. Immortalized human hepatocyte cell line L02 were processed with prepared derivatives and Melphalan in concentration of 20 μM in DMSO for 20, 40, and 80 h.

### **4.3.3 In vitro antitumor activity and cytotoxicity assays [6]**

The viability of cells was determined using an MTT assay. K562, A549, U251 and L02 cells in log-phase were seeded ( $3.5 \times 10^3$  cells per well) in 96-well plates and incubated for 24h at 37 °C. The cells were then treated with 200 μL of the media within various concentrations of the prepared compounds and Melphalan and incubated for 48h in medium. The working concentration of DMSO did not exceed 1%. After incubation for 48h, 5 mg/mL MTT solution (20 μL/well) was added to each well and incubated for a further 4h at 37 °C. The medium in each well was discarded and then DMSO (120 μL) was added respectively. Untreated cells were taken as a control with 100% viability and cells without addition of MTT were used as blank to calibrate the spectrophotometer to zero absorbance. The absorbance at 570 nm was measured using a microplate reader (EL800, BIO-TEK Instruments Inc., USA). IC<sub>50</sub> value for each compound was determined from a dose–response curve that was generated by using nonlinear regression in GraphPad Prism 5 software. All data are average values from triplicate samples, and the experiments were repeated at least twice.

### **4.3.4 Molecular docking**

The crystal structures of oncogenic tyrosine phosphatase SHP2 structures (PDB ID: 3O5X), human epidermal growth factor receptor-2, HER2 (PDB ID: 5MY6), epidermal growth factor receptor (PDB ID: 6DUK), human CC Chemokine

Receptor 7 (PDB ID: 6QZH) were downloaded from the Protein Data Bank PDB. Protein preparation was done using Schrödinger's Protein Preparation Wizard by adding hydrogen atoms, assigning protonation states and minimizing the protein. Ligands were prepared in MOE from smiles in the neutral form. Docking was processed into the catalytic site to sample possible binding geometries<sup>18-21</sup> using the software package Schrödinger's Protein Preparation Wizard.

## 4.4 Results and discussion

### 4.4.1 Synthesis of products

Through simple and efficient methods, new chiral 1, 4-disubstituted-3, 4-dihydroquinazolin-2(*1H*)-one derivatives were synthesized with extended substituent modification. The synthetic routes are shown in Fig. 4.2. Compound **4** reacts with halogenated benzene ring compound to produce compound **5** through Grignard reaction. Compound **5** reacts with PCC and undergoes oxidation to produce compound **6**. Compound **6** reacts with iron powder for one hour and then hydrochloric acid is added to produce compound **7**. For compound **8**, we performed the reaction using Tetraethyl Titanium in THF with microwave irradiation and maintained the reaction temperature at 118°C in a pressurized microwave reaction tube. It is faster and the yield is higher compared with traditional method [7]. Reduction of the sulfinimide is realized through diisobutylaluminium hydride DIBAL-H next, in which a chiral diamine in excellent yield and enantiomeric excess was induced with (*S*)-(-)-*tert*-butylsulfonamide as a chiral inducer according to a previous study [8]. Enantiomeric excess of chiral diamine was characterized representatively. The resulting **12** was determined to be higher than 95% ee value using chiral reagent. After removing sulfinyl group by HCl/MeOH, additional (identical) N-substitutions can be introduced to the free amine of **10** to generate compound **11**. Next, reaction of

aniline with ketone and sodium triacetoxyborohydride [9] is applied for construction of C-N bonds, which is alkyl chain substitution of the amine. The reactions performed under moderate temperatures and short reaction time conditions, which simplify reaction process. Compound **11** is unstable and was purified by column chromatography quickly. Triethylamine was then added followed by treatment with *Bis* (trichloromethyl) carbonate to form directly cyclized products **12**. In this step, CDI was also applied; by which field was significantly lower than that of *Bis* (trichloromethyl) carbonate yet [10]. All seven new compounds are listed in Fig. 4.3. Synthesis details and spectrums are listed in Supplementary Information (SI).

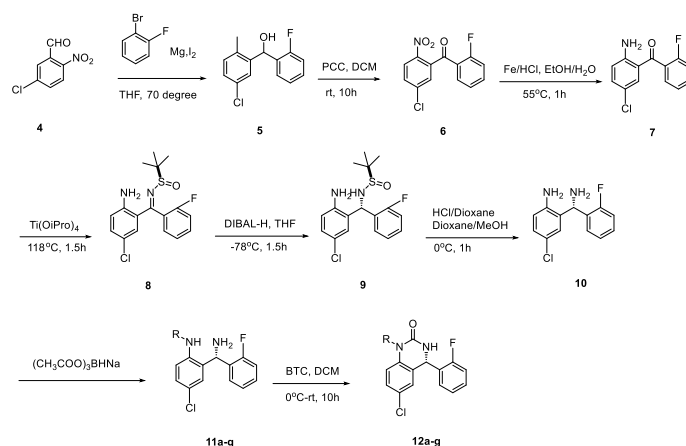


**Fig. 4.2** Synthetic routes of chiral 1, 4-disubstituted-3, 4- dihydroquinazolin-2(1H)-one.

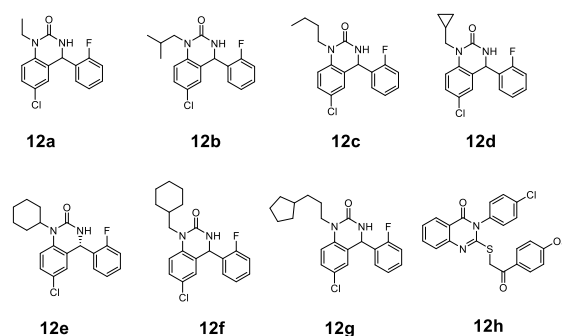


**Fig. 4.3** Structures of 7 synthetic compounds, as well as one known quinazolines derivative **12h** with antitumor activity in Table 4.1.

#### 4.4.2 Antitumor activities towards three kinds of tumor cells

Antitumor activities towards three kinds of tumor cells were investigated, including lung cancer cell A549, leukemia cell K562 and glioma cell U251. The response parameter  $IC_{50}$  was calculated for each cell line, using the known drug Melphalan as a positive control [11]. Cells in well containing only phosphate buffer saline and DMSO at identical dilutions were also prepared in the same manner as blank control. The immortalized human hepatocyte cell line L02 was used for cell cytotoxicity test.

Previous study showed that compounds with R of alkyl substituent possessed good tumor cell validity among the first 10 compounds (Fig. 4.4), so we designed and synthesized another 7 compounds and examined with the same process.

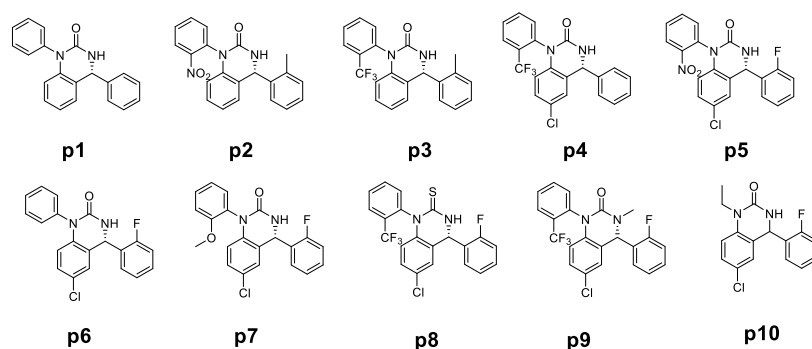


**Fig. 4.4** 10 compounds were synthesized in previous study. It showed that compounds with R of alkyl substituent (compound **p10**) possessed best tumor cell validity.

Table 4.1 shows half maximal inhibitory concentrations ( $IC_{50}$ ,  $\mu M$ ) in vitro tumor cell lines and L02 of 8 compounds. Among these compounds, compound **12d** showed a broad spectrum of antitumor activity and are more effective than other compounds. Compound **12d** (S)-6-chloro-1-(cyclopropylmethyl)-4-(2-fluorophenyl)-3,4-dihydroquinazolin 2(1H)-one containing R substituent of cyclopropylmethyl exhibited best anticancer activity against 3 tumor cell lines, with  $IC_{50}$  values of 5.9  $\mu M$  against A549, 12.3  $\mu M$  against K562, 14.4  $\mu M$  against U251. The presence of nitrogen heterocyclic at position R implied effect for activity rather than the benzene ring substituent. Compared with compounds in Fig. 4.4, ester substituents at R position

promotes antitumor activity than aryl substituents. And as for three cell lines, the skeleton analogue synthesized here possesses the best inhibitory effect on lung cancer cell A549. The IC<sub>50</sub> value higher than 100 μM showed that tested compounds displayed no obvious cytotoxicity against L02 cell line. As far as we know, no other quinazolinone derivatives was explored for antitumor activity, but some 3-substituted-4(3*H*)-quinazolines derivatives were evaluated as antitumor agents in previous study [12], we synthesized one of those compounds, compound 3-(4-Methoxyphenyl)-2-[2-(4-methoxyphenyl)-2-oxo-ethylthio] quinazolin-4(3*H*)-one (**12h**) (Fig. 4.3) for comparison. The results showed that 1, 4-disubstituted-3, 4-dihydro-2(3*H*)-quinazolinone compounds herein are of similar level in terms of antitumor activity (Table 4.1). Compared with known drugs Melphalan (15-40 μM), compound **12d** (5-15 μM) showed better antitumor effect.

**Table 4.1** Half maximal inhibitory concentrations (IC<sub>50</sub>, μM) in vitro tumor cell lines and L02 of 8 compounds.

Compound	Substituent R	Cell line/ IC <sub>50</sub> (μM)			
		A549	K562	U251	L02
12a	Ethyl	62.6±1.5	49.6±2.1	50.2±1.7	152.3±6.5
12b	<i>i</i> -Bu	-	52.0±0.9	51.9±2.0	144.5±7.5
12c	3-Methylbutyl	21.1±1.9	47.9±1.0	51.8±4.7	130.2±3.6
12d	Cyclopropylmethyl	5.9±0.4	12.3±2.6	14.4±1.1	140.5±3.1
12e	Cyclohexyl	21.5±0.7	62.5±2.2	55.7±2.9	129.6±6.3
12f	Cyclohexylmethyl	61.2±1.2	41.5±0.7	54.1±3.1	141.1±1.9
12g	3-Cyclopentylpropyl	30.9±1.5	60.0±4.4	59.3±3.1	160.1±3.5
12h <sup>a</sup>		>100	>100	16.2±1.9	145.7±1.7
Melphalan		37.9±3.1	25.1±2.	19.4±5.0	172.1±2.9

-, precipitated;

a, reference [12]



### 4.4.3 Molecular docking studies

In order to rationalize the experimental biological data all the prepared compounds were docked to 4 different enzymes, oncogenic tyrosine phosphatase SHP2 structures (PDB ID: 3O5X), human epidermal growth factor receptor-2, HER2 structures (PDB ID: 5MY6), epidermal growth factor receptor structures (PDB ID: 6DUK) and retinoic acid receptor related orphan C (RORC) (PDB ID: 4WPF) respectively, which are proved to be closely related to cancer incentives. Through comparison, we found that the final docking scores of compounds with oncogenic tyrosine phosphatase SHP2 (PDB ID: 3O5X) is roughly consistent with actual cell inhibition experiment (data not shown). The compound **12d** with best docking effect are shown in fig. 4.5.

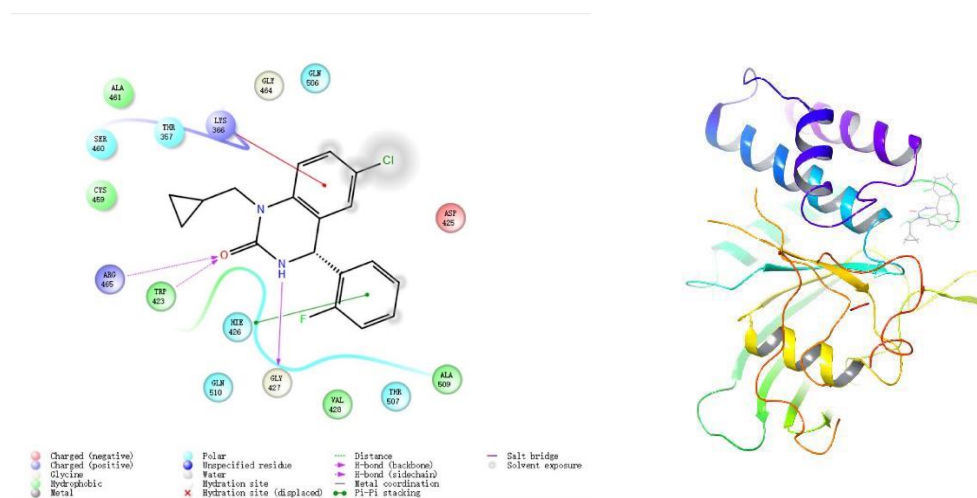


**Fig. 4.5** (A) Schematic depiction of the compound **12d** within the binding pocket. Pink arrows denote hydrogen-bonding to backbone (solid lines) or side chains (dotted), while straight line (green) represents  $\pi$ -stacking interactions, and straight line (red) represents salt bridge; (B) Compound **12d** in oncogenic tyrosine phosphatase SHP2 in the crystal structure

To investigate the possible binding mode, all of the compounds were employed to dock into the binding site of 20 Å sphere around position (31, 10, 3.51, 6.29), and a hydrogen bond to N1547 of Arg465. The detailed two- and three-dimensional binding modes of it in this binding site at an atomic level were revealed by conformation clustering analysis. **12d** consists of a chlorine atom and an O-fluorobenzene substituent. The O-fluorobenzene substituent of **12d** is surrounded by Ala509, Thr507, Val428, Gly427 and Hie426 of oncogenic tyrosine phosphatase SHP2, suggesting that compound **12d** forms  $\pi$ -stacking interactions with surrounding residues. The double bond oxygen interacts with Arg465 and Trp423 by hydrogen-bonding, while the substituent of benzene ring interacts with Lys366 by salt bridge. What's in common, the tertiary ammonia on Imidazole scaffold interacts with Gly427 by hydrogen-bonding in all derivatives. The docking poses derived for the individual isoforms show good agreement with the biological data. But the derivatives are only bound at the edge of the protein rather than the middle according to the relative position in 3D figure.

#### 4.5 Conclusions

Herein a series of novel chiral 1, 4-disubstituted-3,4-dihydroquinazolin-2(*IH*)-one derivatives were synthesized through 8-step route with (*S*)-(-)-*tert*-butylsulfonamide as chiral inducer. In vitro antitumor activity was evaluated on 3 tumor cell lines including lung cancer cell A549, leukemia cell K562 and glioma cell U251 using MTT assay. Among these compounds, compound **12d** (*S*)-6-chloro-1-(cyclopropylmethyl)-4-(2-fluorophenyl)-3,4-dihydroquinazolin 2(*IH*)-one containing R substituent of cyclopropylmethyl exhibited best anticancer activity against 3 tumor cell lines, with IC<sub>50</sub> values of 5.9  $\mu$ M against A549, 12.3  $\mu$ M against K562, 14.4  $\mu$ M against U251. Molecular docking studies suggested that compound **12d** forms  $\pi$ -stacking interactions with surrounding Ala509, Thr507, Val428, Gly427 and Hie426 of oncogenic tyrosine phosphatase SHP2. The double bond oxygen interacts with

Arg465 and Trp423 by hydrogen-bonding, while the substituent of benzene ring interacts with Lys366 by salt bridge.

## 4.6 References

- [1] Hasegawa H, Muraoka M, Matsui K, Kojima A (2003) Pharmaceutical prospects of naturally occurring quinazolinone and its derivatives. *Bioorg Med Chem Lett* 13: 3471-3475.
- [2] Hasegawa H, Muraoka M, Ohmori M, Matsui K, Kojima A (2005) A Novel Class of Sodium/calcium Exchanger Inhibitor: Design, Synthesis, and Structure-Activity Relationships of 3,4-Dihydro-2(1H)-Quinazolinone Derivatives. *Bioorg Med Chem* 13: 3721-3735.
- [3] Hasegawa H, Muraoka M, Matsui K, Kojima A (2006) A novel class of sodium/calcium exchanger inhibitors: Design, synthesis, and structure–activity relationships of 4-phenyl-3-(piperidin-4-yl)-3,4-dihydro-2(1H)-quinazolinone derivatives. *Bioorg Med Chem Lett* 16: 727-730.
- [4] Wang Y, You J, Ye C, Zhu J, Liu J (2008) Quinazoline ketone anticoccidial medicament. CN Patent CN101255138A, filed April 17, 2008, issued September 3, 2008.
- [5] Jiang B, Dong J (2006) 4,4-disubstituted-3,4-dihydro-2(1H)-quinolones and synthesis process and use thereof. CN Patent CN1827605A, filed April 7, 2006, issued September 6, 2006.
- [6] Guo Q, Luo Y, Zhai S, Jiang Z, Zhao C, Xu J, Wang L (2019) Discovery, biological evaluation, structure–activity relationships and mechanism of action of pyrazolo[3,4-b]pyridin-6-one derivatives as a new class of anticancer agents. *Org Biomol Chem* 17: 6201-6214.
- [7] Robak MT, Herbage MA, Ellman JA (2010) Synthesis and Applications of tert-Butanesulfinamide. *Chem Rev* 110: 3600-3740.
- [8] Huang L, Cao Y, Zhao M, Tang Z, Sun ZH (2014) Asymmetric borylation of  $\alpha,\beta$ -unsaturated esters catalyzed by novel ring expanded N-heterocyclic carbenes based on chiral 3,4-dihydro-quinazolinium compounds. *Org Biomol Chem* 12: 6554-6556.

- [9] Li Y, Zhang S, Zhang J, Hu Z, Xiao Y, Huang J, Dong C, Huang S, Zhou H (2019) Exploring the PROTAC degron candidates: OBHSA with different side chains as novel selective estrogen receptor degraders (SERDs). *Eur J Med Chem* 172: 48-61.
- [10] Seitz W, Geneste H, Backfisch G, Delzer J, Graef C, Hornberger W, Kling A, Subkowski T, Zimmermann N (2008) Design and synthesis of novel potent and selective integrin  $\alpha\text{v}\beta\text{3}$  antagonists—Novel synthetic routes to isoquinolinone, benzoxazinone, and quinazolinone acetates. *Bioorg Med Chem Lett* 18: 527-531.
- [11] Al-Rashood ST, Aboldaha IA, Nagi MN, Abouzeid LA, Abdel-Aziz AAM, Abdelhamide SG, Youssef KM, Al-Obaid AM, El-Subbagh HI (2006) Synthesis, dihydrofolate reductase inhibition, antitumor testing, and molecular modeling study of some new 4(3H)-quinazolinone analogs. *Bioorg Med Chem* 14: 8608-8621.
- [12] Gawad NMA, Georgey HH, Youssef RM, El-Sayed NA (2010) Synthesis and antitumor activity of some 2,3-disubstituted quinazolin-4(3H)-ones and 4,6-disubstituted-1,2,3,4-tetrahydro-quinazolin-2H-ones. *Eur J Med Chem* 45: 6058-6067.

## **Chapter 5**

### **Synthesis of phenylpropionate compounds and their potential antiproliferative activities.**

#### **5.1 Abstract**

L-Phenylalanine is one of the essential amino acids. The isothioureia moiety is an important feature present in many small molecules used in chemical and biological applications, such as approved drugs, potent inhibitors of biological targets/pathways and cancer inhibitor.

In this chapter, several high-docking scores compounds were selected. Active molecules of isothioureia with phenylalanine group were successfully synthesized. A multicomponent protocol that involves electrophilic center and isocyanide is proved to be suitable for the formation of these and other important isothioureia compounds, including an anti-gout drug and CXCR4 antibody. The advantages of mild reaction conditions, reduced purification steps, and ease of starting material accessibility is a useful addition to existing methodologies. Considering the seemingly unlimited functional versatility of natural and unnatural amino acids, our derivatives as chiral building blocks and molecular scaffolds can be promising in constructing peptidic drugs in biomedical applications.

#### **5.2 Introduction**

The process of synthesizing the compounds in Chapter 3 and conducting cell tests took one year, but the value of the compounds was only moderate. In order to shorten the working time and improve the value of the compounds, we decided to screen the compounds from the laboratory compound library through computer aided drug design first, then select the ones with high simulated activity from the results for actual synthesis and cancer cell activity test. Computer-aided drug design is a method of designing and optimizing lead compounds through computer simulation, calculation and budgeting of the relationship between drugs and receptor biomacromolecules.

L-Phenylalanine (Fig. 5.1 left) is one of the essential amino acids, catalyzed by phenylalanine hydroxylase to form important neurotransmitters and hormones together with tyrosine, and participate in the body's sugar metabolism and fat metabolism. Metabolic abnormalities of phenylalanine can cause mental retardation phenylketonuria (PKU) and liver cancer [1]. In the pharmaceutical industry, phenylalanine is an intermediate of certain amino acid drugs for the treatment of cancer. It can also be used for treatment for chronic pain resulted from rheumatoid arthritis, muscle pain and osteoporosis. Wu et al. found that L-phenylalanine functionalized Nano-PAAM (Nano-pPAAM) can be used as a novel nanotherapeutics with excellent intrinsic anticancer and cancer-selective properties [2]. Jaskółka et al. described the antiproliferative effects of l-phenylalanines  $\alpha$ -derivatized with a terminal alkyne moiety [3]. Su et al. disclosed that diblock copolypeptides based on lysine and phenylalanine have had a similar antibacterial pore-forming mechanism to natural cationic peptides and high selectivity to bacteria, which can be excellent candidates to replace traditional antibiotics [4].

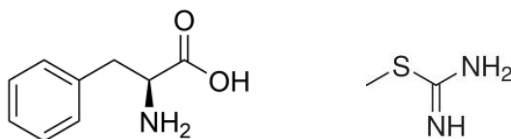


**Fig. 5.1** Molecular structures of L-Phenylalanine (left) and isothioureas (right).

The isothiourea moiety (Fig. 5.1 right) is an important feature present in many small molecules used in chemical and biological applications, such as approved drugs [5], potent inhibitors of biological targets/pathways [6] and cancer inhibitor [7]. While synthetic procedures for a standard isothiourea with open loop structure such as that present in compound **c** are straightforward, synthesis of some heterocyclic compounds such as those S-alkyl or S-aryl sulfanyl substituted [1,2,4] triazoles with fused rings found in compounds **a**, **b**, or **c** can be a challenge. In the past two years, our lab has developed some new compounds based on the structure of isothiourea, and found that the direct connection between N, S and C is achievable. We thought that if the three parts with different functional groups (compound **d** in Fig. 5.2) can be formed

respectively first and spliced together in a simple way next, the reaction steps will be greatly simplified. In this regard, we developed a new methodology and aimed to develop a synthetic methodology based on a multicomponent reaction of isocyanides with an electrophilic sulfur center and a broad range of nucleophiles. Synthesis of compound **a** and compound **c** in Fig. 5.2 have been realized through our synthetic methodology, the reaction paths are showed in Fig. 5.4.

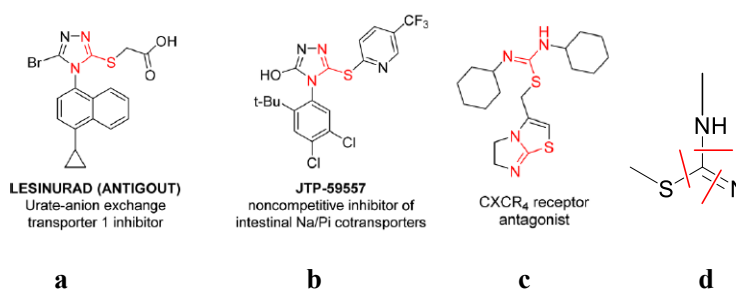


**Fig. 5.2** Structures of Lesinurad (a), JTP-59557 (b), CXCR<sub>4</sub> (c) and resolution of isothiurea structure synthesis (d).

## 5.3 Materials and methods

### 5.3.1 Synthesis and substance testing methods

All commercially available reagents were used without purification unless otherwise noted. Column chromatography was performed using silica gel (200 - 300 mesh). Reactions were magnetically stirred and monitored by NMR spectroscopy or analytical thin-layer chromatography (TLC). TLC plates were visualized by exposure to ultraviolet light (UV, 254 nm) and/or exposure to iodine. <sup>1</sup>H NMR and <sup>13</sup>C NMR spectra were recorded in CDCl<sub>3</sub> operating at 400 MHz and 100 MHz, respectively. Proton chemical shifts are reported relative to the residual proton signals of the deuterated solvent CDCl<sub>3</sub> (7.28 ppm) or TMS. Carbon chemical shifts were internally referenced to the deuterated solvent signals in CDCl<sub>3</sub> (77.10 ppm). Chemical shifts are reported in δ (parts per million)



values. Coupling constants J are reported in Hz. Proton coupling patterns were described as singlet (s), doublet (d), triplet (t), quartet (q), and multiple (m). High-resolution mass spectra were recorded on a Liquid Chromatograph Mass Spectrometer (LCMS - IT - TOF).

### 5.3.2 Molecular docking studies

Eight reported receptor proteins on the surface of cancer cells were selected, including CXC chemokine receptor 4 (CXCR4) (PDB ID: 3ODU), P38 mitogen-activated protein kinase  $\alpha/\beta$  (PDB ID: 2YIS), retinoic acid receptor related orphan C (RORC) (PDB ID: 4WPF), Epidermal growth factor receptor (EGFR) (PDB ID: 6DUK), Epidermal growth factor receptor-2 (HER2) (PDB ID: 5MY6), Human C-C chemokine receptor type (CCR-7) (PDB ID: 6QZH) and Oncogenic tyrosine phosphatase SHP2 (PDB ID: 3O5X). The target protein crystal information found in the Protein Data Bank (PDB) (the ligands were deleted manually) were imported into Discovery studio<sup>TM</sup> (DS) for small molecule-protein docking simulation and score. More than 100 small molecule compounds were designed related to S-N triangle structure possessing anticancer pharmacodynamic groups, such as trifluoromethyl (-CF<sub>3</sub>), sulfanilamide group (-SO<sub>2</sub>NH<sub>2</sub>) and indole et al. One reported tumor inhibitor compound **10** was used for docking as a reference [8] (Table 5.1), which is valuable for subsequent tumor cell viability test.

## 5.4 Results and discussion

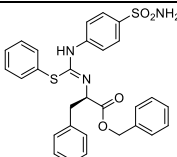
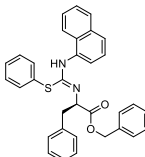
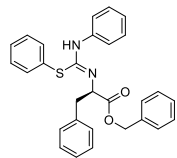
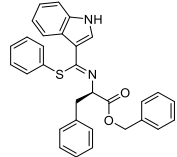
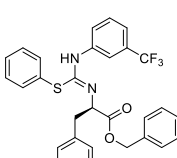
### 5.4.1 Molecular docking studies

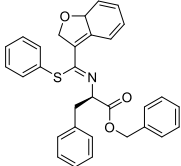
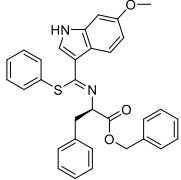
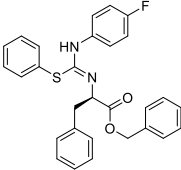
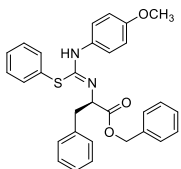
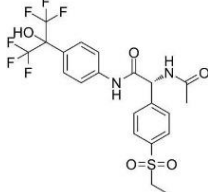
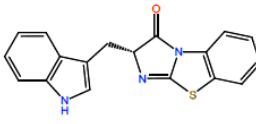
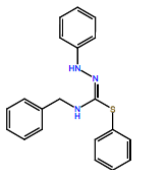
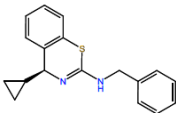
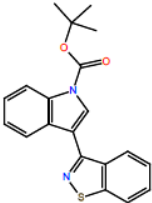
More than 100 small molecule compounds were designed related to S-N triangle structure possessing anticancer pharmacodynamic groups, such as trifluoromethyl (-CF<sub>3</sub>), sulfanilamide group (-SO<sub>2</sub>NH<sub>2</sub>) and indole *etc.* One reported tumor inhibitor

compound **10** was used for docking as a reference, which is valuable for subsequent tumor cell viability test.

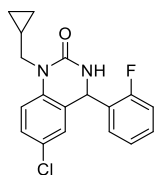
Among the eight reported receptor proteins on the surface of cancer cells, These molecules have the highest binding scores with retinoic acid receptor related orphan C (RORC), rather than CXC chemokine receptor 4 (CXCR4), P38 mitogen-activated protein kinase  $\alpha/\beta$ , Epidermal growth factor receptor (EGFR), Epidermal growth factor receptor-2 (HER2), Human C-C chemokine receptor type (CCR-7) and Oncogenic tyrosine phosphatase SHP2. The docking scores of 9 preferred compounds are listed in Table 5.1, as well as several other compounds of low scores which is convenient for comparison.

**Table 5.1** The docking scores of 9 preferred compounds, one reported tumor inhibitor and other 5 compounds for comparison.

Number	Structure	docking score	XP GScore	glide gscore
1		-14.135	-14.319	-14.319
2		-13.774	-14.049	-14.049
3		-13.742	-13.742	-13.742
4		-13.711	-13.77	-13.77
5		-13.652	-13.711	-13.711

6		-13.548	-13.608	-13.608
7		-13.233	-13.417	-13.417
8		-13.145	-13.204	-13.204
9		-13.098	-13.709	-13.709
10		-11.854	-11.854	-11.854
11		-10.777	-10.777	-10.777
12		-10.532	-10.539	-10.539
13		-10.223	-10.35	-10.35
14		-9.847	-9.847	-9.847

15



-6.021

-6.021

-6.021

The scores of -11 to -15 showed the first 10 compounds are of high level, whose simulation results are much better than quinazolinone derivatives in Chapter 3 (Number 11 in Table 5.1), The common denominator of high-scoring compounds is possessing phenylalanine and isothiourreas structures simultaneously. Schematic depiction of compound 4 with retinoic acid receptor related orphan C (RORC) (PDB ID: 4WPF) within the binding pocket is shown in Fig. 5.3. Molecular docking studies suggested it interacted mainly with residues located in the subdomains IIA of 4WPF, including GLU 379, GLU 326, ARG364, HIS479, GLN 286, HIE323 and GLY380. The benzene ring is observed to make  $\pi$ -stacking interactions with residues HIS479 and TRP317, and PHE388.

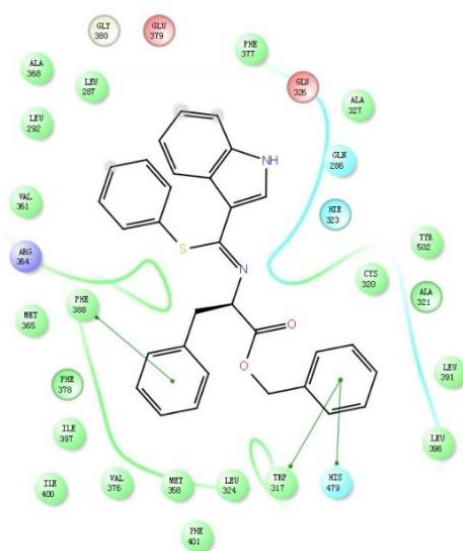
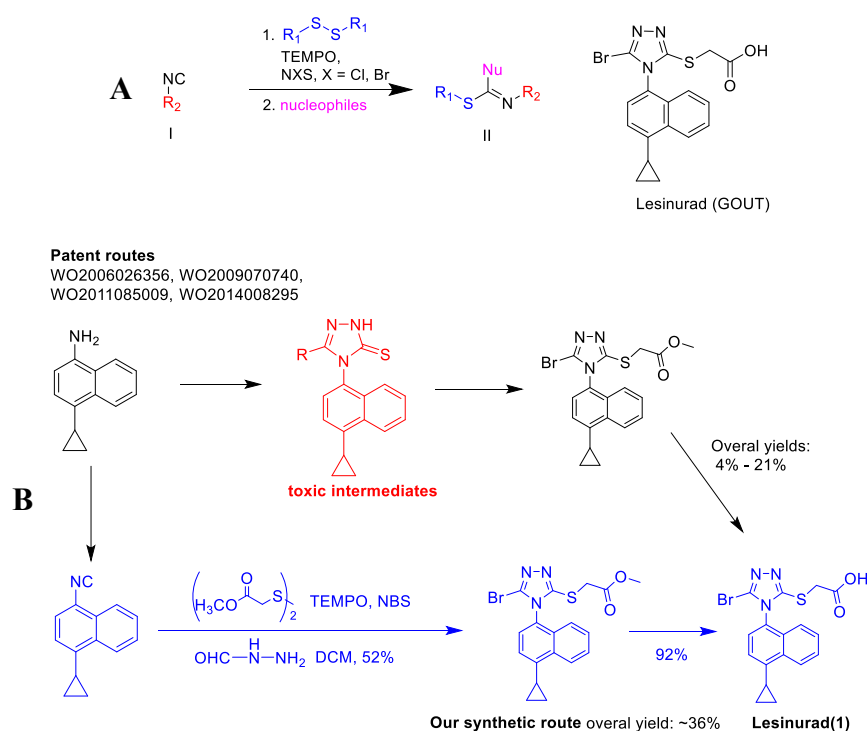


**Fig. 5.3** Schematic depiction of compound 4 with retinoic acid receptor related orphan C (RORC) (PDB ID: 4WPF) within the binding pocket. Straight line (green) represents  $\pi$ -stacking interactions.

From the comparison of simulation calculations in previous studies and actual cell experiment results, a simulated value of -7 to -9 indicates that the compound may have cell activity, and a simulated value higher than -10 means that the compound should have good cell activity. Considering their potential, we decided to synthesize these compounds.

#### 5.4.2 Synthesis of target products

Patent literature synthesized FDA approved drug Lesinurad (compound **a** in Fig. 5.1) with four or more steps in 4%-21% overall yield, involving the formation and handling of the toxic [1,2,4] triazole-3-thiol intermediates [9]. In comparison, the ester precursor to lesinurad can be synthesized in one step from the corresponding isocyanide using our three-component protocol in 36% overall yield, which improving the yield while simplifying the steps (Fig 5.4 A and B) [10]. This reaction principle has been verified by successful synthesis of CXCR4 by methods in Fig 5.4 C, so it is reasonable that the above compounds with good docking effect can be realized in similar routes (Fig 5.4 D).



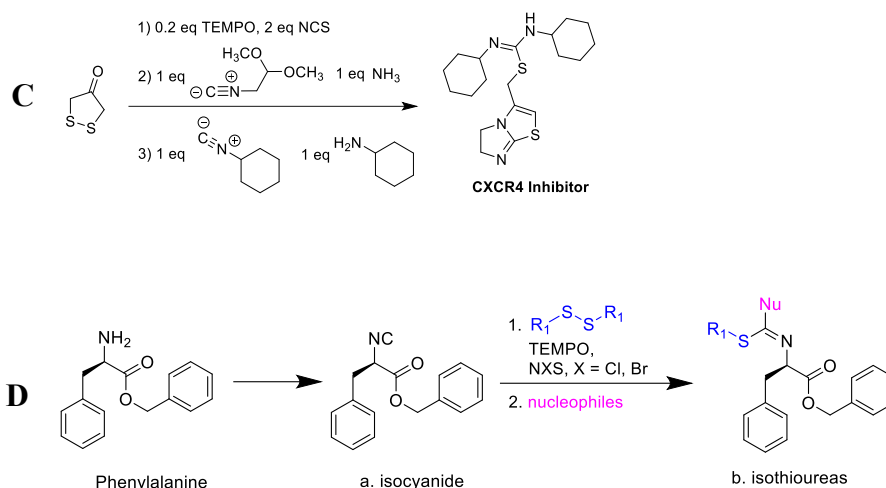
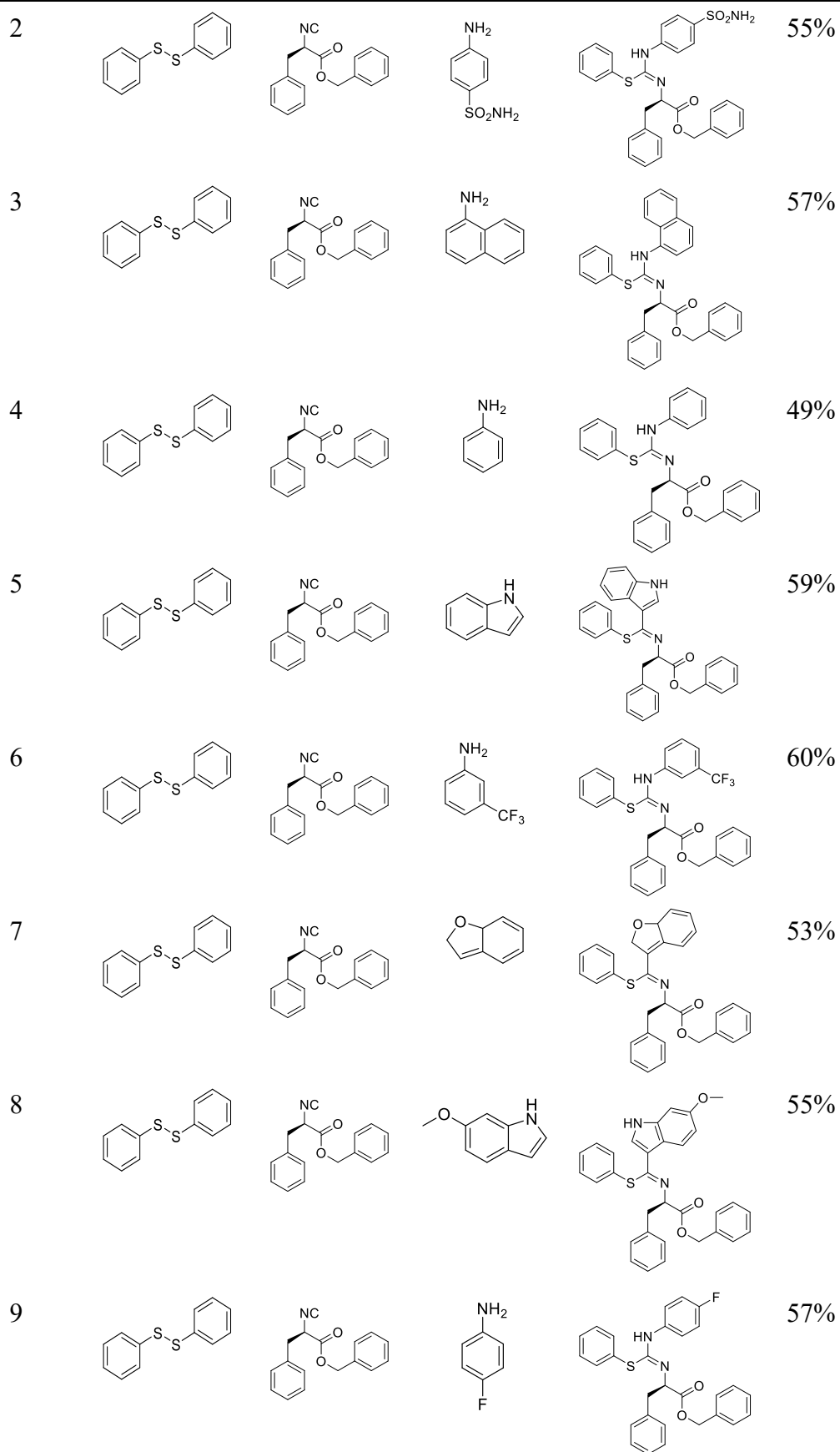


**Fig. 5.4** **A** Synthetic route of Lesinurad explored by us in previous study. **B** Compared with existing synthetic methods, our method has advantages in synthetic pathway and yield. **C** Synthesis of CXCR4 through our synthesis method. **D** Synthesis method of potential cancer cell inhibitor with phenylalanine group and isothiourea group.

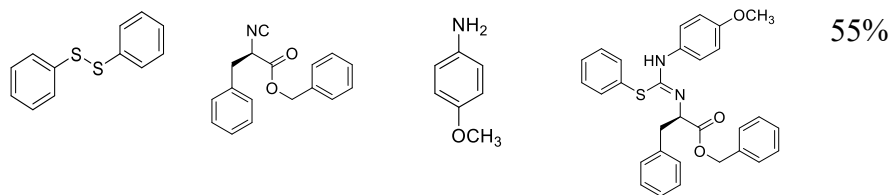
In our protocol, L-phenylalanine was oxidized to benzyl(*R*)-2-isocyano-3-phenylpropanoate by phosphorus oxychloride or *Burgess* reagent, as one of the reactants for main reaction. Diphenyl disulfide was activated to be an electrophilic sulfur center by N-halogen succinimide (NBS/NCS) in the presence of 2,2,6,6-tetramethylpiperidine-1-oxyl (TEMPO) in solvent dichloromethane (DCM), and benzyl(*R*)-2-isocyano-3-phenylpropanoate was then added in the solution after sufficient activation. The reaction is monitored by thin layer chromatography (TLC). Next, nucleophiles were added after isonitrile was consumed to produce phenylpropionate compounds. The nucleophiles used in this study were shown in Table 5.2. As a result, a three-component reaction involving electrophilic sulfur centers, isocyanides and nucleophiles was developed.

**Table 5.2 Synthesis of final products**

Compound Number	disulfides	isocyanide	nucleophiles	Product	Yield
-----------------	------------	------------	--------------	---------	-------



10



Synthesis details and spectrums are listed in Supplementary Information (SI). In the next step, all specific compounds will undergo biological tests for cancer cells inhibitory activity.

### 5.5 Conclusions

In summary, this multicomponent protocol that involves electrophilic center and isocyanide is suitable for the formation of isothiourea, such as anti-gout drugs, CXCR4 antibody, active molecules of isothiourea with phenylalanine group were successfully synthesized. The advantages of mild reaction conditions, reduced purification steps, and ease of starting material accessibility is a useful addition to existing methodologies. Finally, in consideration of the seemingly unlimited functional versatility of unnatural amino acids, we propose our derivatives as chiral building blocks and molecular scaffolds in constructing peptidic drugs can be investigated in biomedical applications.



## 5.6 References

- [1] Fan Yang, Jingjing Li, Haijun Deng, Yihao Wang, Chong Lei, Qiujie Wang, Jin Xiang, Li Liang, Jie Xia, Xuanming Pan, Xiaosong Li, Quanxin Long, Lei Chang, Ping Xu, Ailong Huang, Kai Wang, Ni Tang (2019) GSTZ1-1 Deficiency Activates NRF2/IGF1R Axis in HCC via Accumulation of Oncometabolite Succinylacetone. *EMBO J.* 38: e101964.
- [2] Z. Wu, H. K. Lim, S. J. Tan, A. Gautam, H. W. Hou, K. W. Ng, N. S. Tan, and C. Y. Tay (2020) Potent-By-Design: Amino Acids Mimicking Porous Nanotherapeutics with Intrinsic Anticancer Targeting Properties. *Small*, 2003757.
- [3] M. A. Fik-Jaskólká, A. F. Mkrtchyan, A. S. Saghyan, R. Palumbo, A. Belter, L. A. Hayriyan, H. Simonyan, V. Roviello and G. N. Roviello (2020) Biological macromolecule binding and anticancer activity of synthetic alkyne-containing l-phenylalanine derivatives. *Amino Acids.* 52: 755–769.
- [4] X. Su, X. Zhou, Z. Tan, C. Zhou (2017) Highly efficiency antibacterial diblock copolypeptides based on lysine and phenylalanine. *Biopolymers*, 107(11): e23041.
- [5] Hoy, S. M. Lesinurad: First global approval. *Drugs* 76, 509–516, doi:10.1007/s40265-016-0550-y (2016).
- [6] Kawakami Hiroshi, Kitao Yuki, Matsuo Akira. JP Patent WO03048134A1. TRIAZOLE COMPOUND AND MEDICINAL USE THEREOF. Jun 12, 2003.
- [7] Gebhard Thoma, Markus B. Streiff, Jiri Kovarik, Fraser Glickman, Trixie Wagner, Christian Beerli, and Hans-Günter Zerwes. Orally Bioavailable Isothioureas Block Function of the Chemokine Receptor CXCR4 In Vitro and In Vivo. *J. Med. Chem.* 2008, 51, 24, 7915–7920.
- [8] Olivier René, Benjamin P. Fauber, Gladys de Leon Boenig, Brenda Burton, Céline Eidenschenk, Christine Everett, Alberto Gobbi, Sarah G. Hymowitz, Adam R. Johnson, James R. Kiefer, Marya Liimatta, Peter Lockey, Maxine Norman, Wenjun Ouyang, Heidi A. Wallweber, and Harvey Wong. Minor Structural Change to Tertiary Sulfonamide RORc Ligands Led to Opposite Mechanisms of Action. *ACS Med. Chem. Lett.* 2015, 6, 276–281.

[9] Galvin Gabriel, Gunic Esmir. Manufacture of 2- (5- bromo-4 (-cyclopropyl)naphthalen-1-yl) -4H-1,2,4-Triazol-3-ylthio) acetic acid (2014). US Patent WO2014008295A1. 2014-01-09.

[10] Xiaofang Lei, Yuanyuan Wang, Erkang Fan, and Zhihua Sun. In Situ Activation of Disulfides for Multicomponent Reactions with Isocyanides and a Broad Range of Nucleophiles. *Org. Lett.* 2019, 21, 1484–1487.

## **6 Conclusions**

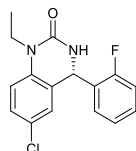
Nitrogen-containing aryl compounds including fenitrothion, GABA, quinazolin derivatives and phenylpropionate compounds. Interaction and application by cell surface technology or potential antiproliferation to tumor cells. The cell Biotechnology, as well as useful chemical molecules by biosynthesis and chemical synthesis should be emphasized, so that they can cooperate and complement with each other.

## Supplementary Information (SI)

### 1. Synthesis of quinazolinone derivatives (Chapter 4)

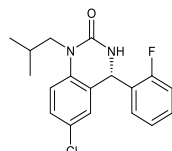
#### Synthesis of 1, 4-disubstituted-3,4-dihydroquinazolin-2(*IH*)-one derivatives

##### (*S*)-6-chloro-1-ethyl-4-(2-fluorophenyl)-3,4-dihydroquinazolin-2(*IH*)-one (12a)



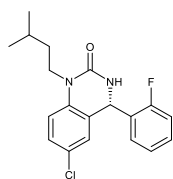
2-(amino(2-fluorophenyl)methyl)-4-chloro-N-ethylcyclohexa-1,5-dien-1-amine (145mg, 0.5mmol) and triethylamine (100mg, 0.9mmol) were added in 10 ml DCM. The solution was cooled down to 0°C, then bis(trichloromethyl) carbonate (190mg, 0.6mmol) was added and the reaction was kept for 12 h. The mixture was quenched with saturated ammonium chloride and extracted with ethyl acetate. The organic layer was dried over anhydrous sodium sulfate and concentrated by a rotary evaporator. The obtained crude product was purified by silica gel column chromatography. 0.105 g, 68% yield, white solid. <sup>1</sup>H NMR (400 MHz, CDCl<sub>3</sub>) δ 7.34 – 7.18 (m, 11H), 7.18 – 6.91 (m, 18H), 7.20 – 6.82 (m, 1H), 6.93 (d, *J* = 8.8 Hz, 3H), 6.93 (d, *J* = 8.8 Hz, 3H), 5.89 (d, *J* = 1.8 Hz, 3H), 5.31 (d, *J* = 10.0 Hz, 4H), 4.09 – 3.69 (m, 8H), 1.35 – 1.21 (m, 19H). <sup>13</sup>C NMR (100 MHz, CDCl<sub>3</sub>) δ 171.1, 160.5, 158.7, 153.7, 136.2, 130.2, 130.1, 129.4, 129.3, 128.6, 128.1, 128.1, 127.3, 127.1, 124.8, 124.8, 123.8, 122.1, 116.1, 115.8, 114.7, 113.4, 50.9, 50.8, 37.3, 29.7, 12.5, 1.0. HRMS (ESI-TOF) *m/z*: calcd for C<sub>16</sub>H<sub>14</sub>ClFN<sub>2</sub>O [M+H]<sup>+</sup> 305.0779, found 305.0779.

##### (*S*)-6-chloro-4-(2-fluorophenyl)-1-isobutyl-3,4-dihydroquinazolin-2(*IH*)-one (12b)



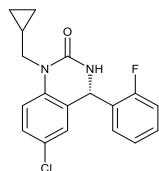
63% yield, white solid. <sup>1</sup>H NMR (400 MHz, CDCl<sub>3</sub>) δ 7.55 – 7.21 (m, 7H), 7.19 – 7.04 (m, 6H), 7.01 (d, *J* = 2.2 Hz, 2H), 6.90 (d, *J* = 8.8 Hz, 2H), 5.92 (d, *J* = 1.8 Hz, 2H), 5.28 (s, 2H), 3.97 (m, 2H), 3.66 (m, 2H), 2.47 – 1.78 (m, 3H), 1.00 (d, *J* = 6.7 Hz, 6H), 0.93 (d, *J* = 6.6 Hz, 6H). <sup>13</sup>C NMR (100 MHz, CDCl<sub>3</sub>) δ 171.1, 161.5, 158.8, 154.2, 136.6, 130.2, 130.13, 129.4, 129.2, 128.5, 128.3, 128.2, 127.3, 127.2, 124.8, 124.7, 123.6, 116.1, 115.9, 115.2, 50.9, 50.9, 48.5, 26.4, 20.1, 19.9. HRMS (ESI-TOF) *m/z*: calcd for C<sub>18</sub>H<sub>18</sub>ClFN<sub>2</sub>O [M+H]<sup>+</sup> 333.1092, found 333.1091.

##### (*S*)-6-chloro-4-(2-fluorophenyl)-1-isopentyl-3,4-dihydroquinazolin-2(*IH*)-one (12c)



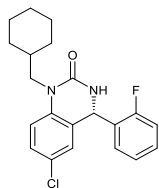
59% yield, white solid.  $^1\text{H}$  NMR (400 MHz,  $\text{CDCl}_3$ )  $\delta$  7.65 – 7.22 (m, 18H), 7.18 – 6.96 (m, 17H), 6.90 (d,  $J$  = 8.8 Hz, 4H), 5.89 (d,  $J$  = 2.0 Hz, 4H), 5.23 (s, 5H), 4.02 (m, 5H), 3.97 – 3.74 (m, 5H), 1.95 – 1.49 (m, 36H), 1.01 (m, 24H).  $^{13}\text{C}$  NMR (100 MHz,  $\text{CDCl}_3$ )  $\delta$  171.1, 160.5, 153.8, 136.4, 130.2, 130.1, 129.3, 128.6, 128.2, 127.3, 127.1, 124.8, 124.8, 123.8, 116.1, 115.8, 114.9, 50.9, 40.8, 35.7, 26.3, 22.6, 22.5. HRMS (ESI-TOF)  $m/z$ : calcd for  $\text{C}_{19}\text{H}_{20}\text{ClFN}_2\text{O}$   $[\text{M}+\text{H}]^+$  347.1248, found 347.1247.

(S)-6-chloro-1-(cyclopropylmethyl)-4-(2-fluorophenyl)-3,4-dihydroquinazolin-2(1H)-one (12d)



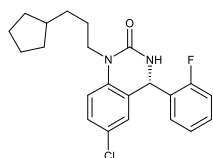
57% yield, white solid.  $^1\text{H}$  NMR (400 MHz,  $\text{CDCl}_3$ )  $\delta$  7.98 – 7.26 (m, 5H), 7.26 – 6.99 (m, 5H), 5.92 (d,  $J$  = 1.8 Hz, 1H), 5.22 (s, 1H), 3.89 (m, 2H), 0.94 – 0.30 (m, 5H).  $^{13}\text{C}$  NMR (100 MHz,  $\text{CDCl}_3$ )  $\delta$  171.1, 160.5, 154.1, 136.6, 130.2, 130.1, 128.6, 128.3, 127.4, 127.1, 124.8, 124.8, 123.9, 116.0, 115.8, 115.3, 50.8, 45.9, 9.5, 4.1, 3.9, -0.01. HRMS (ESI-TOF)  $m/z$ : calcd for  $\text{C}_{18}\text{H}_{16}\text{ClFN}_2\text{O}$   $[\text{M}+\text{H}]^+$  331.0935, found 331.0930.

(S)-6-chloro-1-(cyclohexylmethyl)-4-(2-fluorophenyl)-3,4-dihydroquinazolin-2(1H)-one (12e)



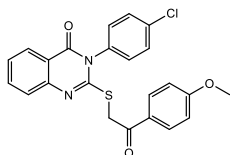
67% yield, white solid.  $^1\text{H}$  NMR (400 MHz,  $\text{CDCl}_3$ )  $\delta$  7.61 – 7.21 (m, 3H), 7.19 – 7.04 (m, 3H), 7.00 (d,  $J$  = 2.2 Hz, 1H), 6.91 (d,  $J$  = 8.8 Hz, 1H), 5.91 (d,  $J$  = 1.7 Hz, 1H), 5.28 (s, 1H), 3.97 (m, 1H), 3.86 – 3.54 (m, 1H), 2.03 – 1.51 (m, 9H), 1.38 – 1.25 (m, 1H), 1.11 (m, 5H).  $^{13}\text{C}$  NMR (100 MHz,  $\text{CDCl}_3$ )  $\delta$  171.10, 161.29, 158.84, 154.26, 136.73, 130.22, 130.14, 129.39, 129.26, 128.53, 128.30, 128.26, 127.26, 127.12, 124.68, 124.64, 123.68, 116.08, 115.87, 115.22, 50.93, 50.90, 47.42, 35.87, 30.80, 26.33, 25.87, 25.75, 1.01, -0.01. HRMS (ESI-TOF)  $m/z$ : calcd for  $\text{C}_{21}\text{H}_{22}\text{ClFN}_2\text{O}$   $[\text{M}+\text{H}]^+$  373.1405, found 373.1401.

(S)-6-chloro-1-(3-cyclopentylpropyl)-4-(2-fluorophenyl)-3,4-dihydroquinazolin-2(1H)-one (12f)



60% yield, white solid.  $^1\text{H}$  NMR (400 MHz,  $\text{CDCl}_3$ )  $\delta$  7.61 – 7.22 (m, 4H), 7.19 – 7.02 (m, 3H), 7.01 (d,  $J = 2.3$  Hz, 1H), 6.90 (d,  $J = 8.8$  Hz, 1H), 5.90 (d,  $J = 1.9$  Hz, 1H), 5.24 (s, 1H), 3.99 (m, 1H), 3.84 (m, 1H), 2.06 – 1.59 (m, 12H), 1.59 – 1.24 (m, 6H), 1.09 (s, 3H).  $^{13}\text{C}$  NMR (100 MHz,  $\text{CDCl}_3$ )  $\delta$  171.10, 161.20, 158.75, 153.84, 136.47, 130.17, 130.09, 129.47, 129.34, 128.60, 128.20, 128.17, 127.26, 127.11, 124.80, 124.77, 123.74, 116.05, 115.83, 114.83, 50.89, 50.85, 49.92, 42.36, 41.17, 39.87, 37.54, 33.19, 32.70, 32.69, 30.85, 29.68, 27.17, 26.28, 25.51, 25.18. HRMS (ESI-TOF)  $m/z$ : calcd for  $\text{C}_{22}\text{H}_{24}\text{ClFN}_2\text{O}$   $[\text{M}+\text{H}]^+$  387.1561, found 387.1560.

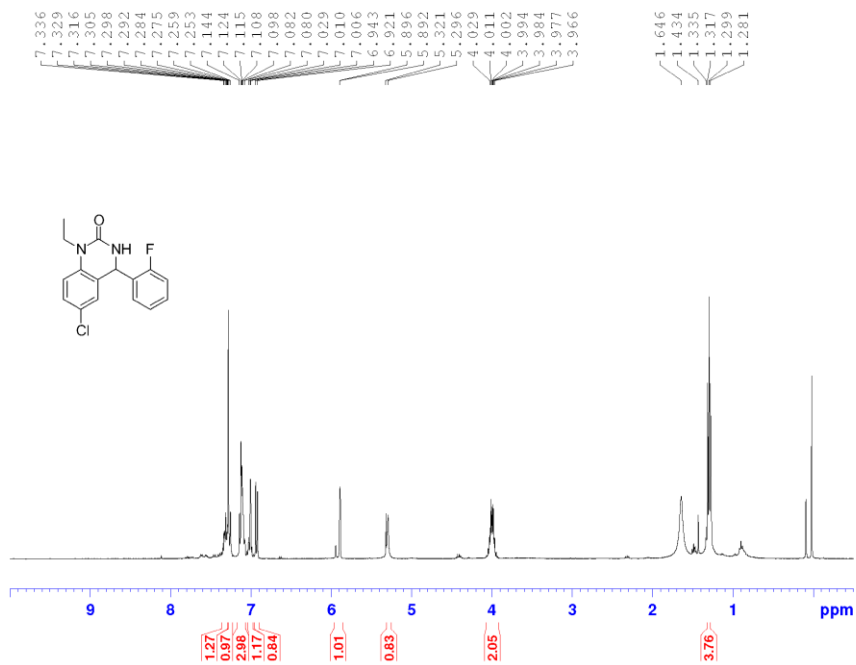
2-[2-(4-Chlorophenyl)-2-oxo-ethylthio]-3-(4-methoxyphenyl)-quinazolin-4(3H)-one (12g)



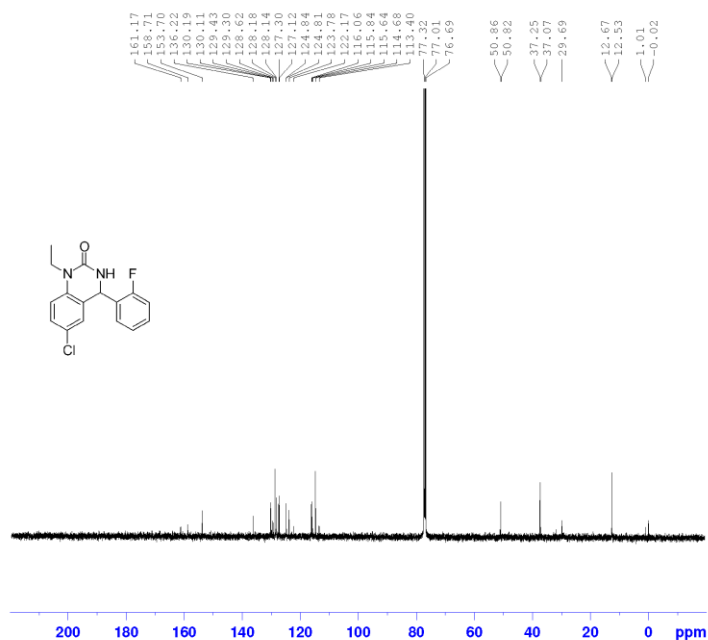
A mixture of 3-Phenyl-2-thioxo-2,3-dihydro-4(*1H*)-quinazolinone (10 mmol) and the 2-Bromo-4'-methoxyacetophenone (10 mmol) was refluxed in dry acetone (30 mL) in the presence of anhydrous potassium carbonate (1.37 g, 10 mmol) for 20h. The reaction mixture was then filtered while hot and the filtrate was concentrated by a rotary evaporator, then recrystallization with acetone. The obtained crude product was purified by silica gel column chromatography. 71% yield, white solid.  $^1\text{H}$  NMR (400 MHz, DMSO)  $\delta$  3.86 (s, 3H), 4.67 (s, 2H), 7.03 – 8.15 (m, 12H); HRMS (ESI-TOF)  $m/z$ : calcd for  $\text{C}_{23}\text{H}_{17}\text{ClN}_2\text{O}_3\text{S}$   $[\text{M}+\text{H}]^+$  437.0705, found 437.0704.

## 2. $^1\text{H}$ NMR and $^{13}\text{C}$ NMR spectra of quinazolinone derivatives

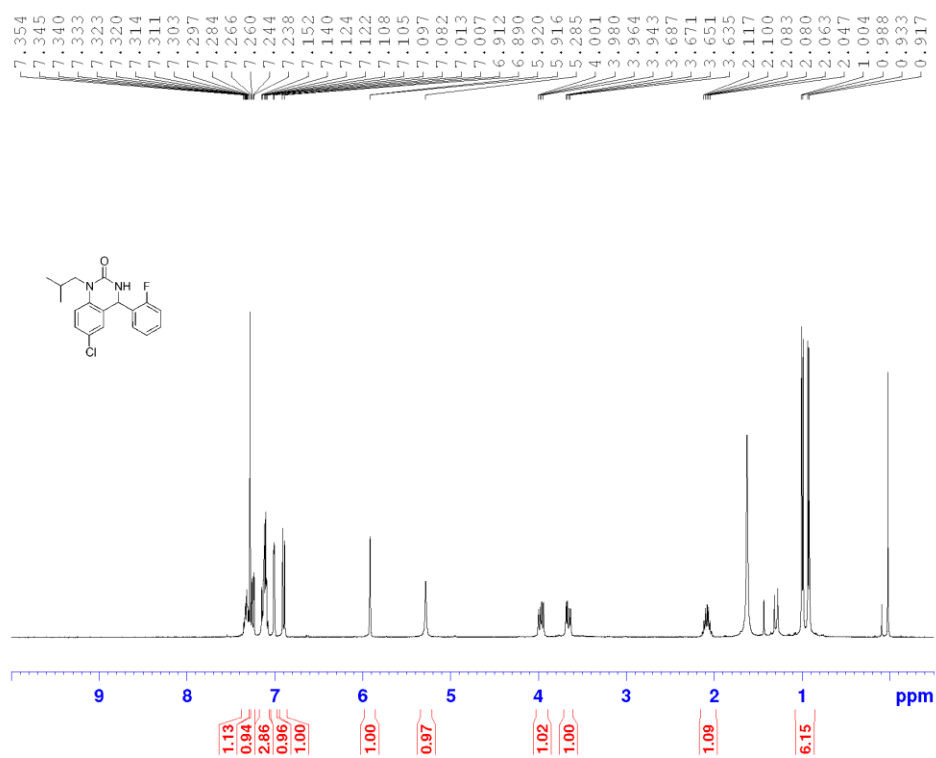
$^1\text{H}$  NMR (400 MHz,  $\text{CDCl}_3$ ) of 12a



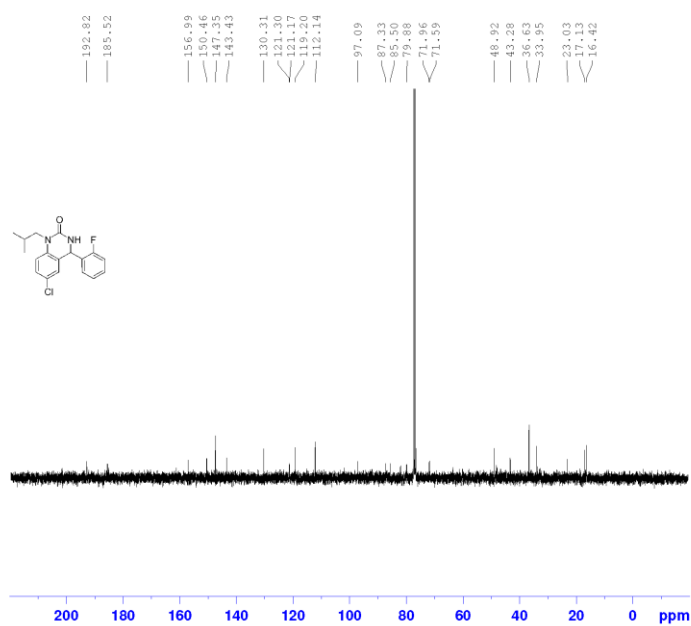
$^{13}\text{C}$  NMR (100 MHz,  $\text{CDCl}_3$ ) of 12a



$^1\text{H}$  NMR (400 MHz,  $\text{CDCl}_3$ ) of 12b

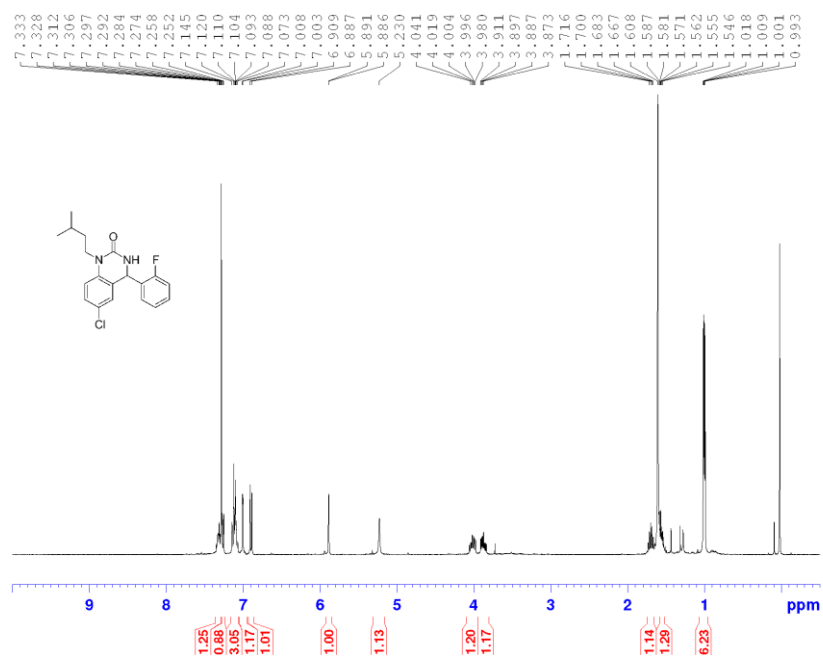


$^{13}\text{C}$  NMR (100 MHz,  $\text{CDCl}_3$ ) of 12b

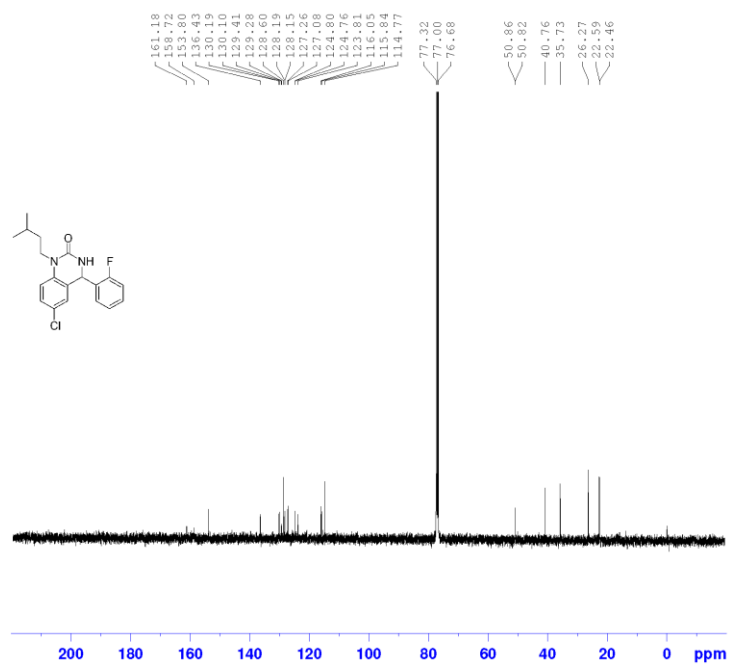




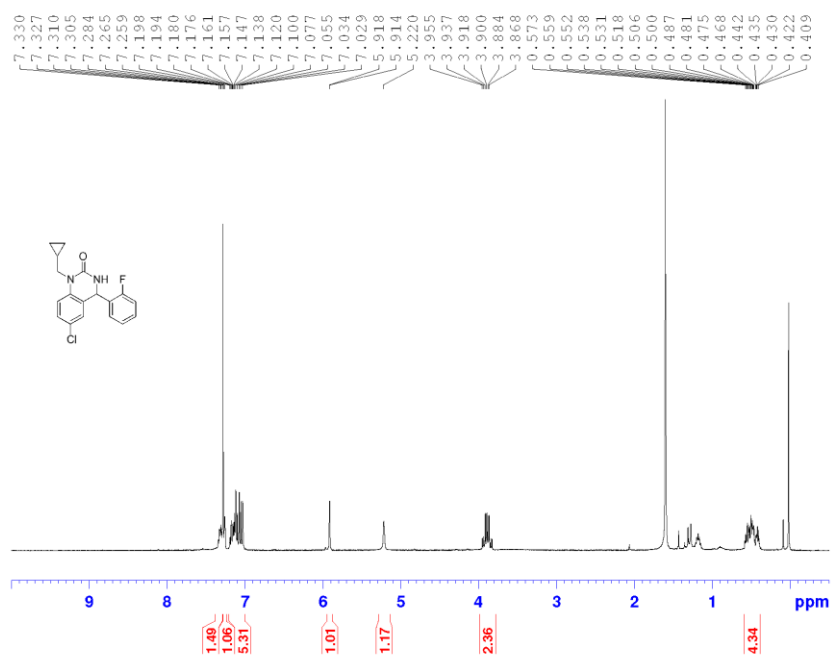
$^1\text{H}$  NMR (400 MHz,  $\text{CDCl}_3$ ) of 12c



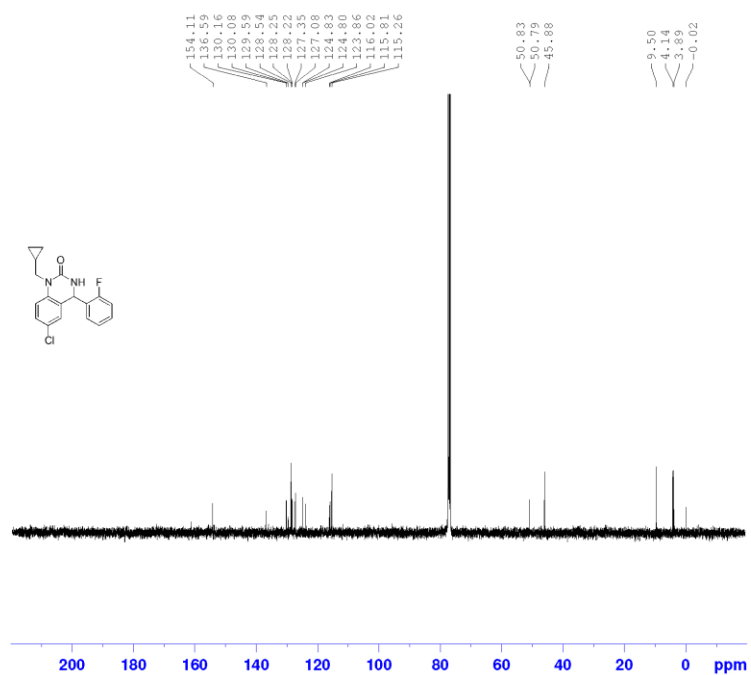
$^{13}\text{C}$  NMR (100 MHz,  $\text{CDCl}_3$ ) of 12c



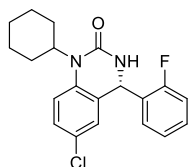
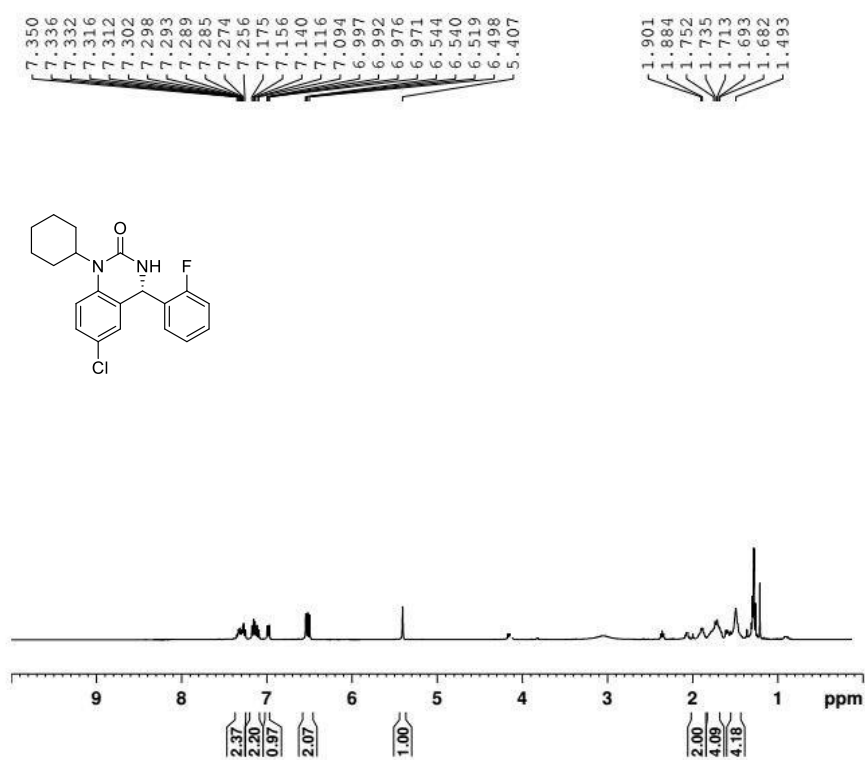
$^1\text{H}$  NMR (400 MHz,  $\text{CDCl}_3$ ) of 12d



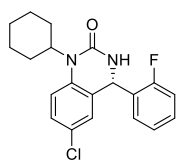
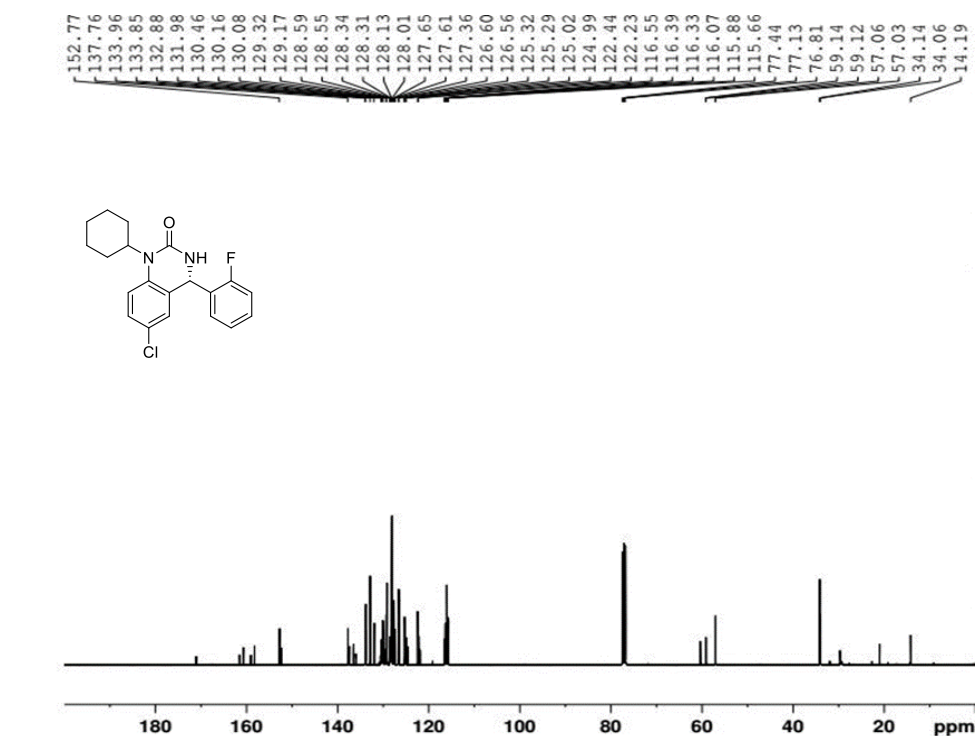
$^{13}\text{C}$  NMR (100 MHz,  $\text{CDCl}_3$ ) of 12d



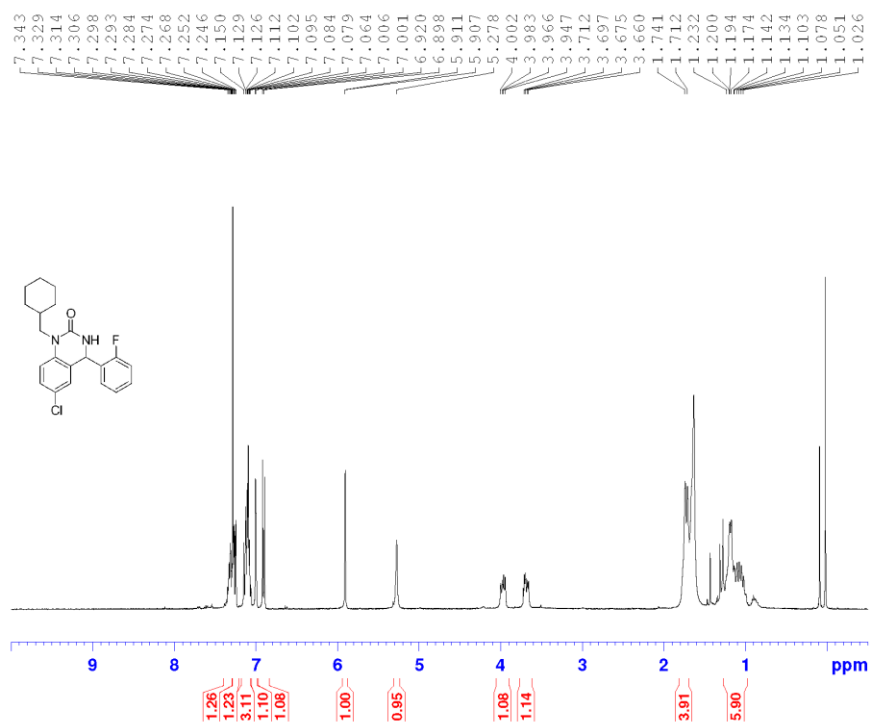
$^1\text{H}$  NMR (400 MHz,  $\text{CDCl}_3$ ) of 12e



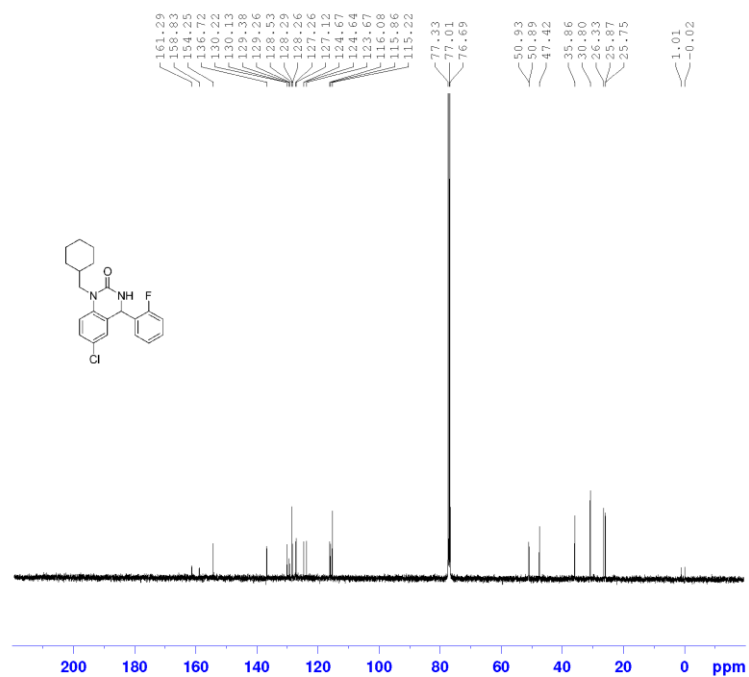
$^{13}\text{C}$  NMR (100 MHz,  $\text{CDCl}_3$ ) of 12e



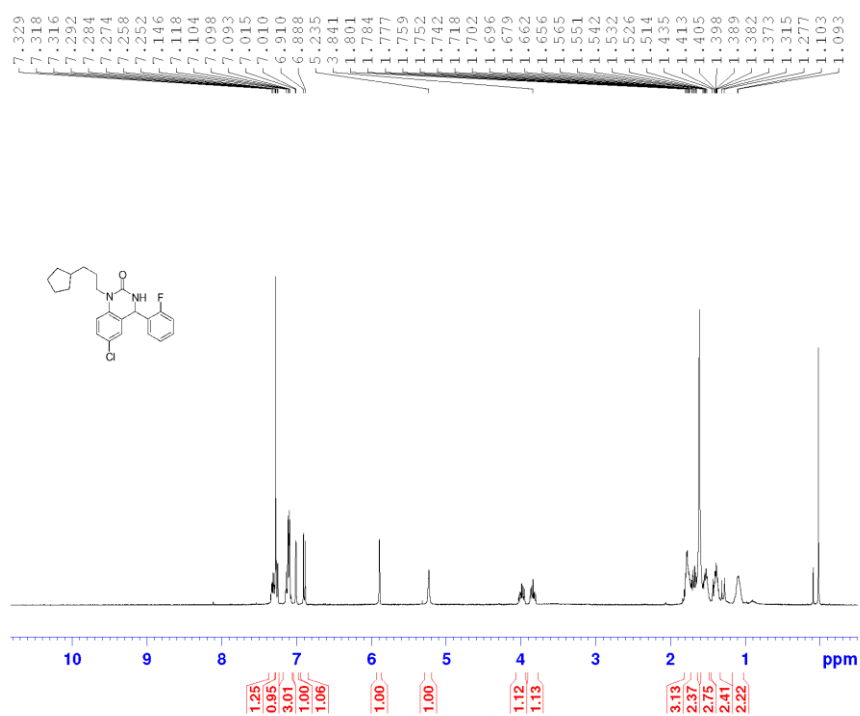
$^1\text{H}$  NMR (400 MHz,  $\text{CDCl}_3$ ) of 12f



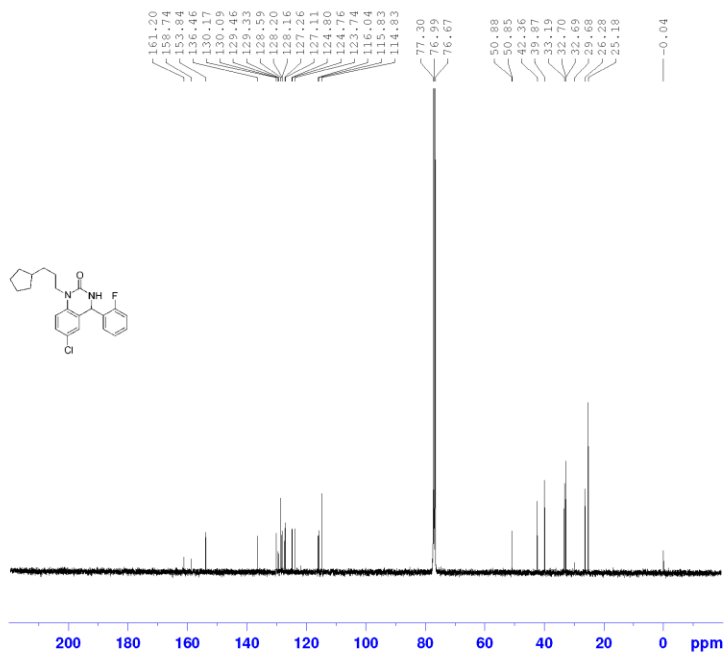
$^{13}\text{C}$  NMR (100 MHz,  $\text{CDCl}_3$ ) of 12f



$^1\text{H}$  NMR (400 MHz,  $\text{CDCl}_3$ ) of 12g

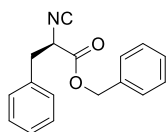


$^{13}\text{C}$  NMR (100 MHz,  $\text{CDCl}_3$ ) of 12g



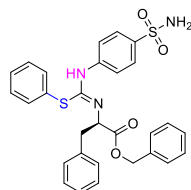
### 3. Synthesis of phenylpropionate compounds (Chapter 5)

#### Synthesis of benzyl (R)-2-isocyano-3-phenylpropanoate (2)



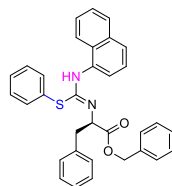
5 mmol (826 mg) of L-Phenylalanine hydrochloride and 2eq triethylamine was added to 30 ml of DCM and stirred vigorously for 2 h. The organic phase was then extracted with DCM. Acetic anhydride (2 eq), dried formic acid (0.5 eq) and L-Phenylalanine (1 eq) were added in 20 ml DCM and stirred at room temperature for overnight. The organic layer was washed with concentrated sodium bicarbonate solution and dried over magnesium sulfate. Next, 6 mmol (1.5 g) Burgess reagent was added as well as 20 ml DCM, the mixture was stirred at room temperature for 2 h under nitrogen protection. The progress of the reaction was thoroughly monitored by TLC. The organic layer was washed with concentrated sodium bicarbonate solution and dried over magnesium sulfate. The obtained crude product was evaporated under reduced pressure and purified by silica gel column chromatography. 1.2g, 90% yield, yellow oil.

#### Synthesis of benzyl (R, Z)-3-phenyl-2-(((phenylthio)((4-sulfamoylphenyl) amino) methylene) amino) propanoate (3).



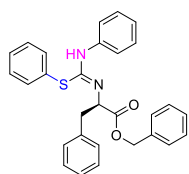
2 mmol of diphenyl disulfide (440 mg) , 1 mmol of N-Bromosuccinimide (NBS) (178 mg) and 0.2mmol of 2,2,6,6-tetramethylpiperidine-1-oxyl (TEMPO) (32 mg) were added in 10 ml DCM and stirred at room temperature for 2 h under nitrogen protection. 1mmol of compound 2 was then added in the solution. 1 mmol of sulfanilamide (173 mg) was added 2 hours later. The reaction is monitored by thin layer chromatography (TLC). The mixture was quenched with saturated ammonium chloride and extracted with ethyl acetate. The organic layer was dried over anhydrous sodium sulfate and concentrated by a rotary evaporator. The obtained crude product was purified by silica gel column chromatography. 0.300 g, 55% yield, yellow liquid.

#### Synthesis of benzyl (R, Z)-2-(((naphthalen-1-ylamino) (phenylthio) methylene) amino)-3-phenylpropanoate (4).



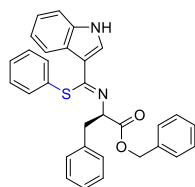
2 mmol of diphenyl disulfide (440 mg) , 1 mmol of N-Bromosuccinimide (NBS) (178 mg) and 0.2mmol of 2,2,6,6-tetramethylpiperidine-1-oxyl (TEMPO) (32 mg) were added in 10 ml DCM and stirred at room temperature for 2 h under nitrogen protection. 1mmol of compound 2 was then added in the solution. 1 mmol of 1-naphthylamine (144 mg) was added 2 hours later. The reaction is monitored by thin layer chromatography (TLC). The mixture was quenched with saturated ammonium chloride and extracted with ethyl acetate. The organic layer was dried over anhydrous sodium sulfate and concentrated by a rotary evaporator. The obtained crude product was purified by silica gel column chromatography. 0.295 g, 57% yield, yellow liquid.

**Synthesis of benzyl (R, Z)-3-phenyl-2-(((phenylamino)(phenylthio)methylene) amino) propanoate (5).**



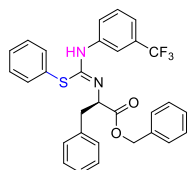
2 mmol of diphenyl disulfide (440 mg) , 1 mmol of N-Bromosuccinimide (NBS) (178 mg) and 0.2mmol of 2,2,6,6-tetramethylpiperidine-1-oxyl (TEMPO) (32 mg) were added in 10 ml DCM and stirred at room temperature for 2 h under nitrogen protection. 1mmol of compound 2 was then added in the solution. 1 mmol of aniline (95 mg) was added 2 hours later. The reaction is monitored by thin layer chromatography (TLC). The mixture was quenched with saturated ammonium chloride and extracted with ethyl acetate. The organic layer was dried over anhydrous sodium sulfate and concentrated by a rotary evaporator. The obtained crude product was purified by silica gel column chromatography. 0.228 g, 49% yield, yellow liquid.

**Synthesis of benzyl (R, Z)-2-(((1H-indol-3-yl) (phenylthio)methylene) amino)-3-phenylpropanoate (6).**



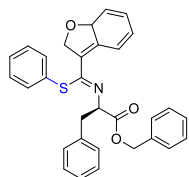
2 mmol of diphenyl disulfide (440 mg) , 1 mmol of N-Bromosuccinimide (NBS) (178 mg) and 0.2mmol of 2,2,6,6-tetramethylpiperidine-1-oxyl (TEMPO) (32 mg) were added in 10 ml DCM and stirred at room temperature for 2 h under nitrogen protection. 1mmol of compound 2 was then added in the solution. 1 mmol of indole (120 mg) was added 2 hours later. The reaction is monitored by thin layer chromatography (TLC). The mixture was quenched with saturated ammonium chloride and extracted with ethyl acetate. The organic layer was dried over anhydrous sodium sulfate and concentrated by a rotary evaporator. The obtained crude product was purified by silica gel column chromatography. 0.290 g, 59% yield, yellow liquid.

**Synthesis of benzyl (R, Z)-3-phenyl-2-(((phenylthio)((3-(trifluoromethyl) phenyl) amino) methylene) amino) propanoate (7).**



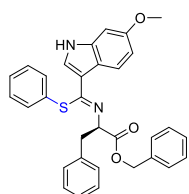
2 mmol of diphenyl disulfide (440 mg) , 1 mmol of N-Bromosuccinimide (NBS) (178 mg) and 0.2mmol of 2,2,6,6-tetramethylpiperidine-1-oxyl (TEMPO) (32 mg) were added in 10 ml DCM and stirred at room temperature for 2 h under nitrogen protection. 1mmol of compound 2 was then added in the solution. 1 mmol of 3-trifluoromethylaniline (162 mg) was added 2 hours later. The reaction is monitored by thin layer chromatography (TLC). The mixture was quenched with saturated ammonium chloride and extracted with ethyl acetate. The organic layer was dried over anhydrous sodium sulfate and concentrated by a rotary evaporator. The obtained crude product was purified by silica gel column chromatography. 0.327g, 60% yield, yellow liquid.

**Synthesis of benzyl (2R)-2-(((Z)-(2,7a-dihydrobenzofuran-3-yl) (phenylthio) methylene) amino)-3-phenylpropanoate (8).**



2 mmol of diphenyl disulfide (440 mg) , 1 mmol of N-Bromosuccinimide (NBS) (178 mg) and 0.2mmol of 2,2,6,6-tetramethylpiperidine-1-oxyl (TEMPO) (32 mg) were added in 10 ml DCM and stirred at room temperature for 2 h under nitrogen protection. 1mmol of compound 2 was then added in the solution. 1 mmol of 2,3-benzofuran (120 mg) was added 2 hours later. The reaction is monitored by thin layer chromatography (TLC). The mixture was quenched with saturated ammonium chloride and extracted with ethyl acetate. The organic layer was dried over anhydrous sodium sulfate and concentrated by a rotary evaporator. The obtained crude product was purified by silica gel column chromatography. 0.260 g, 53% yield, yellow liquid.

**Synthesis of benzyl (R, Z)-2-(((6-methoxy-1H-indol-3-yl) (phenylthio) methylene) amino)-3-phenylpropanoate (9).**

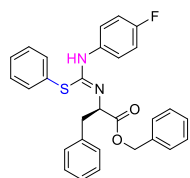


2 mmol of diphenyl disulfide (440 mg) , 1 mmol of N-Bromosuccinimide (NBS) (178 mg) and 0.2mmol of 2,2,6,6-tetramethylpiperidine-1-oxyl (TEMPO) (32 mg) were



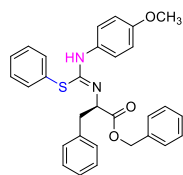
added in 10 ml DCM and stirred at room temperature for 2 h under nitrogen protection. 1mmol of compound 2 was then added in the solution. 1 mmol of 5-methoxyindole (148 mg) was added 2 hours later. The reaction is monitored by thin layer chromatography (TLC). The mixture was quenched with saturated ammonium chloride and extracted with ethyl acetate. The organic layer was dried over anhydrous sodium sulfate and concentrated by a rotary evaporator. The obtained crude product was purified by silica gel column chromatography. 0.285 g, 55% yield, yellow liquid.

**Synthesis of benzyl (R, Z)-2-(((4-fluorophenyl) amino) (phenylthio) methylene) amino)-3-phenylpropanoate (10).**



2 mmol of diphenyl disulfide (440 mg) , 1 mmol of N-Bromosuccinimide (NBS) (178 mg) and 0.2mmol of 2,2,6,6-tetramethylpiperidine-1-oxyl (TEMPO) (32 mg) were added in 10 ml DCM and stirred at room temperature for 2 h under nitrogen protection. 1mmol of compound 2 was then added in the solution. 1 mmol of 4-fluoroaniline (112 mg) was added 2 hours later. The reaction is monitored by thin layer chromatography (TLC). The mixture was quenched with saturated ammonium chloride and extracted with ethyl acetate. The organic layer was dried over anhydrous sodium sulfate and concentrated by a rotary evaporator. The obtained crude product was purified by silica gel column chromatography. 0.276 g, 57% yield, yellow liquid.

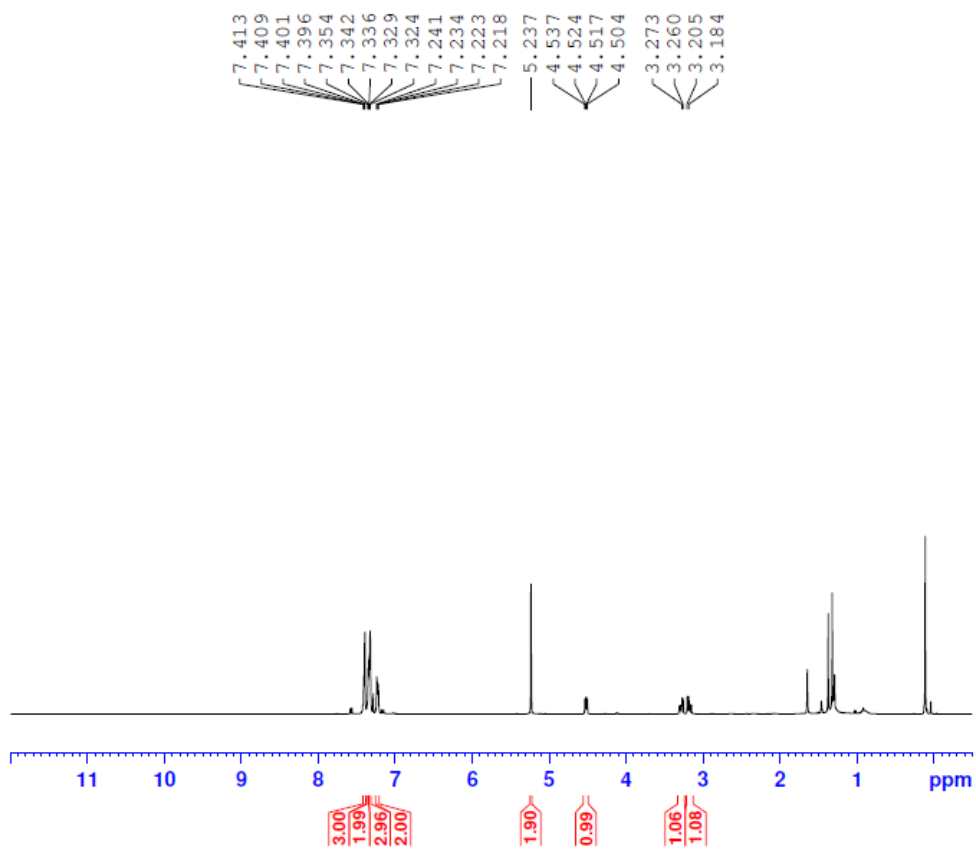
**Synthesis of benzyl (R, Z)-2-(((4-methoxyphenyl) amino) (phenylthio) methylene) amino)-3-phenylpropanoate (11).**



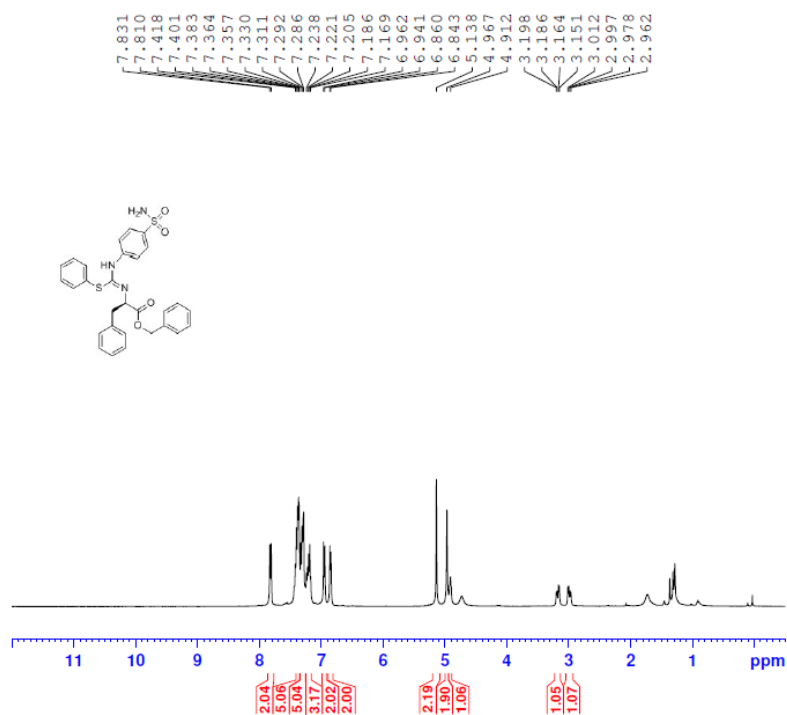
2 mmol of diphenyl disulfide (440 mg) , 1 mmol of N-Bromosuccinimide (NBS) (178 mg) and 0.2mmol of 2,2,6,6-tetramethylpiperidine-1-oxyl (TEMPO) (32 mg) were added in 10 ml DCM and stirred at room temperature for 2 h under nitrogen protection. 1mmol of compound 2 was then added in the solution. 1 mmol of para-anisidine (124 mg) was added 2 hours later. The reaction is monitored by thin layer chromatography (TLC). The mixture was quenched with saturated ammonium chloride and extracted with ethyl acetate. The organic layer was dried over anhydrous sodium sulfate and concentrated by a rotary evaporator. The obtained crude product was purified by silica gel column chromatography. 0.286 g, 55% yield, yellow liquid.

#### 4. $^1\text{H}$ NMR and $^{13}\text{C}$ NMR spectra of phenylpropionate compounds

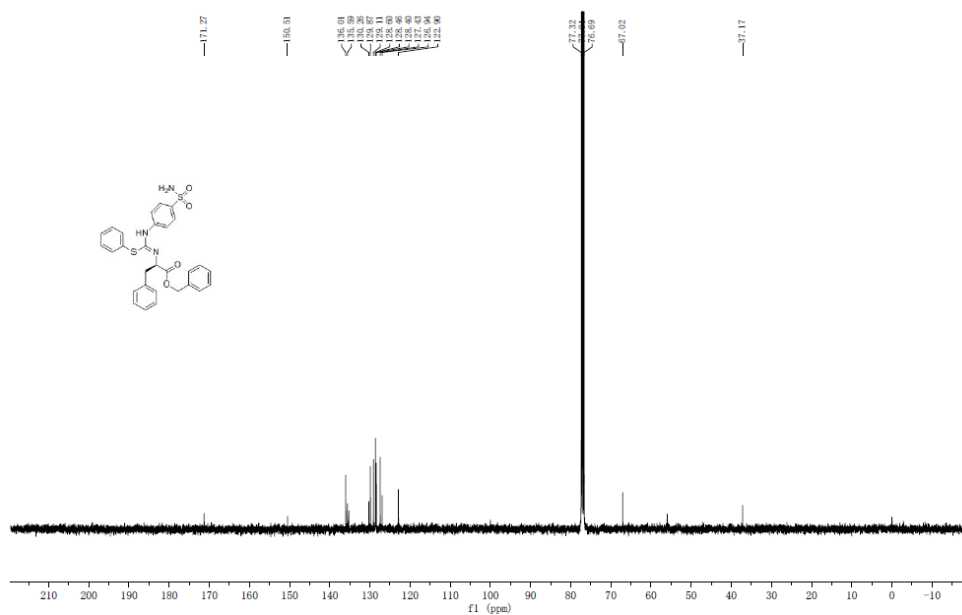
$^1\text{H}$  NMR (400 MHz,  $\text{CDCl}_3$ ) of 2



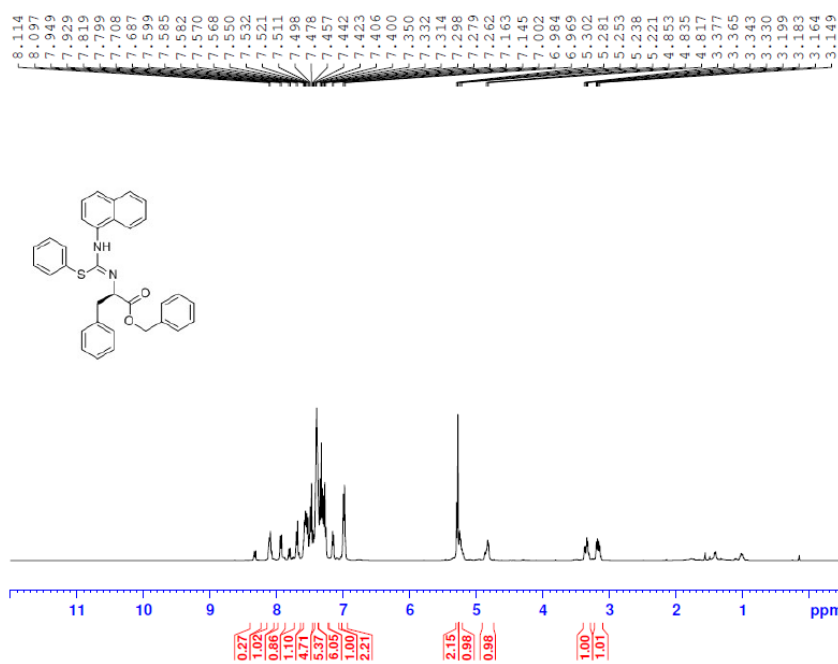
$^1\text{H}$  NMR (400 MHz,  $\text{CDCl}_3$ ) of 3



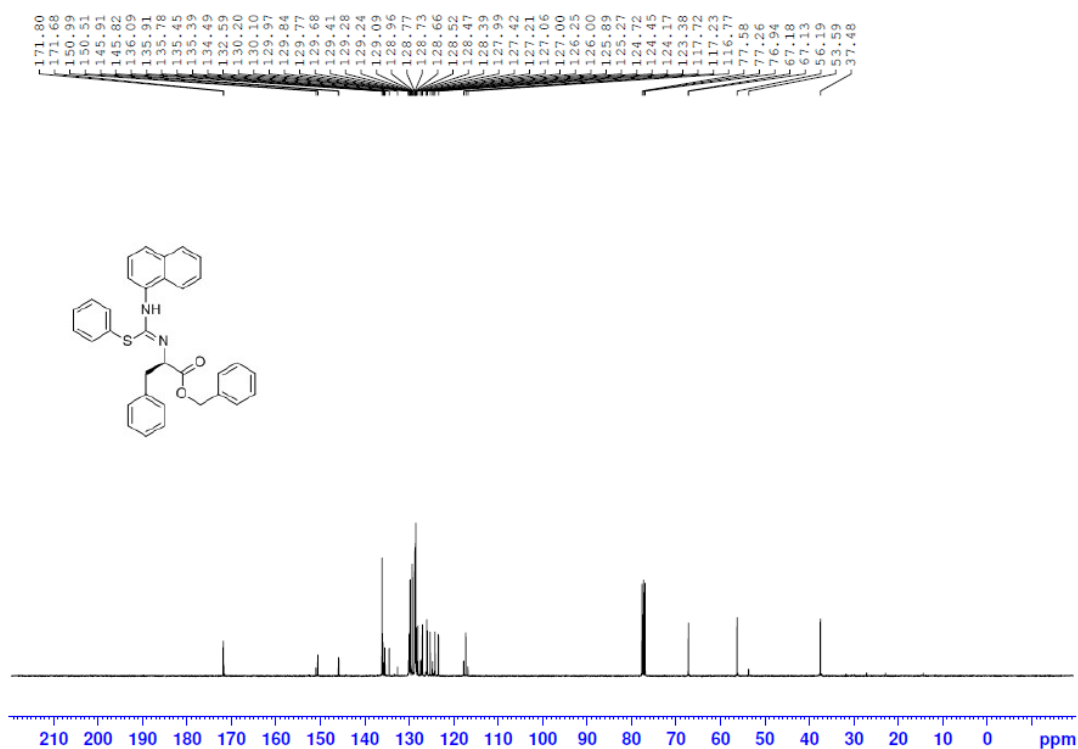
$^{13}\text{C}$  NMR (100 MHz,  $\text{CDCl}_3$ ) of 3



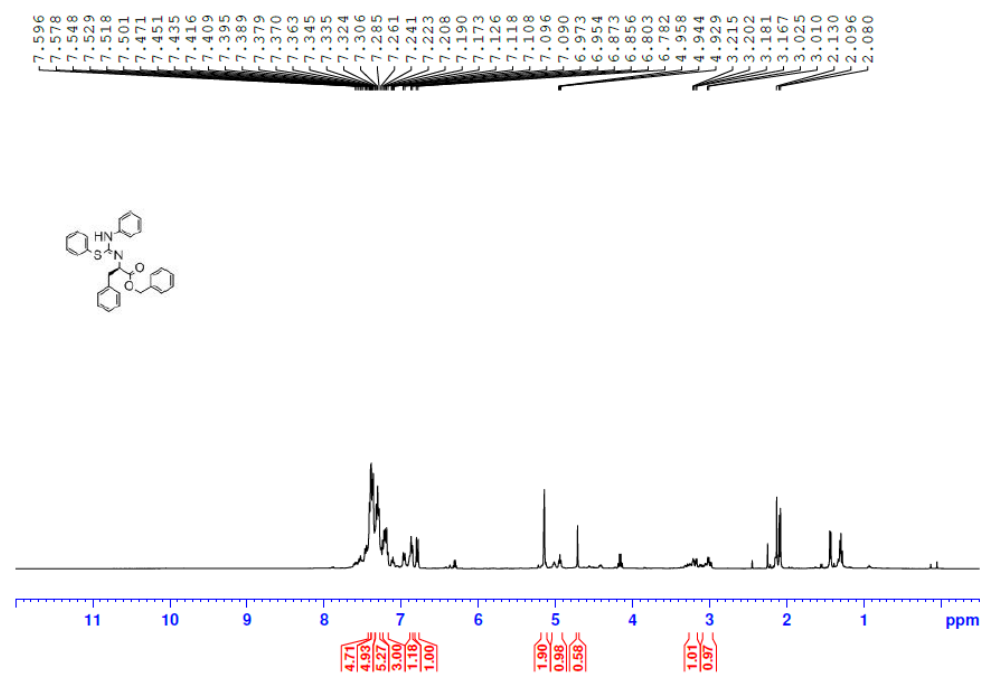
$^1\text{H}$  NMR (400 MHz,  $\text{CDCl}_3$ ) of 4



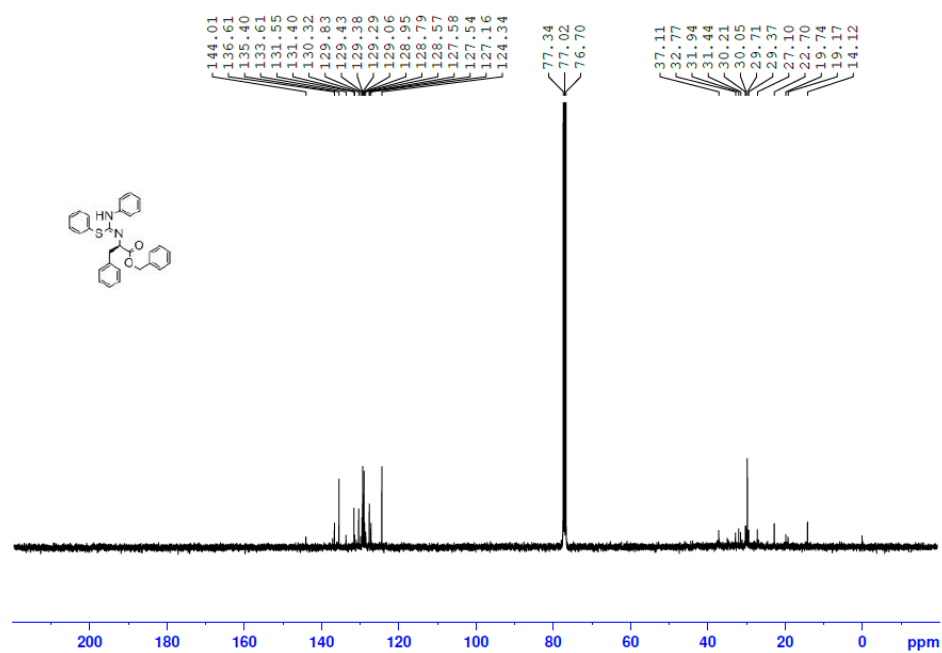
$^{13}\text{C}$  NMR (100 MHz,  $\text{CDCl}_3$ ) of 4



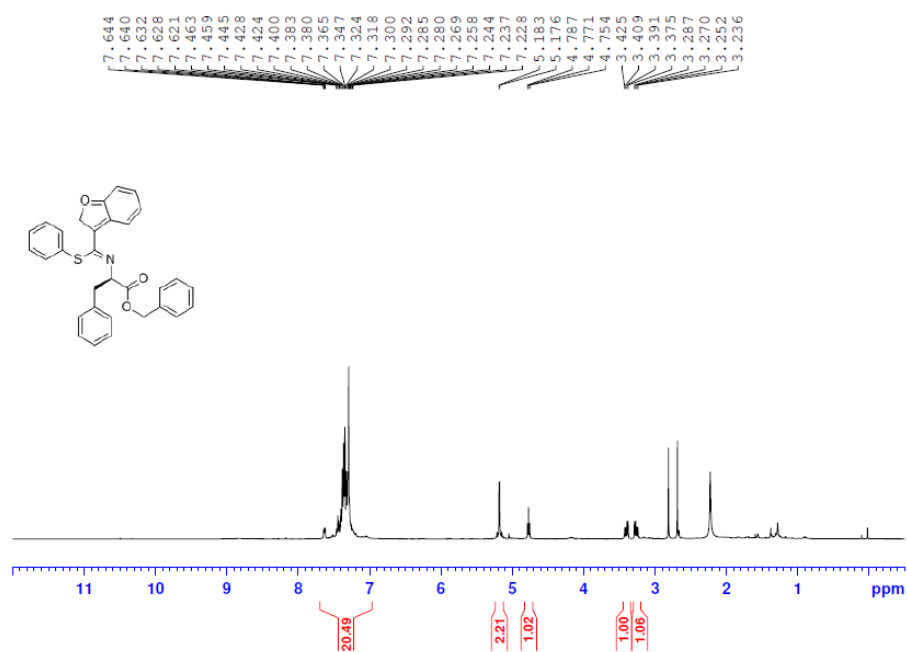
$^1\text{H}$  NMR (400 MHz,  $\text{CDCl}_3$ ) of 5



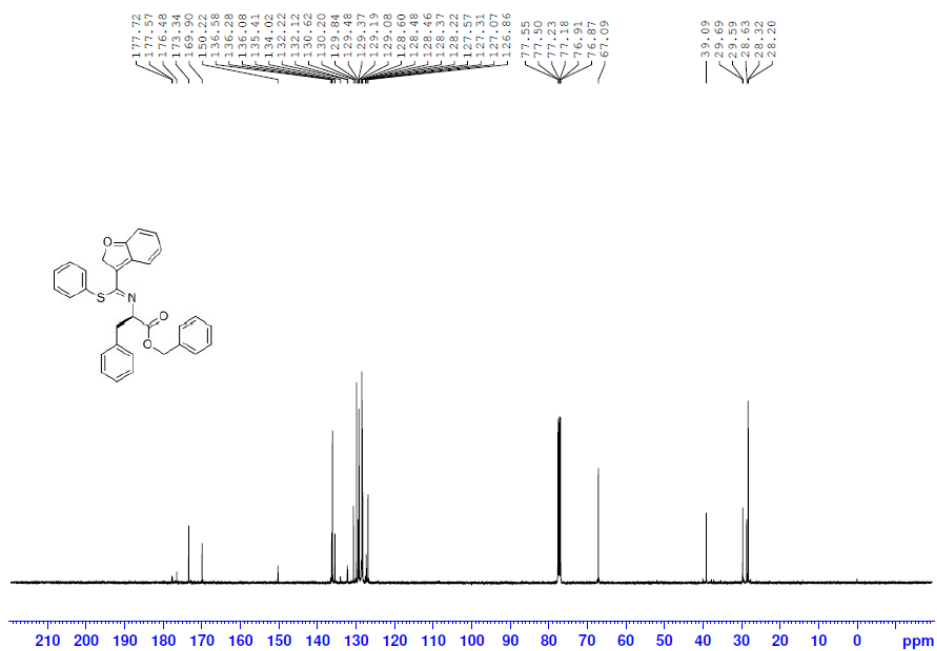
$^{13}\text{C}$  NMR (100 MHz,  $\text{CDCl}_3$ ) of 5



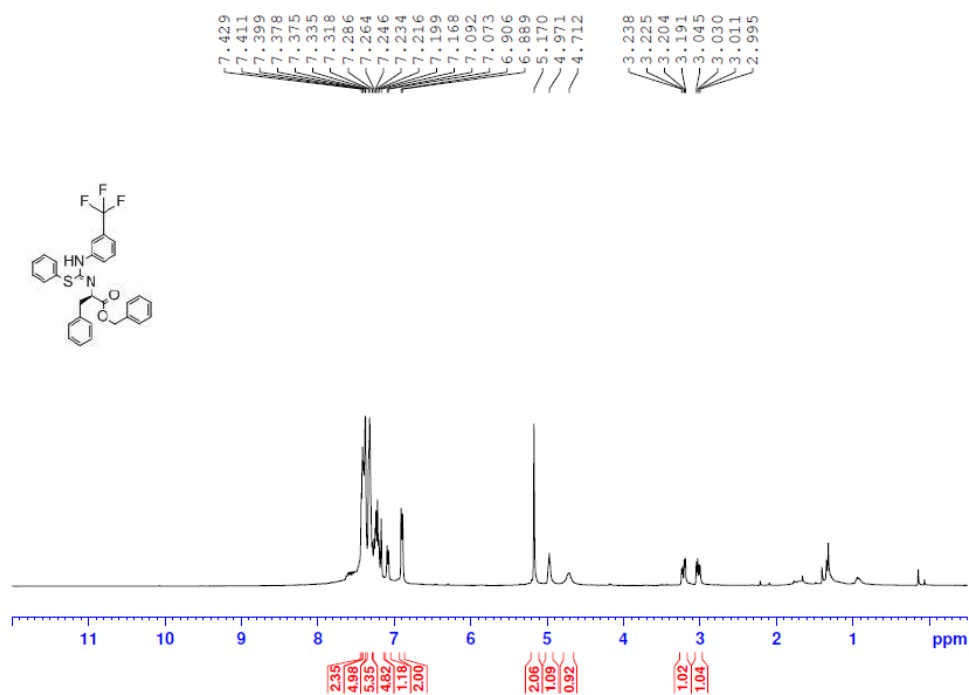
$^1\text{H}$  NMR (400 MHz,  $\text{CDCl}_3$ ) of 6



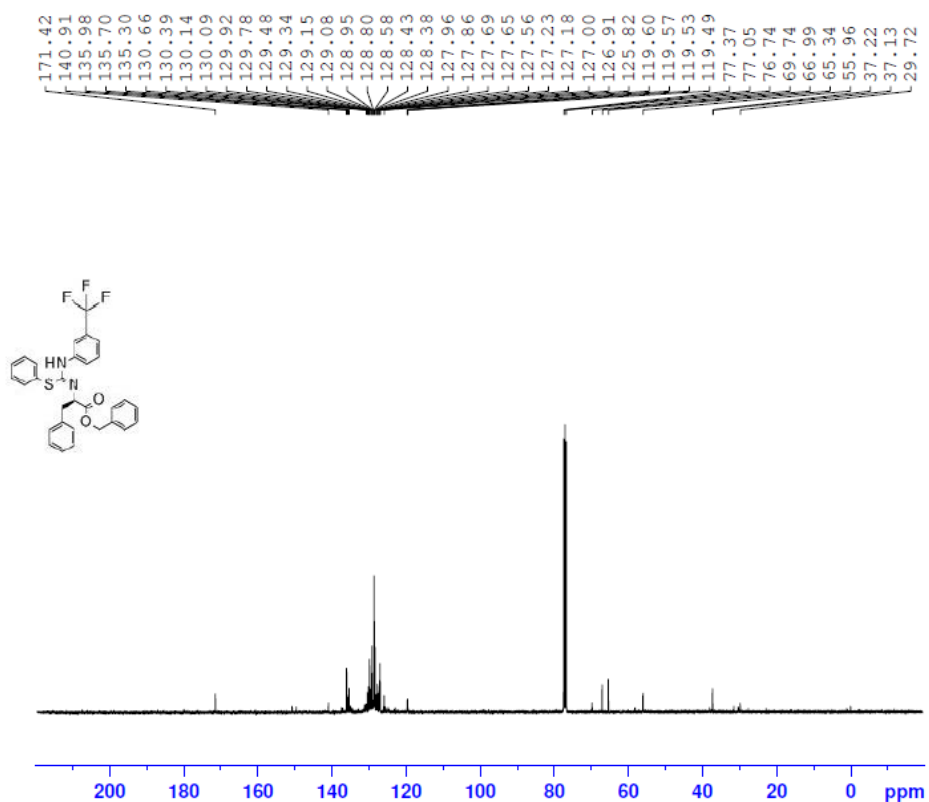
$^{13}\text{C}$  NMR (100 MHz,  $\text{CDCl}_3$ ) of 6



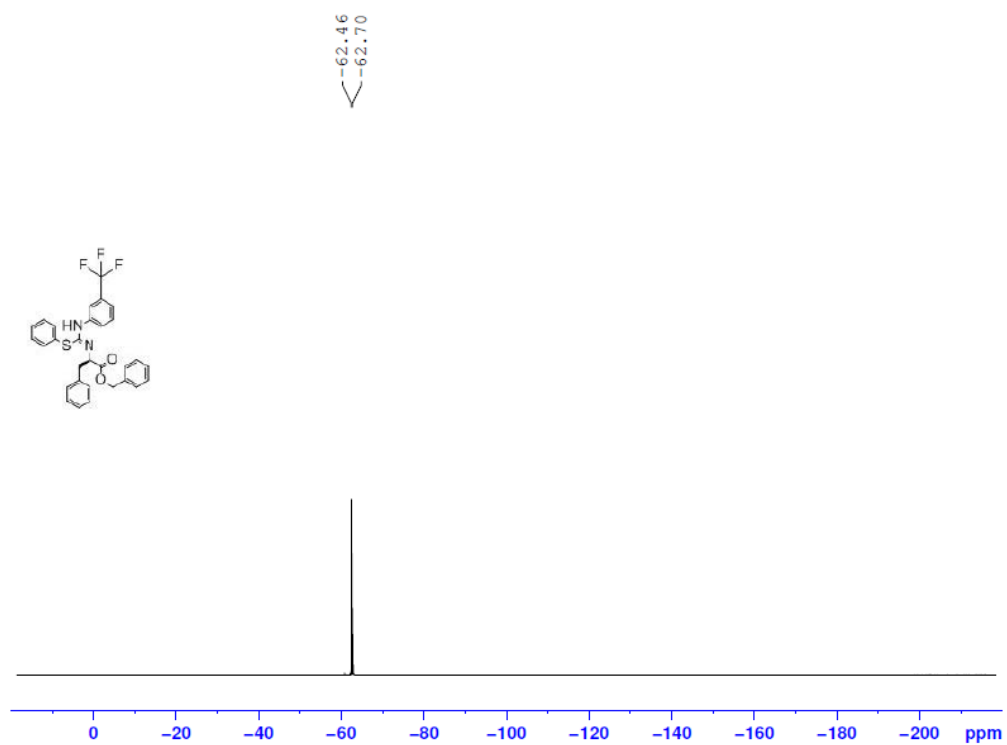
$^1\text{H}$  NMR (400 MHz,  $\text{CDCl}_3$ ) of 7



$^{13}\text{C}$  NMR (100 MHz,  $\text{CDCl}_3$ ) of 7

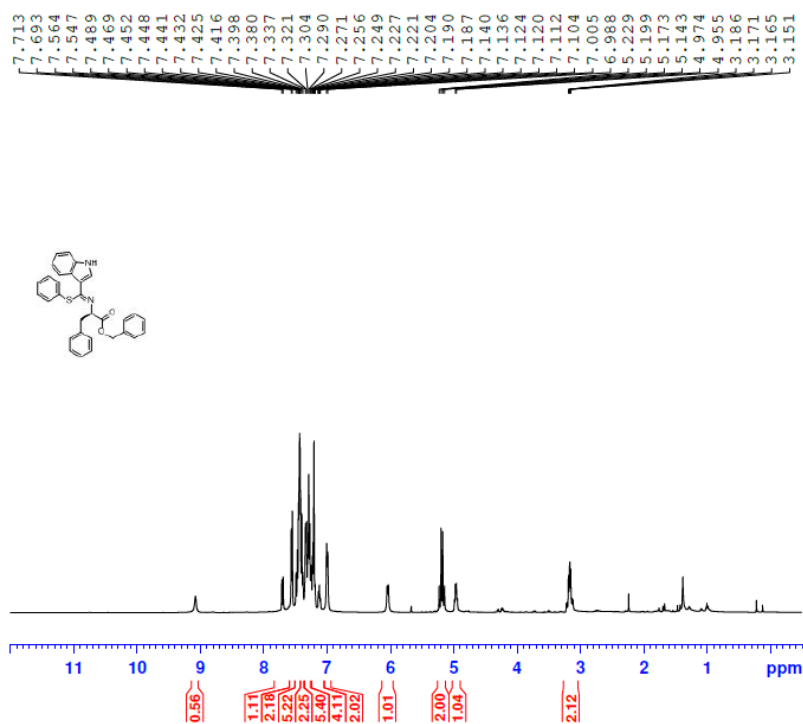


$^{19}\text{F}$  NMR (100 MHz,  $\text{CDCl}_3$ ) of 7

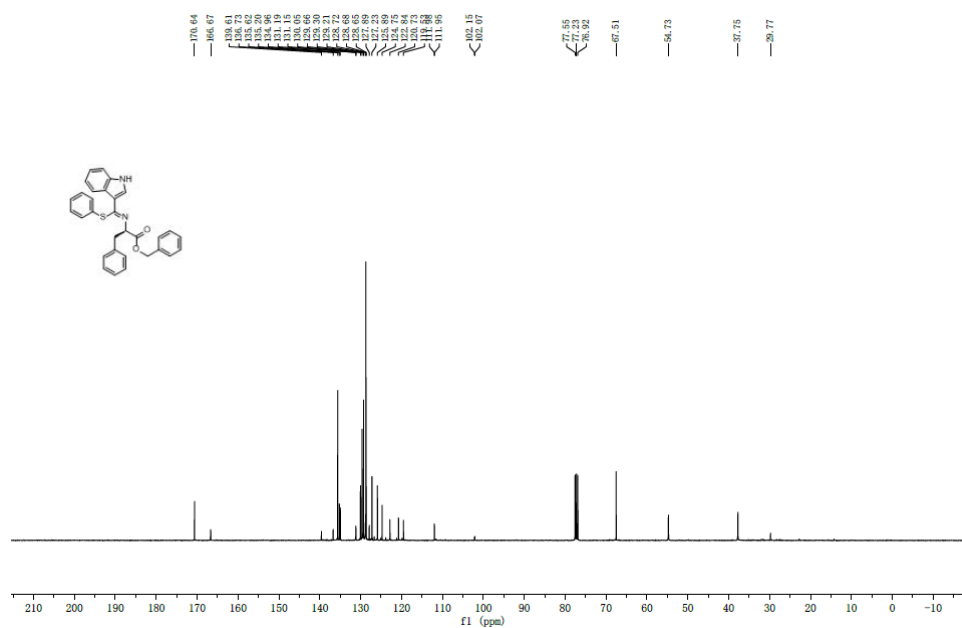




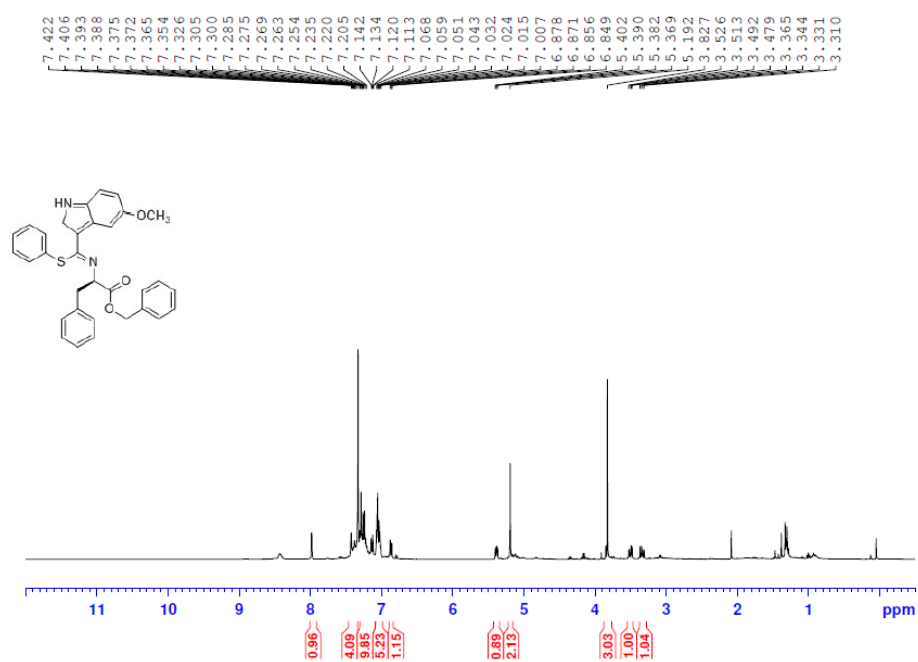
$^1\text{H}$  NMR (400 MHz,  $\text{CDCl}_3$ ) of 8



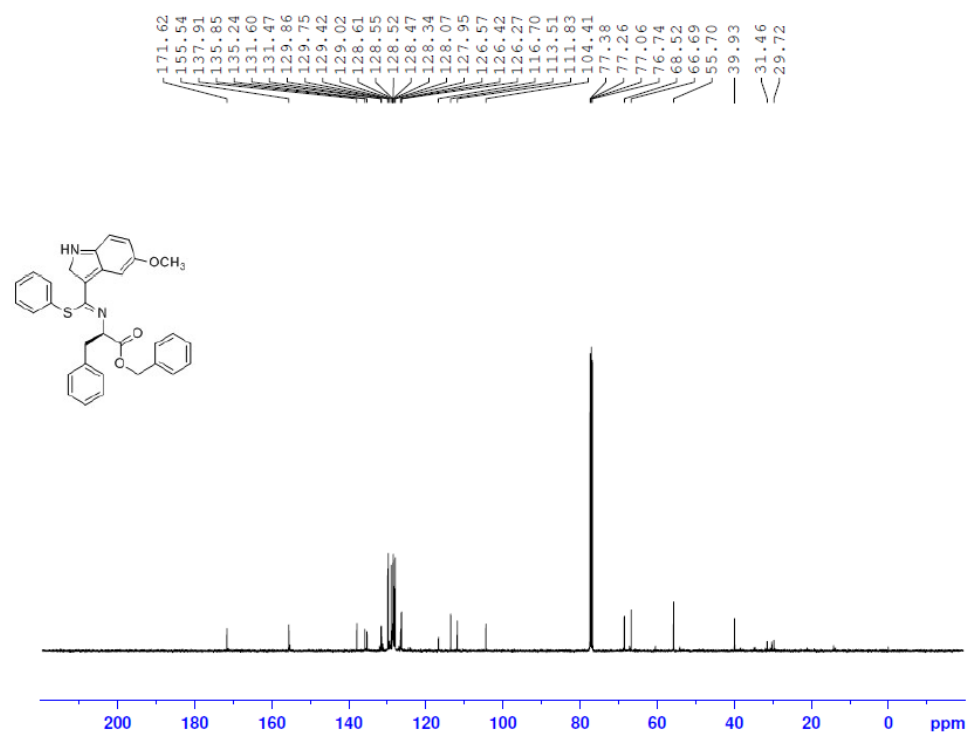
$^{13}\text{C}$  NMR (100 MHz,  $\text{CDCl}_3$ ) of 8



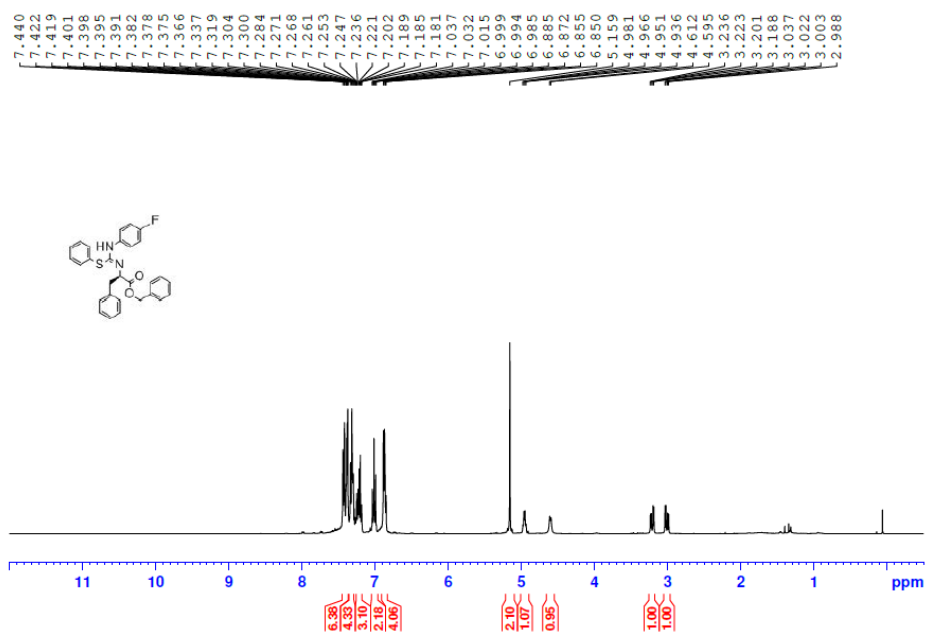
$^1\text{H}$  NMR (400 MHz,  $\text{CDCl}_3$ ) of 9



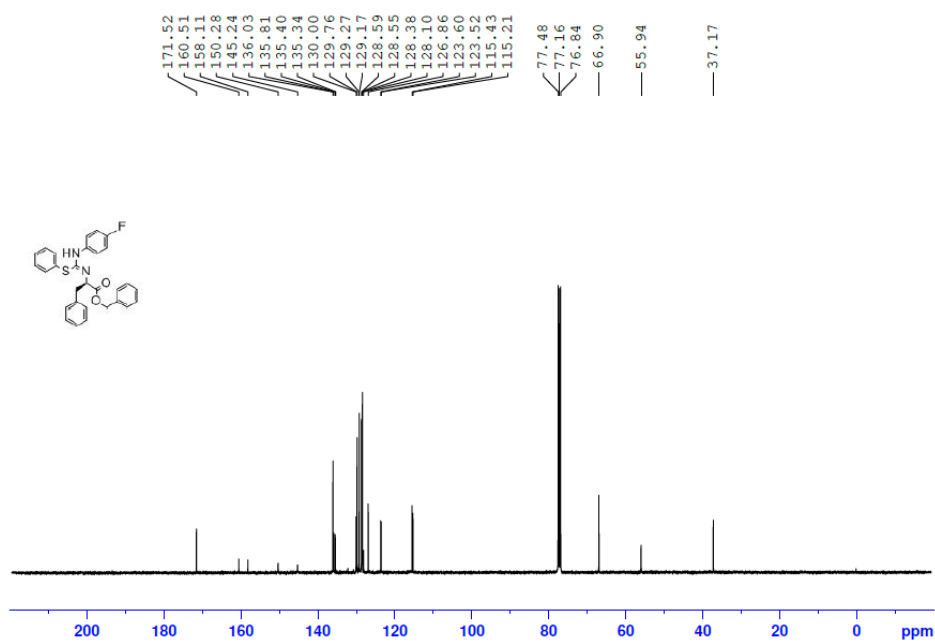
$^{13}\text{C}$  NMR (100 MHz,  $\text{CDCl}_3$ ) of 9



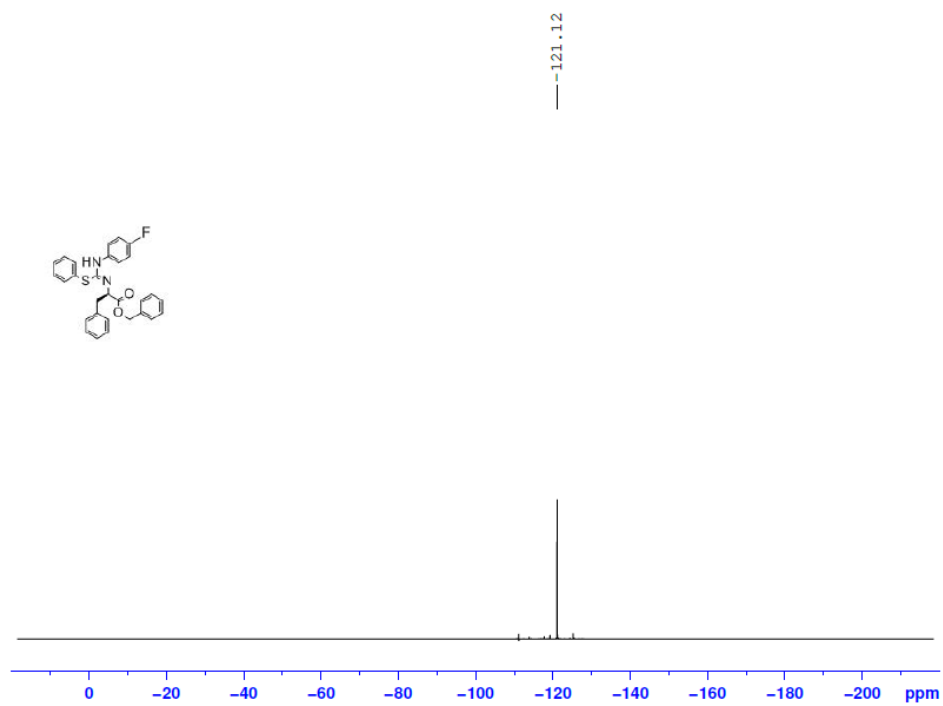
$^1\text{H}$  NMR (400 MHz,  $\text{CDCl}_3$ ) of 10



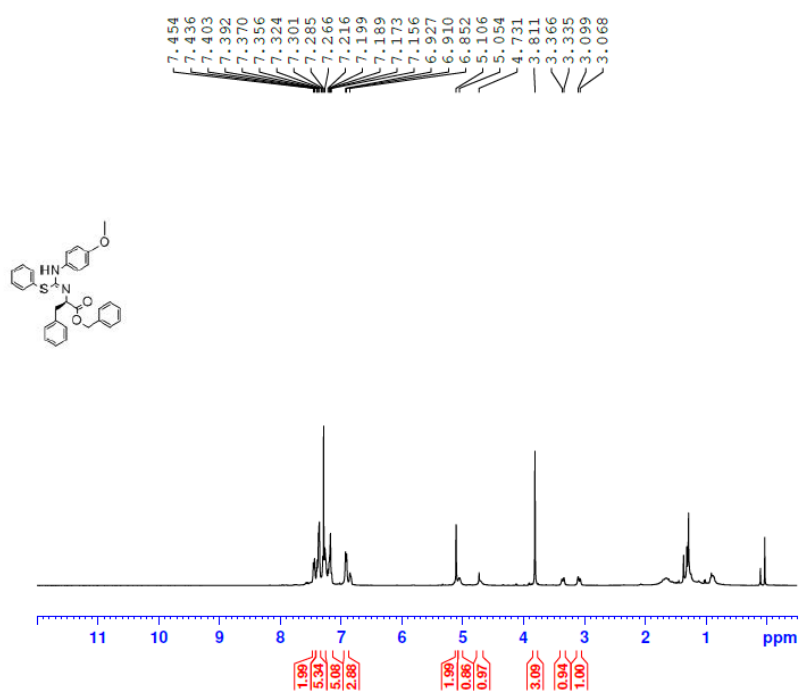
$^{13}\text{C}$  NMR (100 MHz,  $\text{CDCl}_3$ ) of 10



$^{19}\text{F}$  NMR (100 MHz,  $\text{CDCl}_3$ ) of 10



$^1\text{H}$  NMR (400 MHz,  $\text{CDCl}_3$ ) of 11



$^{13}\text{C}$  NMR (100 MHz,  $\text{CDCl}_3$ ) of 11

